

A Study on Parametric Appraisal of Fused Deposition Modelling (FDM) Process

*Dissertation submitted to the
National Institute of Technology Rourkela*

In partial fulfilment of the requirements

for the degree of

Doctor of Philosophy

in

Mechanical Engineering

by

Swayam Bikash Mishra

Roll Number. 512ME111

Under the supervision of

Prof. Siba Sankar Mahapatra



January, 2016

Department of Mechanical Engineering
National Institute of Technology Rourkela



Mechanical Engineering Department
National Institute of Technology Rourkela

January 29, 2016

Certificate of Examination

Roll Number: 512ME111

Name: Swayam Bikash Mishra

Title: A Study on Parametric Appraisal of Fused Deposition Modelling (FDM) Process

We the below signed, after checking the dissertation mentioned above and the official record book (s) of the student, hereby state our approval of the dissertation submitted in partial fulfilment of the requirements for the degree of Doctor of Philosophy in Mechanical Engineering at National Institute of Technology Rourkela. We are satisfied with the volume, quality, correctness, and originality of the work.

Siba Sankar Mahapatra
Principal Supervisor

Raj Kishore Patel
Member, DSC

Anindya Basu
Member, DSC

Subrata Kumar Panda,
Member, DSC

Examiner

Ranjit Kumar Sahoo
Chairman (DSC)



Mechanical Engineering Department
National Institute of Technology Rourkela

Dr. Siba Sankar Mahapatra

Professor

January 29, 2016

Supervisor's Certificate

This is to certify that the work presented in this dissertation entitled "*A Study on Parametric Appraisal of Fused Deposition Modelling (FDM) Process*" by "*Swayam Bikash Mishra*", Roll Number 512ME111, is a record of original research carried out by him/her under my supervision and guidance in partial fulfilment for the requirements of the degree of *Doctor of Philosophy in Department of Mechanical Engineering*. Neither this dissertation nor any part of it has been submitted for any degree or diploma to any institute or university in India or abroad.

Siba Sankar Mahapatra

*This thesis is dedicated to lord Jagannath, my
teachers, my parents and all who have inspired me.*

Declaration of Originality

I, Swayam Bikash Mishra, Roll Number 512ME111 hereby declare that this dissertation entitled "*A Study on Parametric Appraisal of Fused Deposition Modelling (FDM) Process*" represents my original work carried out as a doctoral student of NIT Rourkela and, to the best of my knowledge, it contains no material previously published or written by another person, nor any material presented for the award of any other degree or diploma of NIT Rourkela or any other institution. Any contribution made to this research by others, with whom I have worked at NIT Rourkela or elsewhere, is explicitly acknowledged in the dissertation. Works of other authors cited in this dissertation have been duly acknowledged under the section "Bibliography". I have also submitted my original research records to the scrutiny committee for evaluation of my dissertation. I am fully aware that in case of any non-compliance detected in future, the Senate of NIT Rourkela may withdraw the degree awarded to me on the basis of the present dissertation.

January 29, 2016
NIT Rourkela

Swayam Bikash Mishra

Acknowledgement

While bringing out this thesis to its final form, I came across a number of people whose contributions in various ways helped my field of research and they deserve special thanks. It is a pleasure to convey my gratitude to all of them.

I would like to express my sincere gratitude to all of them. First of all, I would like to express my deep sense of gratitude and indebtedness to my supervisors **Prof. S. S. Mahapatra** for his valuable guidance, suggestions, support, scholarly inputs and invaluable encouragement throughout the research work that instil confidence in me during research and writing of this thesis.

Besides my supervisors, I would like to thank the rest of my doctoral scrutiny committee (DSC) members: **Prof. R. K. Sahoo**, Chairman (DSC Member), **Prof. R. K. Patel**, **Prof. S. K. Panda** and **Prof. A. Basu** for their encouragement and insightful comments.

I am highly grateful to **Prof. S. K. Sarangi**, Director, National Institute of Technology (NIT) for the academic support and the facilities provided to carry out the research work at the Institute.

I also express my thankfulness to the faculty and staff members of the Department of Mechanical Engineering, for their continuous encouragement and suggestions. Among them, **Dr. S. Datta** and **Sri P. K. Pal** deserve special thanks for their kind cooperation in academic and non-academic matters during the research work

I am obliged to, **Chinmaya Prasad Mohanty**, **Sanjita Jaipuria**, **Suman Chatterjee**, **Rameez Malik**, **Mantra Prasad Satpathy**, **Ashutosh Pattanaik**, **Alok Ranjan Biswal**, **P.T.R. Swain** and **Swastik Pradhan** for their support and co-operation that is difficult to express in words. The time spent with them will remain in my memory for years to come.

I owe a lot to my parents, **Mr. Golak Bihari Mishra** (Father) and **Mrs. Saudamini Devi** (Mother), who encouraged and helped me at every stage of my personal and academic life, and longed to see this achievement come true.

I am very much indebted to my brother **Mr. Swayam Prakash Mishra** for his understanding, patience, co-operation and support in every possible way to see the completion of this doctoral work.

Above all, I owe it to almighty **Lord Jagannath** for granting me the wisdom, health and strength to undertake this research task and enabling me to its completion.

Abstract

The manufacturing industries are contemplating to develop new technologies for production of complex end use parts possessing high strength and low product development cycle in order to meet the global competition. Rapid prototyping (RP) is one of the proficient processes having the ability to build complex geometry parts in reasonably less time and material waste. Fused deposition modelling (FDM) is one of the RP processes that can manufacture 3D complex geometry accurately with good mechanical strength and durability. Normally, the FDM process is a parametric dependant process due to its layer-by-layer build mechanism. As FDM build parts are used as end use parts, it is prudent to study the effect of process parameters on the mechanical strength under both static and dynamic loading conditions and wear (sliding) behaviour. In order to investigate the behaviour of build parts in a systematic manner with less number of experimental runs, design of experiment (DOE) approach has been used to save cost and time of experimentation. As the selection of input process parameters influence on build mechanism, the mechanical properties and wear behaviour of FDM build parts change with process parameters. Notably, the raster fill pattern during part building causes FDM build parts to exhibit anisotropic behaviour when subject to loading (static or dynamic). In this research work, an attempt has been made to minimise the anisotropic behaviour through controlling the raster fill pattern during part building by adequate selection of process parameters. Statistical significance of the process parameters is analysed using analysis of variance (ANOVA). Influence of process parameters on performance characteristics like mechanical strength, fatigue life and wear of build part is analysed with the help of surface plots. Internal structure of rasters, failure of rasters, formation of pits and crack are evaluated using scanning electron machine (SEM) micro-graphs. Empirical models have been proposed to relate the performance characteristics with process parameters. Optimal parameter setting has been suggested using a nature inspired metaheuristic firefly algorithm to improve the mechanical strength. Finally, genetic programming (GP) and least square support vector machine (LS-SVM) are adopted to develop predictive models for various performance characteristics

Key words: Rapid prototyping; Fused deposition modelling; Analysis of variance; Genetic programming; least square support vector machine.

Contents

Certificate of Examination.....	ii
Supervisor's Certificate.....	iii
Declaration of Originality.....	v
Acknowledgement.....	vi
Abstract.....	vii
Contents.....	viii
List of Figures.....	xi
List of Tables.....	xiii
Glossary of terms.....	xiv
Chapter 1.....	1
Background and Motivations.....	1
1.1. Introduction.....	1
1.2. Rapid Prototyping process.....	2
1.2.1. Stereolithography (SL).....	4
1.2.2. Selective Laser Sintering (SLS).....	4
1.2.3. Laminated Object Manufacturing (LOM).....	4
1.2.4. Fused Deposition Modelling (FDM).....	5
1.2.5. Three Dimensional Printing (3DP).....	5
1.2.6. Multi Jet Modelling (MJM).....	5
1.2.7. Solid Ground Curing (SGC).....	6
1.3. Need for the research.....	6
1.4. Research objectives.....	7
1.5. Outline of the thesis.....	8
1.6. Conclusion.....	9
Chapter 2.....	10
Literature Review.....	10
2.1. Introduction.....	10

2.2.	Application of RP	13
2.3.	RP process selection	14
2.4.	RP material issue.....	16
2.5.	Assessment of strength of RP build parts	18
2.6.	Assessment of fatigue life of RP build parts	21
2.7.	Wear characteristics of RP build parts	22
2.8.	Discussion on RP issues	23
2.9.	Conclusion.....	23
Chapter 3.....		25
Parametric assessment of static strength of FDM build parts.....		25
3.1.	Introduction.....	25
3.2.	Fuzzy Inference Systems.....	26
3.2.1.	Fuzzifier	27
3.2.2.	Knowledge base	27
3.2.3.	Inference engine	27
3.2.4.	Defuzzifier.....	27
3.3.	Firefly Algorithm.....	28
3.4.	Genetic programming	30
3.5.	Least Square Support Vector Machine	32
3.6.	Experimental Details	33
3.7.	Results and Discussion.....	40
3.8.	Conclusion.....	66
Chapter 4.....		69
Parametric assessment of fatigue life of FDM build parts		69
4.1.	Introduction.....	69
4.2.	Experimental plan	70
4.3.	Results and Discussions.....	76
4.4.	Conclusion.....	92

Chapter 5.....	93
Parametric assessment of wear behaviour of FDM build parts	93
5.1. Introduction.....	93
5.2. Experimental Details	94
5.3. Results and Discussions.....	96
5.4. Conclusion.....	107
Chapter 6.....	108
Executive Summary and Conclusion.....	108
6.1. Introduction.....	108
6.2. Summary of findings	108
6.3. Contribution of the research work	110
6.4. Limitation of the study	111
6.5. Scope for future work.....	111
Bibliography	113
Dissemination	124
Vitae.....	126

List of Figures

Figure 1.1. Main process stage to common RP process	3
Figure 2.1 Research issues in RP	12
Figure 2.2. Percentage of Paper Surveyed	12
Figure 3.1. Structure of fuzzy inference system.....	28
Figure 3.2. GP tree representation of a symbolic expression: $9\tan(x) + 5y$	31
Figure 3.3. Sub-tree crossover between parents.....	31
Figure 3.4. Overlaying raster orientation style	35
Figure 3.5. ASTM D638 standard test specimen for tensile test	37
Figure 3.6. ASTM D695 standard specimen for compressive test	37
Figure 3.7. standard test method for flexural properties of plastics.....	37
Figure 3.8. ASTM D256 standard specimen for izod test	37
Figure 3.9. Instron 1195 series IX automated material testing machine	38
Figure 3.10 FDM Fortus 400mc series	38
Figure 3.11. Monomers in acrylonitrile butadiene styrene (ABS) plastic	39
Figure 3.12. Normal probability plot of residual at 95% confidence interval for tensile strength.....	44
Figure 3.13. Surface plot for tensile strength.....	46
Figure 3.14. SEM image of part showing raster failure	47
Figure 3.15. SEM image of overlaying raster orientation	47
Figure 3.16. Stress strain curve for tensile strength	48
Figure 3.17. Normal probability plot of residual at 95% confidence interval for compressive strength	49
Figure 3.18. Surface plots for compressive strength	51
Figure 3.19. Normal probability plot of residual at 95% confidence interval for Flexural strength	52
Figure 3.20. Surface plots for flexural strength.....	54
Figure 3.21. Stress strain curve for flexural strength	55
Figure 3.22. Normal probability plot of residual at 95% confidence interval for impact strength	56
Figure 3.23. Surface plots for flexural strength.....	58
Figure 3.24. Membership function for each normalised response	59
Figure 3.25. Membership function for MPC1	59

Figure 3.26. Normal distribution of residuals at 95% confidence interval for MPCl	62
Figure 3.27. Diagram of GP formulation of fatigue life of FDM built parts	63
Figure 3.28. Relative errors comparison between GP and LS-SVM models for static strength	66
Figure 4.1. ASTM standard specimen for strain controlled fatigue test.....	74
Figure 4.2. BISS machine (Bangalore Integrated System Solutions).....	75
Figure 4.3. Failure of FDM build parts under static loading	78
Figure 4.4 Failure of FDM build parts under dynamic loading.....	78
Figure 4.5. Strain amplitude vs fatigue life curve for strain controlled fatigue test (ϵ -Nf) for run order 18.....	79
Figure 4.6. Strain amplitude vs fatigue life curve for strain controlled fatigue test (ϵ -Nf) for run order 23.....	80
Figure 4.7. Stress strain-curve for fatigue test for run order 18.....	81
Figure 4.8. Stress strain-curve for fatigue test for run order 23.....	81
Figure 4.9 Normal probability plot of residual at 95% confidence interval for fatigue life.....	83
Figure 4.10 Surface plots for fatigue life	85
Figure 4.11. Raster failure during static loading	86
Figure 4.12 Raster failure in zig-zag manner during cyclic loading.....	86
Figure 4.13 Rupture of adhesive bond during cyclic loading.....	87
Figure 4.14 Crack formation during cyclic loading	87
Figure 4.15. Diagram of GP formulation of Wear of FDM built parts.....	88
Figure 4.16. Relative errors comparison between GP and LS-SVM models for fatigue life.....	91
Figure 5.1 ASTM standard specimen for wear test (all dimensions are in mm)	95
Figure 5.2. Pin on disk wear testing machine	96
Figure 5.3. Response surface plots for wear	100
Figure 5.4. SEM plots of the FDM specimen after wear testing.....	101
Figure 5.5. Wear volume with sliding distance	102
Figure 5.6. Friction coefficient with sliding distance.....	102
Figure 5.7. Diagram of GP formulation of wear of FDM built parts.....	103
Figure 5.8. Relative errors comparison between LS-SVM and GP models for wear behaviour	106

List of Tables

Table 2.1 Materials in rapid prototyping processes (Sood, 2011)	16
Table 3.1. Factors and their levels	36
Table 3.2. Experimental results	40
Table 3.3. Effect of contour number on tensile strength of FDM parts	42
Table 3.4. Effect of delta angle on tensile strength	43
Table 3.5. ANOVA table for tensile strength	44
Table 3.6. ANOVA table for compressive strength	49
Table 3.7. ANOVA table for flexural strength	53
Table 3.8. ANOVA table for Impact Strength	56
Table 3.9. Individual normalised values of responses with MPCl value	59
Table 3.10. Optimum parameter setting to achieve the best MPCl	61
Table 3.11. Parameter setting for genetic programming	63
Table 3.12. Relative error (%) of the GP model and LS-SVM Model	64
Table 3.13. Comparison of strength of injection moulded parts with FDM parts	67
Table 3.14. Comparison of results of present study with previous research work	67
Table 4.1. Experimental results	76
Table 4.2. ANOVA for fatigue life	83
Table 4.3. Optimum parameter setting to achieve the best fatigue life	88
Table 4.4. Parameter setting for genetic programming	89
Table 4.5. Relative error (%) of the GP model and LS-SVM Model	90
Table 5.1. Experimental results	96
Table 5.2. ANOVA table for wear	98
Table 5.3. Optimum parameter setting to achieve the best wear behaviour	103
Table 5.4. Parameter setting for genetic programming	104
Table 5.5. Relative error of LS-SVM model and RSM model	105

Glossary of terms

3D	Three Dimensional
3-DP	3D Printing
ABS	Acrylonitrile Butadiene Styrene
AF	Automated Fabrication
AM	Additive Manufacturing
ANSI	American National Standards Institute
ASCII	American Standard Code for Information Interchange
ASTM	American Society of Testing And Materials
CAD	Computer Aided Design
CAGR	Compound Annual Growth Rate
CAM	Computer Aided Manufacturing
CCD	Central Composite Design
CLI	Common Layer Interface
CNC	Computer Numerical Control
CSG	Constructive Solid Geometry
DFM	Design for Manufacture
DLF	Directed Light Fabrication
DMD	Direct Metal Deposition
DMLS	Direct Metal Laser Sintering
DOE	Design of Experiment
DXF	Drawing Exchange Format
EDM	Electrical Discharge Machining
FCCCD	Face Centred Central Composite Design
FDM	Fused Deposition Modelling
FDMet	Fused Deposition Of Metals
FE	Finite Element
FIS	Fuzzy Inference System
GP	Genetic Programing
IC	Investment Casting
LENS	Laser Engineered Net Shaping
LM	Layered Manufacturing
LOM	Laminated Object Manufacturing
LS-SVM	Least Square Support Vector Machine
LV	Low Vacuum
MADM	Multi Attribute Decision Making
MAPE	Mean Absolute Percentage Error
MJM	Multi Jet Modelling
MPCI	Multi Performance Characteristic Index
NRMS	Normalized Root Mean Square
PC	Polycarbonate

RE	Reverse Engineering
RM	Rapid Manufacturing
RP	Rapid Prototyping
RPI	Rapid Prototyping Interface
RSM	Response Surface Methodology
RT	Rapid Tooling
SEM	Scanning Electron Microscope
SFFF	Solid Free Form Fabrication
SGC	Solid Ground Curing
SL	Stereolithography
SLM	Selective Laser Melting
SLS	Selective Laser Sintering
STL	Stereolithography File
SVM	Support Vector Machine
UC	Ultrasonic Consolidation
UV	Ultra Violet

Chapter 1

Background and Motivations

1.1. Introduction

In the post era of globalisation, the manufacturing industries are facing stiff competitions to sustain in the market place due to reduction in product life cycle. To meet the challenging demands in the global market, the industries depend in technological advancements in the manufacturing field so that design and manufacturing lead time can be reduced. These days, market demands durable parts with complex profiles at reasonable manufacturing time and cost. As the complexity of the part increases, it demands more advanced manufacturing processes in order to reduce manufacturing cost as well as time. In the recent decades, new manufacturing technologies have been developed to address these issues. Among them, additive manufacturing (AM) is one such process that can produce precise durable end use parts in less time. Generally, the manufacturing processes are categorised into two types depending upon the machining processes i.e. additive and subtractive. The subtractive manufacturing (SM) processes include turning, milling, cutting and grinding in which material is removed from the work piece to get the final shape. In case of SM, the work piece has to pass through various machining processes which increases the manufacturing time and wastage of material. On the other hand, AM process develops product by adding material layer one over another in a sequential manner. Since the material is added as defined by the machining software, material wastage and product development time can be subsequently reduced as compared to SM process.

The AM process alternatively known as **Rapid Prototyping** (RP) is widely appreciated for its tremendous ability in producing complex 3D geometry parts directly from computer aided design (CAD) generated models without requirements of tools, dies, fixture and human intervention. The RP process can easily manufacture physical models from conceptual designs processes through computer aided design (CAD) data saved in the .stl (stereolithographic) format. The rapid prototyping (RP) enables quick and easy transition from concept generation in the form of computer images to the fabrication of 3D physical models. Although the RP process can produce durable parts in less time, the availability of material type limits its wide spread application in daily life and industrial applications. However, the ongoing advances in the fields of material and manufacturing technologies

have boosted the wide spread application of RP process to produce end use parts rather than a prototype model (Yan et al., 2009).

In order to increase the industrial application of RP process, some technological advancements are needed. In this direction, overcoming the limitation of materials functionality of RP build parts, the strength and durability of the build parts must be enhanced to face the demands of the customer. The strength of RP build parts under both static loading and dynamic loading condition must be assessed to enhance functionality. The wear behaviour of the RP build parts needs to be examined to assess its durability.

1.2. Rapid Prototyping process

Manufacturing of three dimensional (3D) solid parts directly from the computer aided design (CAD) file (solid modelling softwares like Solid Works, CATIA, Pro-E, UG and Auto CAD) is conventionally adopted by removing or forming of material from a block of work piece to a desirable shape. Conventional machining processes have their own limitation in manufacturing of complex jobs. In case of moulding process, the cost of the mould is very high and accuracy of the mould decreases after batches of production (Tromans, 2003; Ghosh and Mallik, 1985). Generally, the machining process is automated through integration of CAD and computer aided manufacturing (CAM) so that benefits like cost and time reduction can be realized in manufacturing parts with complex geometry. These days, RP is gaining popularity because parts with complex geometry or complete assembly can be built in significantly less time. The RP process involves fabrication of physical part directly from the CAD data without any human intervention. The build mechanism is almost same for all RP processes i.e. addition of layer one over another in the x-y plane. The addition of material occurs in the z- direction (Onuh and Tusuf, 1999; Upcraft and Fletcher, 2003). To form an object, RP processes add and bond materials in a layer wise manner. The RP process is also known as additive manufacturing (AM), solid freeform fabrication (SFF), layered manufacturing (LM), automated fabrication (AF) and other variants.

The RP process came into existence in the mid of 1980 when advanced version of stereolithography (SL) process was commercialised. After several years of research, laminated object manufacturing (LOM), fused deposition modelling (FDM) and 3D printing (3DP) are commercialised. One survey by Wohelers Associates in 2010 reveals that the demand for RP parts has been increased over last 22 years (Wohler, 2010). Industrial applications of RP parts indicate that it is a widely appreciated technology to address variety of problems in a diverse number of industrial problems (Chua et al., 1999; Liu et

al., 2005; Raja et al., 2005). Since the cost of RP machine is prohibitive to be possessed by medium and small enterprises, the web based RP system can improve productivity, manufacturing speed and economic advantage of such firms (Lan H., 2009; Dong et al., 2008).

The main fabrication process is same for all RP process but the mechanism by which individual layers are created and bonded depends upon on the specific system (Kai and Fai, 1997). Figure 1.1. explains the basic steps involved during the RP process.

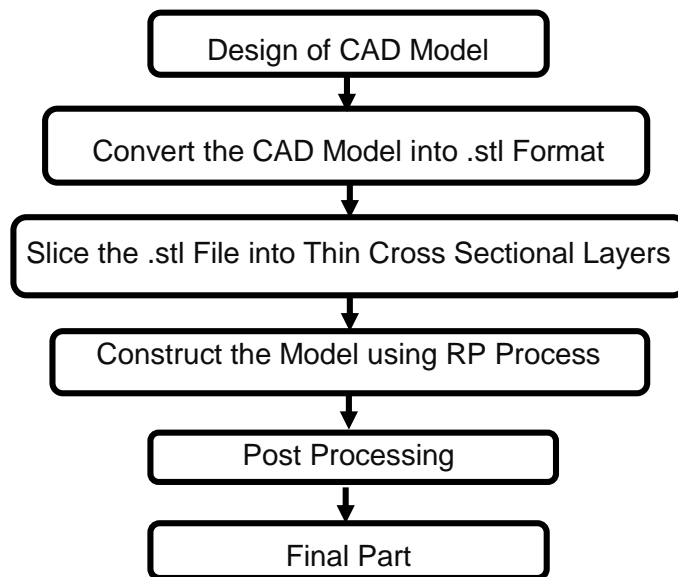


Figure 1.1. Main process stage to common RP process

The primary stage of RP process is to develop the model using any solid modelling software. A solid geometry must be selected from which data is generated to control the fabrication process in an effective manner. Normally, the part generation procedure is divided into two steps.

Step 1: In this step, the CAD file is saved in .stl format after making triangular mesh. The triangular meshed file is sliced and stored in standard formats that could be interpreted by the RP machines at stage 2. In this step, the layer thickness and part orientation act as prime controllable parameter that have the ability to minimise the cost and build time.

Step 2: This step is different for all RP processes and depends upon building mechanism of RP machine. The specific software of the machine guides the laser path or the extrusion head has to get information from the step 1. In this step, various process related information like tolerances, allowances, material and machining types are provided to the controller of the machine (Kai and Fai, 1997; Wang et al., 2000).

Some of well-known RP processes such as Stereolithography (SL), Selective laser sintering (SLS), Laminated object manufacturing (LOM), Fused deposition modelling (FDM), 3D printing (3DP), Multi jet modelling (MJM) and Solid ground curing (SGC) commercialised since 90s have been discussed below (Noorani, 2005).

1.2.1. Stereolithography (SL)

This is the first RP machine commercialised in mid 1980s by 3D Systems, California, USA. In this process, parts are manufactured from a photo curable liquid resin that solidifies when exposed to laser beam. The solidified layer is then lowered into the tank in such a manner that another layer of liquid will come over it to be exposed to the laser. This process continues until all layers are added to develop the model as original as developed in the CAD model. The build platform is removed from the tank and excess liquid polymers are cleaned off. In the post processing stage the build part is cured in an ultra-violet oven.

1.2.2. Selective Laser Sintering (SLS)

This process was developed and patented by Dr. Carl Deckard from University of Texas at Austin and brought into market by DTM Inc. In this process, a thin layer of thermoplastic powder is spread by a roller over the surface of build platform and heated below its melting temperature by infrared heating panels attached to the side of the platform. Then a laser beam traces out the edge of the cross section of the part. The laser beam is used to sinter or fuse together the particle of the layer. After deposition of the first layer, it goes down exactly to layer thickness and another layer of powder is spread over for sintering process. The unsintered powder is removed by brushing off.

1.2.3. Laminated Object Manufacturing (LOM)

In this process, a layer of sheets having an adhesive coating on one side is placed on the build platform with adhesive side down. The sheet sticks to the platform when a heated roller passes over it. Then, a laser beam is pointed to trace the outline of the slice of the part from the sheet. When one layer is formed, the build platform is lowered down up to one layer thickness and another layer of sheet is then stuck onto the previous layer to continue the process. After addition of all layers, the solid block of material is removed from the platform and subjected to post treatment processes.

1.2.4. Fused Deposition Modelling (FDM)

Fused deposition modelling (FDM) was introduced and marketed by Stratasys Inc., USA. In this process, semi molten plastic materials like acrylonitrile butadiene styrene (ABS) or polycarbonate (PC) is extruded from the nozzle over the build platform in the form of thin rasters to build a 3D part. Extruded filaments are placed inside the build chamber in a sequential manner and bonded with the previously placed rasters in the adjacent layer. The build platform is then lowered down relative to the nozzle and next layer of material is deposited over the previous layer. In order to manufacture hanging structures, support material is deposited from a secondary nozzle. Once the part is developed, the support structures are broken away from the part.

1.2.5. Three Dimensional Printing (3DP)

The 3DP technology was invented and patented by the researchers of Massachusetts Institute of Technology (MIT), USA. The inkjet technology is used in 3DP process for model development in a layer-by-layer method. Using the inkjet technology a binder is spread over the powdered material to form a layer. The bed is then lowered by a fixed distance (layer height). Then, powder is deposited and spread evenly over the bed using a roller mechanism to build the next layer. This process continues till the completion of part building. Once the part building is completed, the part is removed from the unprocessed powder and set for post processing.

1.2.6. Multi Jet Modelling (MJM)

In this technology, around ninety six small nozzles are attached to the print head and placed in the x-y plane over the build platform. Thermoplastic polymer are sprinkled over the build platform from the nozzle in droplet form where material is needed. Depending on the shape of layer, jets are activated simultaneously. Hot droplets of material bind with the previously placed material layer. Support structures are also build up inside the part where support is necessary. After completion of a layer, the bed moves down with respect to the print head and the next layer is build up. After completion of the full part, the part is removed from the machine and the support structure is broken off.

1.2.7. Solid Ground Curing (SGC)

In this system, photo polymer resin and ultra-violet (UV) light are used. The computer generated CAD data is used to generate a mask which is placed above the resin surface. Once the layer has been cured, excess resin is wiped away and gaps are filled with wax material. The wax is cooled and the chips are removed. New layer of resin is applied and the process repeated until the object is completed. In this process, large amount of wax is wasted and cannot be recycled.

From above discussions, it has been noted that various RP process have been developed and successfully commercialised for industrial applications. Irrespective of the build mechanism, RP processes are distinguished on their use of material types, strength, durability and surface roughness of the build part. In order to improve the usability and industrial application of RP processed parts, research work needs to be carried out to address the above characteristics. Among all RP processes, fused deposition modelling (FDM) process has the ability to build 3D complex part accurately having reasonable strength and durability. Since the FDM process is parametric dependant, the performance characteristics of the build parts are largely influenced by the selection of process parameters. Therefore, in this research work, efforts have been made to assess the effect of FDM process parameters on the strength, fatigue life and wear behaviour of the FDM build parts.

1.3. Need for the research

Due to design flexibility and ability to handle complex geometry, RP manufacturing processes are gaining significant importance in the industrial application. Manufacturing of functional parts and accurate prototypes without any human intervention can be made using rapid prototyping process only. The application of RP has been diversified in fields like medical, aerospace, automobile, tooling, pattern manufacturing, mould manufacturing and for design verifications (Hopkinson et al., 2006). Apart from these advantages, some limitations exist in the industrial application that drag the popularity of RP. (Wohlert T, 1992). Significant variations are noticed in the geometry and properties of identical parts built using different RP processes. Therefore, industrial standards are required for data transfer between dissimilar RP processes, testing and characterisation of build parts (Campbell et al., 2002; Chockalingam et al., 2005; Ippolito et al., 1995). Use of variable of materials in RP is a major drawback (Gibson et al., 2010).

These limitations of RP technologies open doors for advancements and development as follows:

- Some new design tools and techniques are needed to ease handling of complex geometry that meet specific design as well as strength requirements.
- New RP materials are needed as per the industrial demands.
- To ensure the reliability and predictability of the RP processes, technological and operation related advancements are required.
- In order to predict the performance characteristics of RP build parts, artificial intelligence techniques are needed.
- Some industrial standards for RP processes should be set up to increase the growth rate and further advancement of RP technologies.

1.4. Research objectives

In this context, extensive literature review has been carried out on various efforts directed to improve the industrial feasibility of FDM process. It is well-established fact that FDM build parts are not gaining that much importance in daily life due to limitation of materials used and strength of the part. Therefore, present work focuses on the characterisation of FDM process to make it reliable and predictable like other conventional manufacturing processes simply by extensive study on parametric appraisal rather than resorting to change in the material. Based on these ideas, the objectives of present research are listed below:

- To study the effect of process parameters on static strength, fatigue life and wear resistance of the FDM build parts.
- To effectively control the process parameters to minimise the anisotropic behaviour of the FDM build parts.
- To develop empirical models relating the FDM process parameters with performance characteristics of the FDM build parts.
- To propose predictive models to assess strength, fatigue life and wear resistance of FDM build parts.
- Use of artificial intelligent techniques (AI) to develop models relating process parameters with the performance characteristics of FDM build parts.
- To select optimum parameter setting for the improvement of static strength, fatigue life and wear behaviour of the FDM processes parts.

- To use artificial intelligence techniques for prediction of static strength, fatigue life and wear behaviour of the FDM build part, because prediction models enables to predict the performance measures with reasonable accuracy so that costly experimental time can be minimized.

1.5. Outline of the thesis

The dissertation is organized into six chapters as follows:

Chapter 1. Background and motivation

This chapter introduces fused deposition modelling, its related issues and end use applications. The chapter also provides the problem statements to be addressed in this research.

Chapter 2. Literature survey

This chapter reviews related literature to provide background information on the issues to be considered in the thesis and emphasize the relevance of the present study. The search is restricted on those articles for which full text is available. The study is mainly categorized into six parts such as application of RP, material issue, process selection, assessment of static strength, fatigue life and wear behaviour of FDM build parts.

Chapter 3. Parametric assessment of static strength of FDM build parts

In this chapter, effect of six controlling process parameter such as contour number, layer thickness, raster width, raster orientation, part orientation and air gap on the mechanical strength (tensile, compressive, flexural and impact strength) are studied using design of experiment approach. Empirical models relating process parameters and mechanical strength have been developed using regression analysis. Optimum parameter setting has been suggested using a nature inspired meta-heuristic known as firefly algorithm to improve the mechanical strength of the FDM build parts. To predict the mechanical strength, two latest artificial intelligence techniques known as genetic programming (GP) and least square support vector machine (LS-SVM) have been adopted. The prediction model enables to predict the performance measures with reasonable accuracy so that costly experimental time can be minimized.

Chapter 4. Parametric assessment of fatigue life of FDM build parts

In this chapter, effect of six controlling process parameter on the fatigue life of the build parts has been studied using strain-controlled fatigue test based on ASTM E 606. The failure mechanism of rasters has been analysed and discussed using SEM micrographs. A statically valid empirical model relating process parameters and fatigue life has been

developed using regression analysis. Optimum parameter setting has been suggested firefly algorithm to improve the fatigue life of the FDM build parts. To predict the fatigue life, genetic programming and least square support vector machine have been adopted.

Chapter 5. Parametric assessment of wear characteristics of the FDM build parts

In this chapter, effect of six controlling process parameter on sliding wear behaviour of the build parts have been studied. From the scanning electron microscope (SEM) micrographs, wear surfaces and internal structures of the specimens are evaluated. Empirical model relating process parameter and wear volume has been suggested. Again genetic programming and least square support vector machine have been adopted to predict the wear behaviour of FDM build parts.

Chapter 6. Executive summary and conclusions

In this chapter, conclusions, scope for future work and contribution of the research work have been highlighted.

This chapter also presents the brief summary of findings, major contribution to research work and future scope of the research.

1.6. Conclusion

Present chapter highlights the importance and significance of RP as a manufacturing technology having the ability to build the part accurately without any human intervention. The advantage of RP over traditional manufacturing may be listed as follows:

- An additive manufacturing process (Layer-by-Layer build mechanism).
- Have the ability to build 3D complex geometry of reasonable strength with less time and material wastage.
- Fully automatic process and depends on the CAD data.
- RP process does not require any jig and fixture arrangement.
- Parts can be built directly from CAD data without any human intervention.

The advantages of RP, draws the attention of the manufacturers for direct implementation of RP in industries. To overcome the limitations of RP processes particularly in the application of FDM process, research objectives are set and the work outline is presented in this chapter. An exhaustive literature survey is presented in the next chapter (Chapter 2).

Chapter 2

Literature Review

2.1. Introduction

In order to face the challenging demands of global customers, manufacturing industries are adopting new processes to minimise the product development cycle and wastage of material. Among all processes, rapid prototyping (RP) is widely appreciated for its ability to manufacture accurate and durable parts in reasonable time with less material waste. For proper implementation of RP process, the related issues associated RP process must be addressed. Therefore, in this direction, the current chapter elaborates the development and problems associated with the RP process with specific attention to the fused deposition modelling (FDM) process. RP literature survey in this work begins with journals and books published after 1990. The literature survey is limited to those article for which full text was available. Table 2.1 provides the name of journal and the number of citations from the journal. The International Journal of Advanced Manufacturing Technology and Journal of Material Processing Technology together account 30% of the total cited articles.

Table 2. 1 Summary of publication referred

Journal name	Citation
Advanced Engineering Informatics	1
Advanced Engineering Materials	1
Assembly Automation	1
ASTM standards	6
CIRP Annals-Manufacturing Technology	6
CIRP Journal of Manufacturing Science and Technology	1
Composites Part B: Engineering	1
Computational Materials Science	1
Computer and Geosciences	2
Computer-Aided Design	1
Computers in Industry	4
Expert Systems with Applications	1
ICIC Express Letters	2
International Journal of Current Research	1

International Journal of Engineering Education	1
International Journal of Fatigue	4
International Journal of Innovative Computing, Information and Control	1
International Journal of Machine Tools and Manufacture	2
International Journal of Oral and Maxillofacial Surgery	1
International Journal of Production Economics	1
International Journal of Production Research	1
Journal European Ceramic Society	2
Journal of Cranio-Maxillofacial Surgery	1
Journal of Industrial Technology	1
Journal of Intelligent Manufacturing	7
Journal of Manufacturing Processes	1
Journal of Manufacturing Systems	3
Journal of Manufacturing Technology Management	1
Journal of Material Science and Technology	1
Journal of Materials Processing Technology	17
Journal of Operational Research	1
Journal of the European Ceramic Society	2
Materials and Design	8
Materials and Manufacturing Processes	1
Materials Science and Engineering	2
Medical Engineering and Physics	1
Polymer Engineering and Science	1
Polymer Testing	1
Proceedings of the Institution of Mechanical Engineers, Part B:	
Journal of Engineering Manufacture	2
Rapid Prototyping Journal	12
Robotics and Computer-Integrated Manufacturing	2
Scripta Materialia	3
Small	1
The International Journal of Advanced Manufacturing Technology	30
Tsinghua Science and Technology	3
Virtual and Physical Prototyping	1
Conferences	9

Books	6
Web sites	2
Total	162

All the articles reviewed are classified into an assortment of section dealing with specific issues associated with RP as shown in Figure 2.1. Figure 2.2 provides breakdown of the number of citations reviewed addressing the RP issues. Lastly, this chapter summarized the advancement of RP process and shows direction to continue research work in a well organised manner.

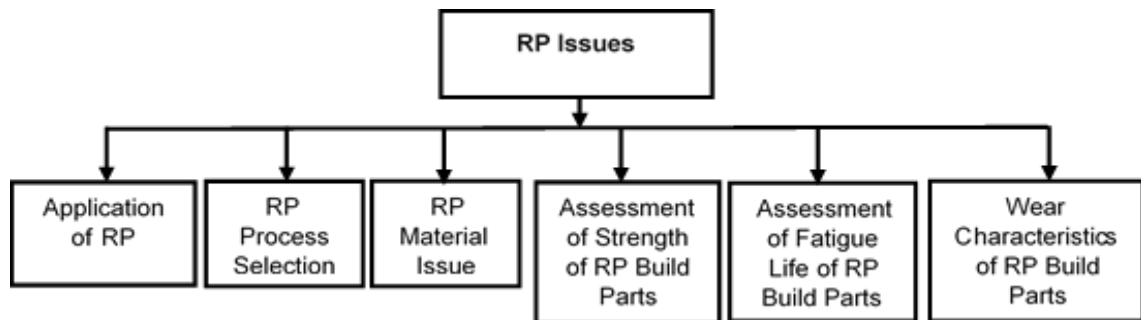


Figure 2.1 Research issues in RP

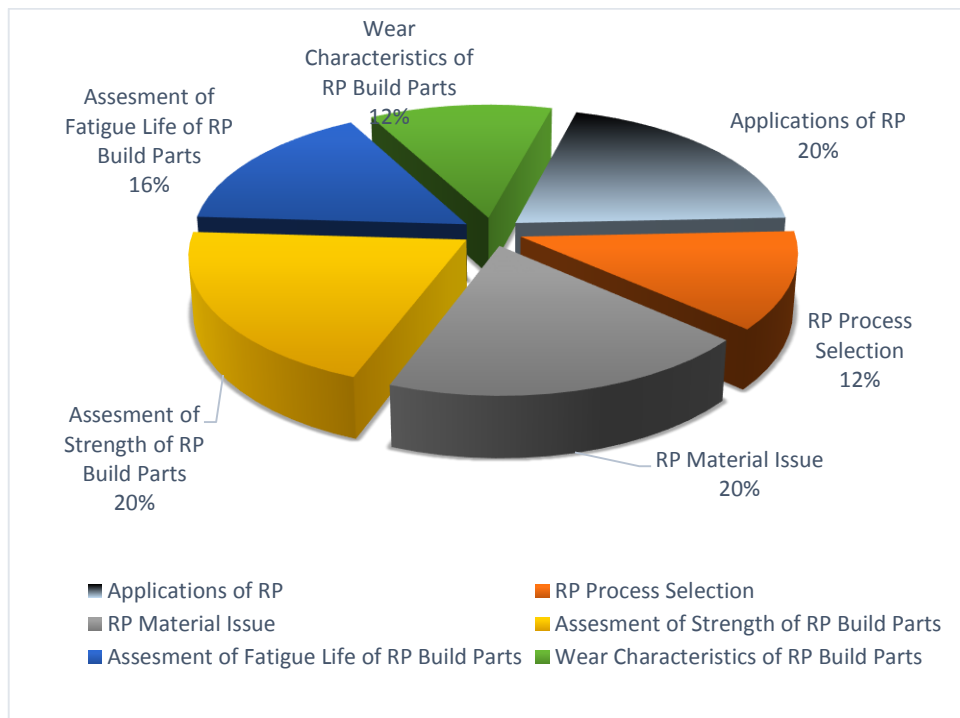


Figure 2.2. Percentage of Paper Surveyed

2.2. Application of RP

In order to decrease the product development cycle time due to stiff competition in the market place, manufacturing industries are forced to adopt new technologies for part design and fabrication. Among all technologies, RP process is distinguished due its ability to develop accurate 3D parts directly from CAD (computer aided design) data without any human intervention. RP helps the manufacturer to get competitive advantage due to reduction of cycle time. Hence the process is widely adopted in manufacturing industries (Krause et al., 1997; Bernard and Fischer, 2002; Kruth et al., 1998). Wiedemann and Jantzen (1999) reveals that complete engine mock-ups for Daimler- Benz can be manufactured using the RP process at a cost of 80% than the conventional manufacturing process.

Application of RP in the medical field increases the possibility of viewing and physical handling of anatomically precision parts so that information can be gathered before any surgical operations (Berry et al., 1997; Giannatsis and Dedoussis, 2009). Some bio-models manufactured through RP processes are used for planning to assist surgery and preparation of implants (Liu et al., 2005; Girod et al., 2001; Heissler et al., 1998; Lohfeld et al., 2007). Studies also reveal that CAD, finite element (FE) analysis and RP techniques can be simultaneously adopted for direct manufacturing of customized implant parts (Colombo et al., 2010). Normally, RP produced parts are porous in nature due to the presence of small air gaps between layers and these porosity is advantageous for the construction of specific scaffolds (Too et al., 2002).

Primarily, RP processes are used to manufacture prototype parts for design verifications but design freedom, less tooling and less human intervention enables RP process to be used for batch production economically. Direct manufacturing of end use and kinematic functional parts from CAD model is termed as rapid manufacturing (RM) process. Using the RM process, the product development cycle and the requirement of equipment can be minimised (Levy et al., 2002; Hon K., 2003). Multi-layer printed circuit board (PCB) can be accurately fabricated using RP technology like solid ground curing (SGC) (Im et al., 2007).

Though RP processes are not well developed to use metal as build material directly but the combination of RP process with metal casting increases the feasibility of rapid manufacturing process. This combination gives rise to a new application of RP known as rapid tooling (RT). The RT process proves its existence in the manufacturing industries by producing complex moulds which are capable of forming millions of parts at a single time.

RT, an application of RP process, describes a technology which either use RP parts as a pattern to develop a mould or use of RP parts directly as a tool (Ding et al., 2004; Dunne et al., 2004; Chua et al., 1999). Depending on the application RT process, it is divided into two type i.e. direct tooling and indirect tooling. In case of indirect tooling, the master pattern is manufactured using a RP process. Now-a-days, RP patterns can be manufactured using almost all RP processes such as stereolithography (SL), selective laser sintering (SLS), laminated object manufacturing (LOM), fused deposition modelling (FDM), 3D printing (3-DP) and solid ground clearing (SGC) (Shan et al., 2003; Rahamati and Dickens, 2007; Mueller and Kochan, 1999; Czyzewski et al., 2009). In case of direct tooling, tool cavities are directly manufactured using the RP processes avoiding the intermediate steps of generating patterns (Cheah et al., 2002; Karapatis et al., 1998). The FDM technology have shown its capability in the manufacturing of acrylonitrile butadiene styrene (ABS) patterns for the investment casting processes (Gosh and Malik, 1985; Cheah et al., 2004). Another interesting area for the application of rapid tooling is in the electrical discharge machining (EDM) process. Some RP processes have already shown their potential in the manufacturing of EDM tools by using abrading process, copper electroforming and spray metal deposition (Tang et al., 2002). To make an EDM tool using RP process, post processing of parts are needed to meet the EDM specifications. For non-conductive material, metallisation is required to make it conductivity i.e. by applying conductive paste over the outer surface (Monzon et al., 2008). One effective method has been proposed by Hsu et al. (2007) for the manufacturing of EDM tool using Zcorp 402 3DP rapid prototyping process and the experimental results indicate that the performance of the EDM tool is reasonable. Zhang et al. (2009) have used the integration of RP with reverse engineering (RE) process for the die making of clutch house of a diesel engine. The LOM process is used to manufacture the die by collecting data from the RE process. Most effective RP processes that are used to fabricate composite structures are laminated object manufacturing (LOM), fused deposition modelling (FDM), stereolithography (SL), 3D printing (3DP), ultrasonic consolidation (UC), laser engineering net shaping (LENS) and selective laser sintering/ melting (SLS/SLM) (Ma et al., 2007; Kumar and Kruth, 2010).

2.3. RP process selection

Appropriate selection of RP process requires a focus on various criteria such part cost, part quality, part properties, temperature of the build platform, build time and other parameters that suits the build condition. In this direction a large number of articles have

been published to proposed decision support systems assisted with software tool for the selection of most suitable RP process. A data base has been developed by Mahesh et al. (2005) that stores all the features of individual RP systems. The data base structure use of queries of the users for the selection of suitable RP process. The selection of RP process depends upon the benchmarking studies which compares different RP system on the basis of part accuracy, part strength, part quality and other aspects (Campbell and Bernine, 1996; Pham and Gault, 1998; Bibb et al., 1999). Comparison of RP processes using benchmark problems has some limitation due to the selection of a standard part for the benchmarking issue.

As selection of RP process can be viewed as multi criteria decision making process, analytic hierarchy process (AHP) is gaining popularity for the selection of RP process to suit the manufacturer's requirements (Vaidya and Kumar, 2006; Bragila and Petroni, 1999; Kengpol and Brien, 2001). A rule based RP process selector has been developed by Industrial Research Institute, Swinburne (IRIS) and it uses selection criteria such as part accuracy, machine cost, surface finish, build envelop, build material and building speed. The database includes the full specification of RP machines and displays it when recommended by the selector program (Masood and Al-alawi, 2002; Masood and Soo, 2002). Byun and Lee (2004) have proposed a modified version of technique order preference by a similarity to ideal solution (TOPSIS), a multi attribute decision making (MADM) approach, for ranking the RP systems. The key factors used for the selection of RP processes are part accuracy, strength, surface roughness, build time, part cost of the build part. Lan et al. (2005) have proposed a method of integrating the expert system with the fuzzy synthetic evaluation (FSE) to select an appropriate RP process as required by the user. The selection process is divided into two stages. In the first stage, possible alternatives are developed while executed under the expert system environment. Subsequently, in the second stage FSE approach is made to produce a ranking order of the RP processes. Chowdary et al. (2007) have implemented a back propagation artificial neural network (ANN) for the selection of different types of machines. The major attributes that are considered during the selection process of SL machines are laser configuration types (wavelength and power), layer thickness, beam diameter, drawing speed, maximum part weight, capacity, maximum build size, part cost build time and operating system. Rao and Padmanabhan (2007) have proposed a methodology for selection of RP process using the graph theory and matrix approach. Subburaj and Ravi (2008) have proposed a computer aided rapid tooling (RT) process selection and manufacturability evaluation

methodology that not only help in RT process selection but also identifies the difficulties to manufacture a part.

2.4. RP material issue

The RP process has the ability to use base material in the form of solid, liquid and powder but choice of material is totally depends upon the selection of RP process by the user. The material used in the RP must satisfy some criteria such as proper range for melting and solidification temperature, minimum shrinkage value, low viscosity, low coefficient of thermal expansion and must be capable of rapid solidification relatively in short time in order to achieve good strength and part quality. Normally, the part building temperature range lies in between 70-100°C. The preferable solidification temperature is 5-10°C below the glass transient temperature of the build material. Thermoplastic material such as polycarbonate (PC), polyphenylsulfone (PPSF) and acrylonitrile butadiene styrene (ABS) satisfy above material properties and preferred as build material for RP processes (Noorani, 2005; Hopkinson, 2006). Based on the above characteristics, each RP process has its own limitations in the use of build material. Table 2. 1 shows some RP processes with their common build materials.

Table 2.1 Materials in rapid prototyping processes (Sood, 2011)

RP Technology	Working Principle	Build Materials
Stereolithography (SL)	Photo sensitive polymer is exposed to UV laser beam.	Liquid photopolymers.
Fused Deposition Modelling (FDM)	Plastic materials are extruded from the heated nozzle.	ABS, PC, Elastomers and wax
Three Dimensional Printing (3DP)	Printer nozzle deposits molten wax on the starch bed	Wax and starch, fragile and powdery
Laminated Object Manufacturing (LOM)	CO ₂ laser is used to cut cross section from layers of paper	Paper; similar to wood
Selective Laser Sintering (SLS)	Laser is used to sinter together the powder material	Polycarbonates, nylons, elastomers and ceramics

Advancement in material technology and RP process increases the number of materials types and metals as base material in RP processes. A high performance powder material namely ZP 140 having smooth and fast processing capability has been introduced by the Z Corporation for 3D printing process (Grimm T., 2008). Zhong et al. (2001) have

shown that the blending of ABS with composite fibres and small amount of plasticizer have improved the strength of the build parts (Zhong et al., 2001). Composite manufacturing using iron particles with nylon matrix have shown better mechanical strength as functional parts when manufactured by direct rapid tooling on FDM process (Masood and Song, 2004). Mostafa et al. (2009) have reported development of a new composite materials involving ABS plastic with iron. A high performance thermoplastic composite has been developed using thermotropic liquid crystalline polymer (TLCP) fibre that can be used as a build material for FDM process. The mechanical strength exhibited by the composite is approximately four times that of ABS (Robert et al., 1998). In medical application, medical grade polymethyl-methacrylate (PMMA) is used in FDM to manufacture porous customised freeform parts for applications in craniofacial reconstruction and orthopaedic spacers (Esplaine et al., 2010). Hinczewski et al. (1998) and Greco et al. (2001) have shown the capability of stereolithography (SL) process for processing of the ceramic slurry containing alumina powder. The study has focused on the necessity of minimising the organic concentration in the suspension and maintaining the viscosity of the suspension as low as possible to make a good coat of liquid monomer on the polymerised layer. Yen et al. (2009) have used ceramic slurry, a mixture of silica powder, clay, silica gel, water and inorganic binders to manufacture interconnected porous structure having high strength and better surface quality using the SLS process. Liu et al. (2011) have fabricated ceramic-metal composites by combining the SLS and gelation techniques. Apart from SLS process which sinter the powdered particles to form an object, they increase the concentration silica solution by evaporation using laser beam. In comparison to other manufacturing processes for making ceramic-metal composites, this approach requires less laser forming energy and the fabrication process is faster. Using the above manufacturing process, a composite prototype is manufactured having bending strength 45MPa, surface finish of 32 μm and dimensional variation of 10% under a laser energy density of 0.4 J/mm². Zhang et al. (2001) have used laminated object manufacturing (LOM) process for the fabrication of Al₂O₃ ceramic parts with complex geometry. Use of ceramic materials in the manufacturing of 3D parts using FDM principle gives rise to new type of process known as fused deposition of ceramics (FDC). In FDC process, the ceramic powder is compounded with binder and solvent and the extruded filaments are joined together by diffusion process. All the organic contents are removed by sintering at a high temperature to form a pure ceramic lattice (Hattiangadi et al., 2000; Grida et al., 2003; Bose et al., 1999).

With the recent advancements in the RP technology, some RP machines have increased their capability to produce metal parts directly. The most emerging technology in this field is selective laser sintering (SLS) which sinter the powder metal to form an object (Kumar, 2009). In order to develop metal parts from RP technology, other RP processes have been involved like direct metal laser sintering (DMLS), laser engineering net shaping (LENS), direct metal deposition (DMD), ultrasonic consolidation (UC), selective laser sintering (SLS) and direct light fabrication (DLF) processes. Now-a-days, a variety of materials is available to operate in DMLS process like bronze-based alloy, low carbon steel based alloy and tool steel based alloy (Luo et al., 2005). Direct metal deposition (DMD) is a laser based fabrication process that produces fully dense metal products using tool steel alloy, stainless steel, cobalt based alloy and copper based alloy (Lewis and Schlienger, 2000). Zaang et al. (2002) and Zhang et al. (2003) have developed a control technology which includes slicing, system implementation and post processing for RP process using gas metal arc welding as the deposition mechanism. The metal transfer control system controls the frequency and size of the droplets to improve the part accuracy. The deposition parameters includes travel speed of head, torch angle, welding current and arc voltage are controlled to get required 3D geometry. A novel method has been designed by researcher of Rutgers University to use metallic and ceramic based materials in the FDM process for rapid fabrication of functional parts having improved mechanical strength (Wu et al., 2002; Allahverdi et al., 2001).

2.5. Assessment of strength of RP build parts

Since RP process is a parametric dependant process, the mechanical properties of the RP parts can be increased by the proper selection of process parameters. Cheah et al., (1997) have studied the mechanical strength of a stereolithography (SL) processed parts fabricated using acrylic-based-polymer (De Solite SCR-300) and post cured using intense ultra violet (UV) light. It was observed that the post cured specimen exhibits high modulus of elasticity, ultimate tensile strength and elongation to fracture. The mechanical properties of the post cured prototype can be increased by decreasing the layer height and increasing the laser exposure density. The effect of part orientation on the tensile, compressive and flexural strength of the laser sintered parts has been investigated by Ajoku et al. (2006). The results indicate that the anisotropy is exhibited by the test specimen manufactured by laser sintering process. Specimens built in the direction parallel to the movement of laser head exhibit highest tensile and compressive strength whereas specimens exhibit highest

flexural strength when the parts are manufacture in the direction perpendicular to the movement of laser head. Chockalingam et al. (2005) have found that the layer thickness, part orientation and post curing time have significant effect on the strength of SL manufactured parts. Using finite element analysis approach, Nickel et al. (2001) have shown that the raster pattern used to build the interior of a layer has significant effect on the resulting residual stresses and deformation of the shape deposition manufacturing (SDM) build parts. Pandey et al. (2008) have improved the tensile strength of SLS build part by optimising the time difference for laser exposer between two points on successive line on a single layer. As the time difference totally depends on the part orientation of build part, an algorithm has been developed and implemented to find out the optimum part orientation for improvement of the tensile strength.

However, FDM is a widely used technology because of its low material cost, less manufacturing time, less material wastage and use of non-toxic materials. The major challenge in industrial applications of FDM build parts lies with production of quality parts for end use applications. This can be achieved if the relation between the performances of the FDM processed parts with the process parameters is clearly understood. Ahn et al. (2002) have studied the effect of raster orientation, air gap, raster width, model temperature and colour on tensile strength of specimen built through FDM route. The results indicate that raster orientation and air gap have strong influence on tensile strength whereas raster width, model temperature and colour have small or no effect. The tensile strength reaches maximum when the raster direction is parallel to the applied force and exhibits failure of individual rasters as load is taken by all rasters in a collective manner. Number of contours at the perimeter (offset contours) helps to reduce stress concentration at the edges and overcomes premature failure of the specimen. Es Said et al. (2000) have studied the effect of raster orientation on tensile strength, modulus of rupture and impact resistance of FDM built parts. It is concluded that the anisotropic property in FDM built parts is observed due to raster fill pattern. The strength is severely affected due to weak interlayer bonding between rasters and the presence of interlayer porosity. An analytical model validated by experimentation has been proposed by Croccolo et al. (2013) to predict the tensile strength and stiffness of FDM processed parts considering number of contours deposited around the edges of perimeter and other deposition parameters. Using design of experiment (DOE) approach, Onwubolu and Rayegani (2004) have experimentally investigated the effect of layer thickness, part orientation, raster angle and air gap on the tensile strength of the specimens. Gurralla et al. (2014) have investigated the effect of bond quality of interlayer and intra-layer rasters on the tensile strength of the specimen, both

experimentally and analytically considering build direction as a variable. A strong correlation between the tensile strength and the neck growth has been developed and the contribution of amalgamation of filaments to the strength of the specimen is studied. Lee et al. (2007) have observed anisotropic behaviour of FDM built parts caused mainly due to build direction when compressive test is carried out on standard specimen. Villalpando et al. (2014) have developed an optimisation model considering the material usages, part build time, surface roughness, strength features and other related FDM parameters. They have concluded that the internal matrix structure inside the part based on normal element deposition style balances the compressive strength, material usage and build time. Bellehumeur et al. (2008) have experimentally demonstrated that the interlayer bond quality and bond quality between adjacent filaments depends on temperature and convective heat transfer condition within the build chamber when FDM specimen is subjected to flexural strength test. The temperature profiles on built parts indicate that temperature at the bottom layers rises above the glass transition temperature and decreases in the direction of movement of extrusion head. It is concluded that strong interlayer bonding between rasters as well as layers can be achieved with less layer number and cooling and heating cycle. Simulation of finite element analysis reveals that part distortion occurs due to accumulation of thermo-residual stress at the bottom surface of the part during manufacturing (Chou and Zhang, 2008). Lee et al. (2005) have studied the effect of layer thickness, raster angle and air gap on elastic behaviour and surface quality of the FDM built parts using Taguchi method.

Sood et al. (2010) have studied the effect of layer thickness, part orientation, raster width, raster angle and air gap on the mechanical strength of the FDM processed parts conducting experiments based on central composite design and proposed functional relationship between process parameters and mechanical strength. It is suggested that deposition parameters largely influence meso-structural configuration of the built parts, distortion and bonding of rasters within the built part. Wang et al. (2007) have investigated the effect of material characteristics, setup of the fabrication parameters, geometrical structure of the CAD model and the deposition path planning on mechanical strength. It is observed that sudden cooling of extruded material from semi-molten temperature to chamber temperature develops thermal residual stresses that affects interlayer bonding strength resulting in layer deformation and cracking in parts. It has been observed that deformation and cracking is more pronounced in bottom layer than the upper layer due to involvement of rapid cooling and heating cycles. However, thermal residual stresses can be minimised by maintaining small difference between the glass transition temperature of

the material and chamber temperature of the FDM machine. Sood et al. (2009) have studied the effect of FDM process parameters on the part quality and dimensional accuracy of the parts manufactured through FDM route. It has been observed that the shrinkage is dominant along length and width direction of FDM built parts affecting dimensional accuracy of built parts. Anitha et al. (2001) have studied the effect of layer thickness, raster width and deposition speed on surface roughness and part quality of FDM built parts using a systematic design of experiments approach and concluded that layer thickness has significant influence. Peng et al. (2014) have studied the effect of raster width, extrusion velocity, filling velocity and layer thickness over dimensional error, warp deformation and build time.

Byun and Lee (2005) have used multi-attribute decision making (MADM) for selection of RP process considering part accuracy, roughness, strength, elongation, part cost and build time. Chang and Huang (2011) have studied the effect of contour width, contour depth, part raster width and raster angle on profile error of FDM built parts. Phatak and Pande (2012) have proposed a methodology to obtain optimum part orientation of the RP parts to minimise the build time and the material used in a hollowed model. Rezaie et al. (2013) have developed an approach for the production of topological optimised FDM built part.

2.6. Assessment of fatigue life of RP build parts

Normally, fatigue occurs due to repetitive cyclic loading of the specimen where the loading is just below the static strength of the material. The fatigue of the material is characterised by the rate of failure which is a function of amplitude and frequency of the stress intensity factor. Starr and Wegener (2013) have investigated the effect of surface finish on the fatigue life of SLM build parts under strain controlled mode. Polishing of the selective laser melting (SLM) build part improves the fatigue life at low stress amplitude fatigue test. Marissen et al. (2001) have shown that the fracture strain during cyclic loading decreases due to the presence of large number of micro-cracks in the build material. These micro cracks initiate the crack growth in the build parts and lead to failure. Riemer et al. (2014) have found that the presence of residual stress and micro-porous gaps inside the part lead to premature failure and lower the performance in many alloys fabricated through SLM process. Edwards et al. (2014) have experimentally found that residual stresses, surface roughness, microstructure and internal porosity are the key factors responsible for lowering fatigue performance of the SLM Ti-6AL-4V build parts. Presence of porous gaps inside the

parts has significant influence on the fatigue behaviour of SLM processed Ti-6-4 specimens. By adopting stress relieving post processing methods, the crack growth in SLM processed Ti-6-4 part is similar to the conventional processes part.

The estimation of fatigue life is not adequately addressed to assess the long term durability and sustainability of the FDM build parts. Therefore, the present research work intends to analyse the effect of process parameters on fatigue life on the FDM build part. Ziemian et al. (2015) have experimentally studied the effect of stress controlled fatigue on the FDM build parts. It is observed that FDM build parts exhibits anisotropic behaviour due to the influence of part orientation. Under stress controlled fatigue mode, the amount of strain energy absorbed by two different types of FDM build materials are examined by Lee and Huang (2013) considering the part orientation as the process parameter. Since the life cycle of acrylonitrile butadiene styrene (ABS) plastic, one of the work materials of FDM process, is less than 10^5 cycles, low cycle fatigue (LCF) test is recommended under strain controlled mode for better characterisation of fatigue life of FDM build parts (ASTM E606). Kallrath et al. (1999) and Tao and Xia (2007) have studied the fatigue crack growth in polymers and their composites under strain controlled low cycle fatigue test.

2.7. Wear characteristics of RP build parts

One of the important characteristics to assess the functionality is the wear resistance of end use parts built through FDM route. To this end, Sood et al. (2012) have experimentally studied the effect of five process parameters such as layer thickness, part orientation, raster angle, raster width and air gap on the sliding wear of the FDM build parts using design of experiment (DOE) approach. It is observed that wear occurs due to rupture of interfacial adhesive bonds and formation of cracks in the surface region. Among all process parameters, layer thickness, part orientation and air gap have significant effect on the sliding wear of the FDM build part. Singh and Singh (2015) have studied the effect of input process parameters on the wear of Al-Al₂O₃ functionally graded material prepared by FDM assisted by investment casting. The wear characteristics of alumide material fabricated through selective laser sintering (SLS) process have been investigated by Minetola and Iuliano (2014). Ramesh and Shrinivas (2009) have observed that the iron silicon carbide metal matrix composites manufactured by direct metal laser sintering (DMLS) process exhibits better micro-hardness and co-efficient of friction. It is concluded that density, micro-hardness and wear resistance of the DMLS manufactured parts can be improved by lowering the laser speed. Kumar and Kurth (2008) have shown that parts

manufactured through selective laser melting (SLM), a variant of selective laser sintering (SLS), exhibit superior fretting wear performance to selective laser sintering.

2.8. Discussion on RP issues

RP processes have increased the capability of manufacturing industries by increasing the ability to develop 3D complex geometry directly from CAD data with reduced time and material waste. Present application of RP is not limited to form, fit and functional testing but it is widely used as an end use product where durable precision components are needed. Moreover, integrating RP technology with other post processes, not only increases the strength but also reduces the cost and product development cycle. The RP parts are mostly used in orthodontic application, aerospace and automobile industries (Wiedemann et al., 1999; Berry et al., 1997; Giannatsis and Dedoussis, 2009). Growing demands and popularity of RP technologies in the industries and research works get rise to development of new integrated RP technologies in the market every year (Onuh and Yusif, 1999; Hopkinson, 2006). The selection of RP process totally depends upon some key factors such as time, cost, surface roughness, temperature of build envelop, material type and part accuracy. Although extensive research work has been reported on RP, very less work has been performed to explore the improvement of fused deposition modelling (FDM) process. Among all RP technologies, fused deposition modelling (FDM) technology is widely appreciated due to ability to manufacture accurate and durable product with less time and material waste. Literature suggests that the FDM process is parametric dependant and the selection of suitable process parameter can increase the strength and durability of the FDM build parts. Therefore, a systematic approach is needed to understand the influence of process parameters on the part quality and part strength. Empirical models should be developed relating the process parameters and the performance characteristics so that the user can easily predict the measures and control the process parameters.

2.9. Conclusion

This chapter provides the various past research and development work in the area of RP technology. For the sake of easy understanding the chapter is divided into six main sections. In the section 2. 2, the application of RP in various fields has been discussed. The material limitation of RP processes is the key factor that decreases the growth rate of

industrial application of RP processes. Many research works have been performed in the past to overcome this limitation by integrating RP process with other post processing technology. In section 2. 3, the proper selection of RP process for appropriate manufacturing task has been explored. The literatures are discussed on the selection of RP process suiting a particular task taking account the quantitative and qualitative data. Each RP process has its own advantage and limitations in terms of strength, accuracy and part quality of the build part, few approaches have been highlighted in this section to enable the user for finding out practical solution to the problem. Section 2. 4, reviews the issue of limitation and advantage of the RP processed materials. The material limitation is the key factor which drag the popularity of RP process for the industrial applications. In section 2. 5, the improvement of mechanical strength has been addressed for the RP processed parts. Since RP processes are parametric dependant, the effect of process parameters on the mechanical strength of RP processed parts have been discussed. Chapter 2 .6 reveals the parametric effect of process parameters on the fatigue life of the RP processed parts. It has been observed that few studies have been devoted to determine the fatigue life of the FDM parts under strain controlled mode. The effect of sliding wear on the RP process parts have been addressed in chapter 2. 7. Major steps taken by the researcher to minimise the sliding wear of the RP processes parts are noted down.

In this direction, present research work attempts to explain the effect of process parameters and their possible interactions with performance characteristics. It is found that proper tuning of process parameter of RP process can enhance the part strength, part life and durability of the build part.

Chapter 3

Parametric assessment of static strength of FDM build parts

3.1. Introduction

To sustain in the competitive market, it is necessary to minimise the product development time. Therefore, manufacturing firms attempt to change to rapid prototyping (RP) technology. The major advantage of RP lies in manufacturing end use assembly parts proficiently directly from computer aided design (CAD) file saved in .stl format (Gibson et al., 2010; Keause et al., 1997; Bernard et al., 2002; Kruth et al., 1998). Although RP is a well-developed manufacturing technology, limitation in availability of compatible material types restrict its wide spread application (Zhang et al., 2001; Hattiangadi et al., 2000; Grida et al., 2003; Bose et al., 1999). In order to overcome material issue, modification has been made to improve the material performance (Zhong et al., 2001; Masood et al., 2004; Mostafa et al., 2004; Greco et al., 2001; Yen et al., 2009). Even with the existing materials, controlling of process parameter may influence the properties of the parts build through RP route due to its inherent building mechanism (Ahn et al., 2009; Galantucci et al., 2009; Cheah et al., 1997; Es-Said et al., 2000; Ahn et al., 2002; Crocclolo et al., 2013). It is noted that RP build part exhibits anisotropic effect under tensile compressive and flexural test (Ajoku et al., 2006; Ahn et al., 2002; Lee et al., 2007). Literature suggests that adjustment of process parameters has significant influence over properties of RP parts (Sood et al., 2010; Chou et al., 2008; Onwubolu and Rayegani, 2004). The influence of process parameters on the mechanical strengths needs a distinct study to select a suitable parameter setting for the improvement of strength. The present chapter is devoted to study the effect of process parameters on the mechanical strength such as tensile, compressive, flexural and impact strength of fused deposition modelling (FDM) build parts.

Exhaustive analysis of literature reveals that relatively less research works address the issue of influence of contour number on the mechanical property of FDM built parts. Similarly, the influence of delta angle, which is capable of reducing the anisotropic behaviour of the built parts and improving the mechanical strength in different directions is not adequately considered in the literature. Therefore, in this research work, contour

number along with five FDM process parameters such as layer thickness, raster width, raster orientation, part orientation and air gap have been considered for analysing their effect on mechanical strength of FDM build parts. A face centred central composite design (FCCCD) of response surface methodology (RSM) approach has been adopted to conduct the experiments in a systematic manner and to obtain maximum information from less number of experimental runs. Empirical relationship between mechanical strength and process variables have been developed and statistical validity ensured. The effect of raster fill pattern (delta angle) is investigated and compared with the default delta angle. The analysis based on fuzzy logic finds applications in vague and uncertain environment. In the recent years, fuzzy logic based multi-criteria decision making approaches have become very popular in optimization of manufacturing processes. Utility of fuzzy logic based optimization technique can be further improved when it is integrated with other optimization methodologies. Therefore, fuzzy inference system (FIS) has been adopted for the sake of converting multiple performance measures into single equivalent performance measure. Finally, the nature inspired meta-heuristic known as firefly algorithm is applied to obtain a best parametric combination for the improvement of all the performance measures simultaneously. To predict the mechanical strength, two latest artificial intelligence techniques known as genetic programming (GP) and least square support vector machine (LS-SVM) have been adopted. The prediction model enables to predict the performance measures with reasonable accuracy so that costly experimental time can be minimized.

3.2. Fuzzy Inference Systems

Fuzzy logic (FL) is a technique that allows evaluation and simplification of complexities with regard to the relationship in a process by presenting the relation between input parameters and responses in a linguistic manner. Fuzzy rules may be formulated based on expert knowledge in the field. Out of two most popular fuzzy inference systems (Mamdani and Sugeno fuzzy model), Mamdani fuzzy model is widely used for solving many real world problems because of its easiness. The Mamdani fuzzy model based on the collection of IF-THEN rules with fuzzy antecedents and consequent can predict the output in an efficient manner. A linguistic variable is a variable whose values are defined in words or in sentences by man-made language. A fuzzy set is commonly defined by its membership function. Normally, triangular or trapezoidal membership functions are used to the crisp inputs because of computational efficiency (Chang et al., 2005; Gungor et al.,

2007; Sapkota et al., 2009; Wang et al., 2010; Li et al., 2010). Various steps involved in fuzzy rule based system consist of four parts as explained below. The pictorial representation of FIS is shown in Figure 3.1.

3.2.1. Fuzzifier

The crisp value is fuzzified using the fuzzification operator inside the fuzzifier. The precise crisp value (input) is converted into imprecise value by using the linguistic terms such as low, medium and high.

3.2.2. Knowledge base

The knowledge base is the main part of the fuzzy system in which both database and rule base are jointly referred. In knowledge base part, the membership function and rules (IF-THEN) are defined

3.2.3. Inference engine

The inference operation on the rules is performed by the inference system. It decides the way in which the rules are combined. It applies reasoning to compute the fuzzy outputs.

3.2.4. Defuzzifier

The output of the inference block is in the form fuzzy value. To translate this fuzzy value to the crisp value or to the real world output value, defuzzifier is used.

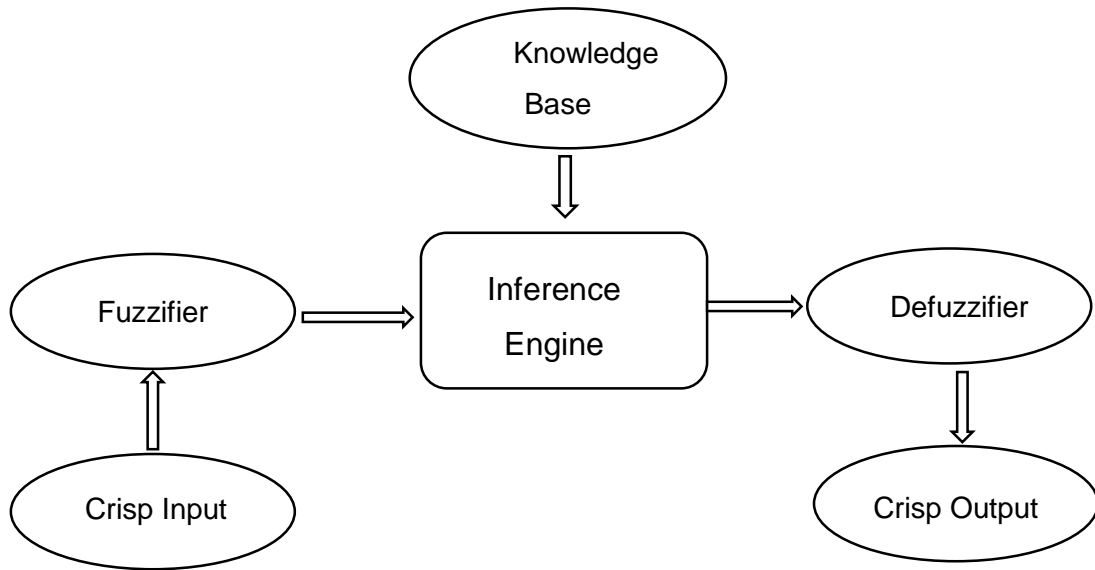


Figure 3.1. Structure of fuzzy inference system

3.3. Firefly Algorithm

The nature inspired meta-heuristic firefly algorithm, suggested by Xin-She Yang (2010) is based on the behaviour of fireflies. The working of firefly algorithm completely depends upon the light intensities of the fireflies. The variation of light intensity between fireflies insist fireflies to move towards the brighter one to get a best optimal solution. In the firefly algorithm, all fireflies are categorised by their light intensity associated with the objective function. Each firefly regularly changes its position to move towards the brighter one. Three basic rules followed by firefly algorithm are listed below:

- All fire flies are unisex so that one firefly will be attracted to other fireflies irrespective of their sex.
- The attractiveness between two fireflies is directly proportional to their brightness and the attractiveness decreases with increase in distance between them. The firefly moves randomly if there is no brighter firefly.
- The brightness of a firefly are influences or controlled by the landscape of the objective function.

The light intensity (I) varies with the distance r between fireflies and is denoted by the following equations 3. 1 and 3. 2.

$$I(r) = I_0 e^{-\gamma r^2} \quad (3.1)$$

where I_0 denotes the light intensity at the source and γ is the light absorption coefficient. The attractiveness (β) is described by monotonically decreasing function of the distance r between any two fireflies.

$$\beta(r) = \beta_0 e^{-\gamma r^2} \quad (3.2)$$

The term β_0 denotes the maximum attractiveness at ($r = 0$) and γ is the light absorption coefficient which controls the decrease of the light intensity. The distance between two fireflies i and j at position x_i and x_j is defined as:

$$r_{ij} = \|x_i - x_j\| = \sqrt{\sum_{k=1}^d (x_{i,k} - x_{j,k})^2} \quad (3.3)$$

Here $x_{i,k}$ is the k -th component of the spatial coordinate, x_i of i -th firefly and d denotes the number of dimensions. The movement of firefly i which is attracted towards the brighter one can be determined by the following equation:

$$x_i = x_i + \beta_0 e^{-\gamma r^2} (x_j - x_i) + \alpha \left(\text{rand} - \frac{1}{2} \right) \quad (3.4)$$

The first term shows the current position of the firefly i , the second term signifies a firefly's attractiveness and the last term shows the random movement of firefly when there is no brighter firefly. For most cases the term of randomisation α is considered between zero to one. The term rand generates random number and distributed uniformly between one and unity. In general practice, the light absorption coefficient γ varies from 0.1 to 10. The firefly algorithm can be presented in the following pseudo code given by Xin-She Yang (2010):

Pseudo code of the firefly algorithm

Objective function $f(x)$, $x = (x_1, \dots, x_d)T$

Generate initial population of fireflies x_i ($i=1, 2, \dots, n$)

Light intensity l_i at x_i is determined by $f(x_i)$

Define light absorption co-efficient γ

While ($t < \text{Max generation}$)

for $i=1:n$ all n fireflies

for $j=1:n$ all n fireflies (inner loop)

if ($l_i < l_j$), Move firefly i towards j ; **end if**

Vary attractiveness with distance r via $\exp[-\gamma r]$

Evaluate new solution and update light intensity

end for j

end for i

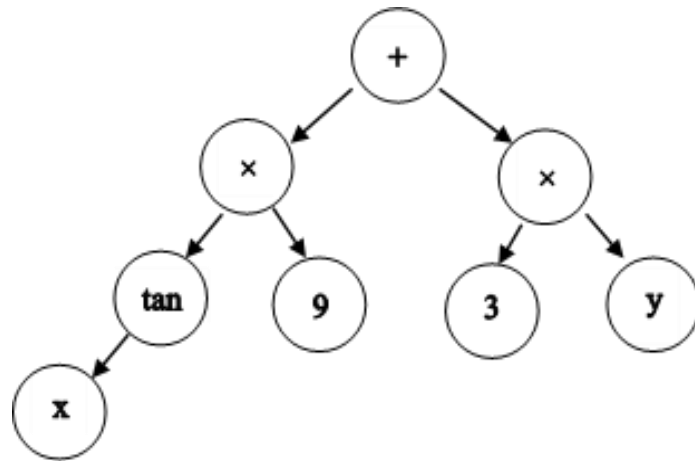
*Rank the fireflies and find the current global best g^**

End while

Post process results and visualisation

3.4. Genetic programming

The genetic programming (GP) is the most powerful tool used to predict the behaviour of various processes and for formation empirical modelling. Normally, GP follows the process of evolution in nature Darwin's theory of 'survival of the fittest' to find out best solution to assigned problem. The GP is known as the generalised form of genetic algorithm (GA) and was extensively studied by Koza (1992). In GP, the model is represented as a hierarchical tree structures of terminals and functions. A well-known implementation of GP is in symbolic regression and is used to determine the mathematical expression for a given set of variable and functions. The function are generated using Boolean operator (AND, OR), nonlinear operators (sin, cos, tan, exp, tanh, log) and from basic mathematical operators (+, -, / and \times). The fitness function is calculated as the error between the actual value and the predicted value of the symbolic expressions. In GP individual terms are randomly initialised and the population is progressed to find out the optimal solutions through various operations such as reproduction, crossover and mutation. The reproduction process produces children as an input to the next generation by replicating a fraction of the parent selected by the current generation. Individuals having highest fitness values in the population are selected as the parent and used for reproduction. Normally, the crossover operation produces children by exchanging some parts of their selected parents. The crossover operation is divided in to two types i.e. sub-tree crossover and node crossover. However the sub-tree crossover has shown more significant effect than the node crossover. Figure 3.2 shows the tree representation of a symbolic expression.

Figure 3.2. GP tree representation of a symbolic expression: $9\tan(x) + 5y$

For better understanding of subtree crossover, an example is considered and is presented in tree manner.

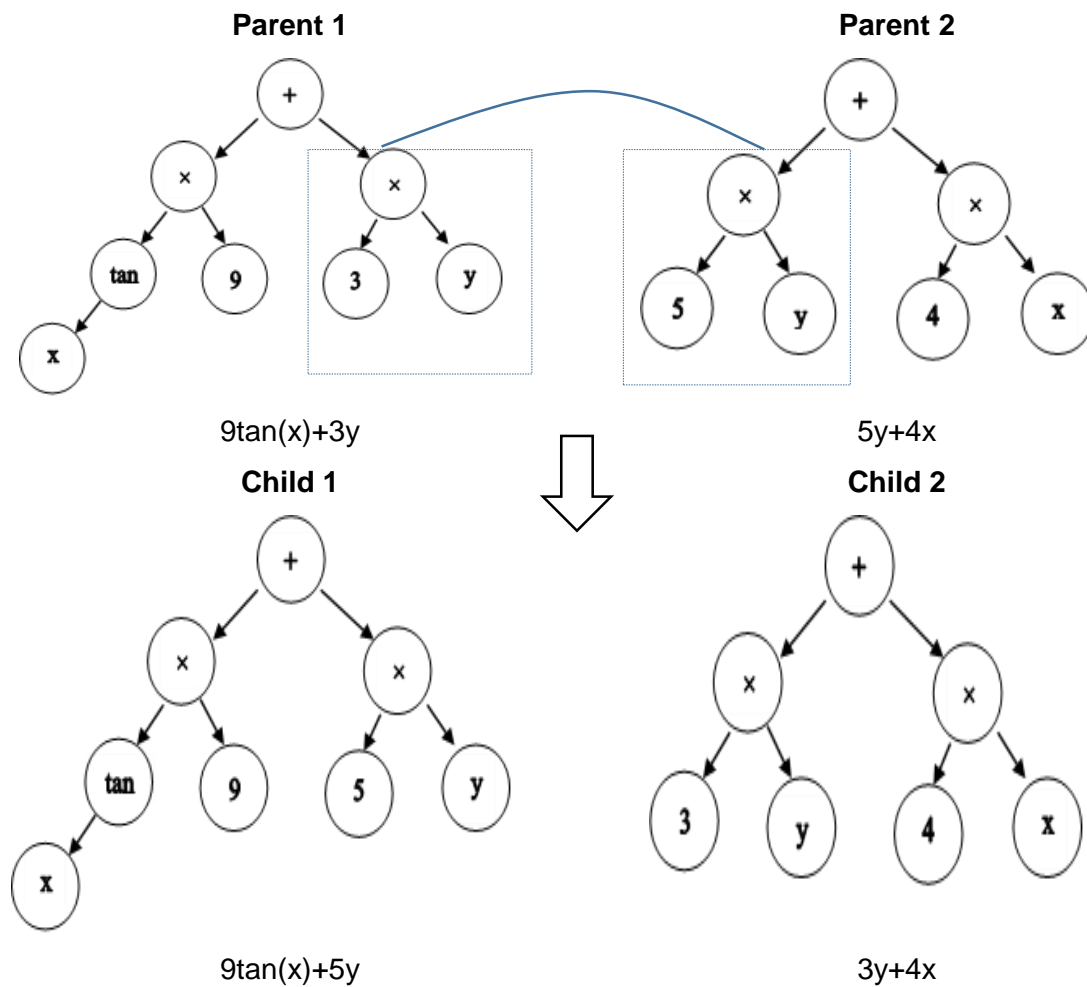


Figure 3.3. Sub-tree crossover between parents

In the present work GPTIPS was applied to perform a genetic programming for prediction of fatigue life of the FDM build parts (Searson, 2009). Some application of GPTIPS have been already successfully reported (Garg et al., 2014a; Garg et al., 2013; Garg et al., 2014b; Baziar et al., 2011). The GPTIPS is an add-on code written based on the multigene GP to compile with MATLAB 14. The mean absolute percentage error (MAPE) between actual value and the GP value is used as a fitness function to evaluate each individual of the population.

3.5. Least Square Support Vector Machine

The most widespread and advanced technique in the field of machine learning is support vector machine (SVM). The SVM technique has been applied to regression problem known as support vector regression (SVR). The SVR is an artificial intelligent tool based on statistical learning process and have the ability to develop appropriately predictive models from given set of data. In a given problem, the training data set is represented in the form x_i and y_i where x_i represents the input data, y_i represents the output data and $i=1, 2, 3 \dots N$. The regression model can be generated using a nonlinear mapping function $\phi(x)$ and the predictive model is given in equation 3.5.

$$y = w^T \phi(x) + b \quad (3.5)$$

where w represents the weight vector and b is the bias term.

The least square vector machine (LS-SVM) is the advance version of the SVR because the error is minimised through least square method. The LS-SVM technique uses quadratic loss function for optimisation purpose whereas SVR uses the inequality constraint which is facing difficulty for solving optimisation problems. Using the cost function (equation 3.6) and constrained function (equation 3.7) the optimisation problems can be handled smoothly (Tripathy et al., 2012).

$$\min C(w, e) = \frac{1}{2} w^T w + \frac{1}{2} \gamma \sum_{i=1}^N e_i^2 \quad (3.6)$$

$$y = w^T \phi(x_i) + b + e_i \quad (i= 1, 2, 3 \dots N.) \quad (3.7)$$

where γ is the penalty factor and e_i is the loss function also known as regression error.

The LS-SVM technique minimises the penalty regression error which is associated with cost function and equality constraint function. The first part of the cost function known as weight degeneration process mainly used to regularise the weight size and convert the large weight in to fixed value. The second part known as the regression error for the

training data and regularisation parameter (γ). For solving the optimisation problem, equation is converted into Lagrange function as given below (equation 3.8).

$$L(w, b, e, \alpha) = \frac{1}{2} \|w\|^2 + \gamma \sum_{i=1}^N e_i^2 - \sum_{i=1}^N \alpha_i \{W^T \phi(X_i) + b + e_i - y_i\} \quad (3.8)$$

where the term α represents the Lagrange multipliers. The term γ must be greater than zero. The term α_i and b can be calculated using Karush-Kuhn-Tucker (KKT) conditions. For the nonlinear system, the LS-SVM model is converted to:

$$y_i = w \cdot \phi(x) + b = \sum_{i=1}^k \alpha_i k(x_i, x) + b \quad (3.9)$$

where $k(x_i, x) = \phi(x_i)^T \phi(x)$ represents the kernel function.

The kernel function plays a vital role in understanding of hyperspace from the training data set. Among all kernel functions, radial basis function (RBF) is chosen for its advantage of shorter training mechanism and high generalisation ability to the model. The mathematical model of the RBF kernel function is represented in equation 3.10.

$$K(x_i, x_j) = \exp\left(-\frac{\|x_i - x_j\|}{\sigma_{sv}^2}\right) \quad (3.10)$$

where σ_{sv}^2 represents the square variation of the Gaussian function. This function should be optimised by the user to get a support vector. For better generalisation of the model, the tuning parameters such as α and γ should be selected very carefully. Using the combination of coupled simulated annealing (CSA) and the grid search method (GSM), the RBF parameters (α , γ) are estimated. All the codes are generated and run through MATLAB 2014 software.

3.6. Experimental Details

The FDM modelling process is one of the wide appreciated technology that produces prototypes from acrylonitrile butadiene styrene (ABS) plastic materials by putting semi molten filaments one over another. The heated filaments are extruded from the extrusion nozzle as defined by the machine software (Insight 10. 2) in a layer wise manner. The semi melted plastic material rapidly solidify to chamber temperature, which develops thermo residual stress inside the build part. This thermo residual stress adversely affects the mechanical strength of the build parts. The mechanical strength of the FDM parts is significantly influenced by some process parameters, among them contour number along with raster orientation, part orientation, layer thickness, air gap and raster width are

considered from experimental work. Some process parameters are kept constant such as delta angle, part fill style, contour width, part interior style, shrinkage factor and perimeter to raster air gap are kept constant. All the process parameters are defined as:

1. Contour Number: Number of offset contour or perimeter added during part building.
2. Raster Orientation: It is the angle between raster and x- axis of the build platform.
3. Part Orientation: Part building orientation refers to placing of the build part with respect to the x, y, z axis of the building platform of the machine.
4. Layer Thickness: it is the thickness of the raster deposited from the extrusion nozzle.
5. Air Gap: This is the distance between two adjacent rasters in a layer.
6. Raster Width: The width of the raster deposited by the extrusion nozzle in a particular layer.
7. Delta Angle: Delta angle refers to the angle of rotation of the raster fill pattern from the previous raster fill pattern. By default, the raster angle alternates every layer based on the delta angle.
8. Part Fill Style: it refers to the filling style of a model. It is of two type i.e. single contour/ rasters and multiple contours. In case of single contour / raster type, single perimeter is present followed by filled rasters at the inner part. Multiple contours include part building with the use of several perimeters.
 - Part Interior style: It defines the interior part filling pattern of the build part using rasters.
 - Solid normal: The part is fully filled with rasters.
 - Sparse: Internal section of the part is filled with unidirectional rasters.
 - Sparse double dense: crisscross sparse structure are used to fill the internal structure of the part. Utilises minimum material than the sparse filling style.
9. Sparse fill pattern: it defines the filling pattern of the build parts. Three types of fill pattern are available i.e. hexagonal, porous hexagonal and saw tooth types.
10. Shrinkage factor: This is the shrinkage allowance applied in all direction such as x, y and z axis during part building.
11. Perimeter to raster air gap: Air gap between inner perimeters to the primary raster inside that perimeter is termed as perimeter to raster air gap.

The variation of delta angle with respect to its adjacent layer has a strong influence over the anisotropic effect and bond strength between the rasters. The raster fill pattern changes at an incremental angle of 30° to its previous raster fill angle as shown in Figure 3. 4. The delta angle is fixed at 30° throughout the study.

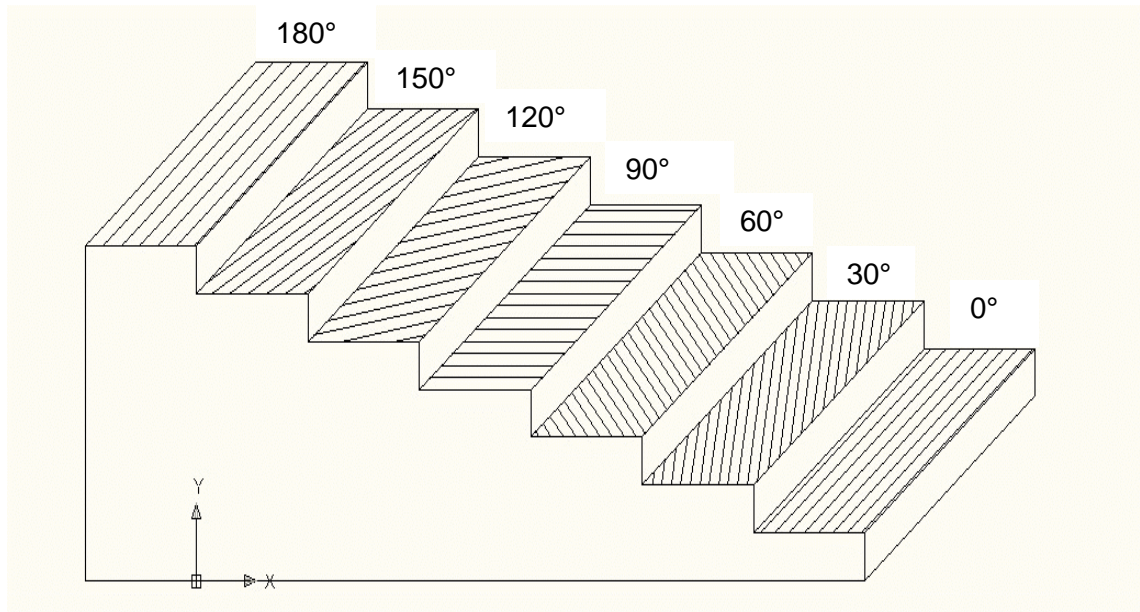


Figure 3.4. Overlaying raster orientation style

In order to develop an empirical model for the mechanical strength of the FDM build parts, experiments have been conducted based on face centred central composite design (FCCCD). The FCCCD is capable of fitting second order polynomial and preferable if curvature is as summed to be present in the system. In order to reduce the experimental runs, half factorial (2^{k-1}) design (k factors, each having three level) having single block is considered using response surface methodology (RSM) technique. Two levels have been considered for each factors and factors are coded as low level (-1) and high level (+1).

$$\xi_{ij} = \left(\frac{x_{ij} - \bar{x}_i}{\Delta x_i} \right) \times 2 \quad (3.11)$$

$$\bar{x}_i = \frac{\sum_{j=1}^2 x_{ij}}{2} \text{ and } \Delta x_i = x_{i1} - x_{i2} \quad (3.12)$$

$$1 \leq i \leq k; 1 \leq j \leq 2,$$

where ξ_{ij} and x_{ij} are the coded and actual value of jth level of ith factor respectively.

Using equation 3.11, all input factors are represented in coded form or in the same range. Zero level (centre point) is created in between high level and low level and $\pm \alpha$ level of each factor is also included. To reduce the number of levels due to machine constraints, face centred central composite design (FCCCD) in which $\alpha = 1$ is considered. This design locates the axial points on the centres of the faces of the cube and requires only three levels for each factor (Montgomery, 2003) In general practice two or three centre points

are sufficient but in order to get a reasonable estimate of experimental error eight centre points are considered. Half factorial (2^{6-1}) unblocked designs having 32 experimental runs, 12 (2^k where $K=6$) axial runs and eight centre runs is considered for experimental work. Table 3. 1 shows the factors along with their levels in terms of uncoded form as per FCCCD.

Table 3.1.Factors and their levels

Symbol	Factor	Unit	Low Level (-1)	Centre Point (0)	High Level (1)
A.	Contour number	magnitude	1	3	5
B.	Layer thickness	mm	0.178	0.254	0.330
C.	Raster width	mm	0.4064	0.4814	0.5564
D.	Part orientation	degree	0	15	30
E.	Raster angle	degree	0	30	60
F.	Air gap	mm	0.0000	0.0254	0.0508

For determining the mechanical strength of ABS built parts, tensile, compressive, flexural and impact tests are conducted according to ASTM standards. The tensile strength is determined according to ASTM D638 (standard test method for tensile properties of plastics) and the standard specimen is shown in Figure 3. 5. The compressive strength of the specimen is determined according to ASTM D695 (standard test method for compressive of rigid plastic) as shown in Figure 3. 6. The flexural strength at yield is determined according to ASTM D790 (standard test method for flexural properties of plastics) as shown in Figure 3. 7. The impact strength of the FDM build parts are found out by performing the Izod impact test according to ASTM D256 (Standard test method for determining the Izod pendulum impact resistance of plastics) as shown in Figure 3. 8. The tensile, compression and flexural tests are conducted using Instron 1195 series IX automated material testing system with crosshead speed 1 mm/s as shown in Figure 3.9. The Izod impact test is performed on VEEKAY TLVS4 impact testing machine. The standard specimens are fabricated using FDM FORTUS 400mc (manufactured by Stratasys, USA) for the measurement of mechanical strength as shown in Figure 3.10. The standard specimens are designed using CATIA V5 R21 software and saved in STL format for importing to the machine. The STL file is then imported to FDM machine software i.e. Insight 10. 2 for product development purpose. All tests are carried out at normal ambient temperature 23 ± 2 °C and relative humidity $50 \pm 10\%$ as per ASTM D618 standard. The material used for fabrication of test specimen is acrylonitrile butadiene styrene (ABS M30). The chemical composition of ABS is $(C_8H_8 \cdot C_4H_6 \cdot C_3H_3N)_n$ and symbolic representation of ABS is given in Figure 3.11. ABS is a combination of monomeric chemical acrylonitrile

butadiene and the styrene in presence of carbon hydrogen and nitrogen. ABS is a carbon chain copolymer and belongs to styrene ter-polymer chemical family. It is made by dissolving butadiene-styrene copolymer in a mixture of acrylonitrile and styrene monomers and then polymerizing the monomers with free-radical initiators. It contains 90-100% acrylonitrile/butadiene/ styrene resin and may also contain mineral oil (0-2%), tallow (0-2%) and wax (0-2%). Its three structural units provide a balance of properties with the acrylonitrile providing heat resistance, butadiene imparting good impact strength and the styrene gives the copolymer its rigidity.

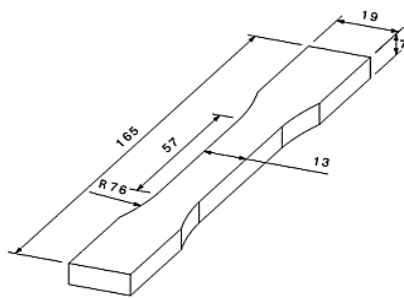


Figure 3.5. ASTM D638 standard test specimen for tensile test

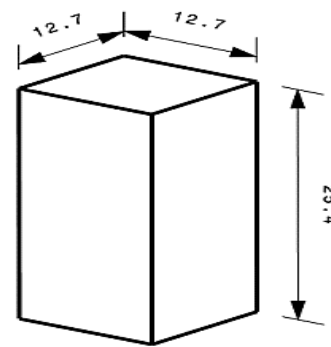


Figure 3.6. ASTM D695 standard specimen for compressive test

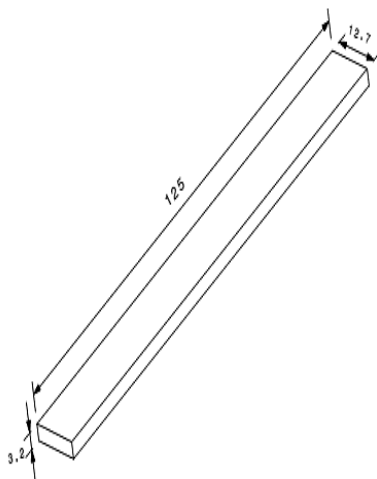


Figure 3.7. standard test method for flexural properties of plastics

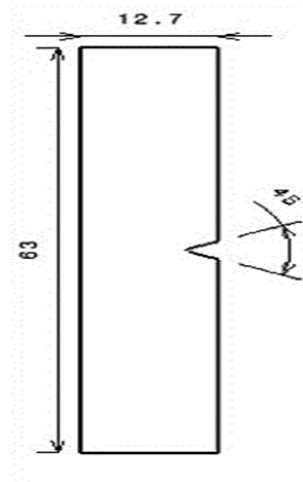


Figure 3.8. ASTM D256 standard specimen for izod test



Figure 3.9. Instron 1195 series IX automated material testing machine



Figure 3.10 FDM Fortus 400mc series

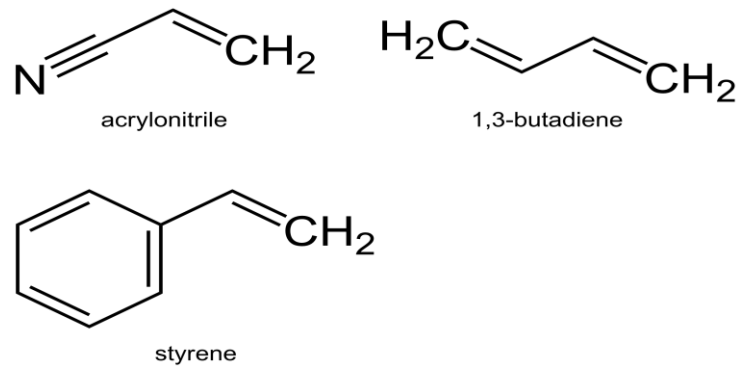


Figure 3.11. Monomers in acrylonitrile butadiene styrene (ABS) plastic

3.7. Results and Discussion

For each experimental run, build parameters are set as per FCCCD design matrix and three specimens are prepared. Tests have been conducted on the specimens and the average value for each run is listed in Table 3.2.

Table 3.2. Experimental results

Run Order	Factors in coded form						Average Strengths			
	A	B	C	D	E	F	Tensile Strength (MPa)	Compressive Strength (MPa)	Flexural Strength (MPa)	Impact Strength (J/m)
1	-1.00	-1.00	-1.00	-1.00	-1.00	-1.00	25.90	98.41	56.634	243.438
2	+1.00	-1.00	-1.00	-1.00	-1.00	+1.00	23.70	21.57	50.728	350.000
3	-1.00	+1.00	-1.00	-1.00	-1.00	+1.00	20.41	95.34	52.618	301.250
4	+1.00	+1.00	-1.00	-1.00	-1.00	-1.00	31.30	93.75	65.933	321.250
5	-1.00	-1.00	+1.00	-1.00	-1.00	+1.00	20.63	89.12	35.492	031.563
6	1.00	-1.00	+1.00	-1.00	-1.00	-1.00	27.87	102.4	44.764	266.563
7	-1.00	1.00	+1.00	-1.00	-1.00	-1.00	26.58	91.14	52.024	169.063
8	+1.00	+1.00	+1.00	-1.00	-1.00	+1.00	25.12	67.47	46.949	402.188
9	-1.00	-1.00	-1.00	+1.00	-1.00	+1.00	14.43	66.73	23.681	176.250
10	1.00	-1.00	-1.00	+1.00	-1.00	-1.00	19.97	79.91	11.811	133.438
11	-1.00	+1.00	-1.00	+1.00	-1.00	-1.00	24.85	51.30	25.866	184.063
12	+1.00	+1.00	-1.00	+1.00	-1.00	+1.00	20.16	45.55	11.102	301.563
13	-1.00	-1.00	+1.00	+1.00	-1.00	-1.00	19.42	105.5	21.791	133.438
14	+1.00	-1.00	+1.00	+1.00	-1.00	+1.00	19.42	64.21	08.858	243.438
15	-1.00	+1.00	+1.00	+1.00	-1.00	+1.00	15.35	40.89	06.614	243.438
16	+1.00	+1.00	+1.00	+1.00	-1.00	-1.00	22.49	69.52	04.823	169.063
17	-1.00	-1.00	-1.00	-1.00	+1.00	+1.00	18.57	82.89	28.791	205.938
18	+1.00	-1.00	-1.00	-1.00	+1.00	-1.00	27.05	50.37	40.445	281.875
19	-1.00	+1.00	-1.00	-1.00	+1.00	-1.00	29.18	73.85	63.248	243.438
20	+1.00	+1.00	-1.00	-1.00	+1.00	+1.00	22.50	64.48	55.866	273.750
21	-1.00	-1.00	+1.00	-1.00	+1.00	-1.00	26.00	106.8	53.268	278.750

22	+1.00	-1.00	+1.00	-1.00	+1.00	+1.00	25.23	44.50	50.315	318.750
23	-1.00	+1.00	+1.00	-1.00	+1.00	+1.00	19.75	81.62	45.472	243.438
24	+1.00	+1.00	+1.00	-1.00	+1.00	-1.00	29.18	78.20	66.555	274.688
25	-1.00	-1.00	-1.00	+1.00	+1.00	-1.00	22.05	54.88	40.335	311.250
26	+1.00	-1.00	-1.00	+1.00	+1.00	+1.00	17.23	46.80	28.185	243.438
27	-1.00	+1.00	-1.00	+1.00	+1.00	+1.00	17.69	35.95	29.232	276.875
28	+1.00	+1.00	-1.00	+1.00	+1.00	-1.00	25.26	52.08	33.661	065.000
29	-1.00	-1.00	+1.00	+1.00	+1.00	+1.00	17.66	74.00	30.709	361.250
30	+1.00	-1.00	+1.00	+1.00	+1.00	-1.00	21.50	91.10	32.185	361.250
31	-1.00	+1.00	+1.00	+1.00	+1.00	-1.00	23.92	32.19	45.472	343.750
32	+1.00	+1.00	+1.00	+1.00	+1.00	+1.00	21.47	47.15	33.661	361.250
33	-1.00	0.00	0.00	0.00	0.00	0.00	22.93	72.91	42.520	236.875
34	+1.00	0.00	0.00	0.00	0.00	0.00	26.44	59.70	36.969	266.563
35	0.00	-1.00	0.00	0.00	0.00	0.00	23.26	71.05	34.614	217.188
36	0.00	+1.00	0.00	0.00	0.00	0.00	23.92	51.46	34.016	245.625
37	0.00	0.00	-1.00	0.00	0.00	0.00	23.70	61.36	36.614	215.313
38	0.00	0.00	+1.00	0.00	0.00	0.00	24.36	71.82	34.783	232.188
39	0.00	0.00	0.00	-1.00	0.00	0.00	25.91	81.11	55.866	276.875
40	0.00	0.00	0.00	+1.00	0.00	0.00	22.38	61.91	29.232	276.250
41	0.00	0.00	0.00	0.00	-1.00	0.00	23.45	62.92	30.784	169.063
42	0.00	0.00	0.00	0.00	+1.00	0.00	23.59	62.22	35.661	237.188
43	0.00	0.00	0.00	0.00	0.00	-1.00	27.02	66.72	39.567	266.250
44	0.00	0.00	0.00	0.00	0.00	+1.00	21.61	59.89	30.709	281.875
45	0.00	0.00	0.00	0.00	0.00	0.00	24.91	62.84	34.783	218.125
46	0.00	0.00	0.00	0.00	0.00	0.00	25.11	67.87	36.562	211.875
47	0.00	0.00	0.00	0.00	0.00	0.00	23.76	64.73	33.040	221.875
48	0.00	0.00	0.00	0.00	0.00	0.00	23.58	60.33	35.170	218.125
49	0.00	0.00	0.00	0.00	0.00	0.00	25.11	66.61	34.780	208.125
50	0.00	0.00	0.00	0.00	0.00	0.00	23.68	64.41	33.390	213.125
51	0.00	0.00	0.00	0.00	0.00	0.00	24.90	62.03	32.100	214.063
52	0.00	0.00	0.00	0.00	0.00	0.00	23.68	57.81	35.519	213.125

Due to the complexity of the problem, a full quadratic model is attempted for suitably explaining the performance measures like tensile, compressive, flexural and impact strength. In this present context, experimental data obtained using FCCCD design runs are fitted with following empirical model (equation 3.13):

$$y = \beta_0 + \sum_{i=1}^k \beta_i x_i + \sum_{i=1}^k \beta_{ii} x_i^2 + \sum_{i < j} \sum \beta_{ij} x_i x_j \quad (3.13)$$

where y is the performance measure and x_i and x_j are i^{th} and j^{th} factor respectively, k is the total number of factors. In the analysis of variance (ANOVA) table, the terms which have the P value less than 0.05 are considered as the significance parameters with 95% confidence level.

To analyse the effect of contour number on the tensile strength of FDM built parts, two new experimental run sets are considered having contour numbers 1 and 5 keeping other process parameters at their fixed level. The experimental results are shown in Table 3. 3.

Table 3.3. Effect of contour number on tensile strength of FDM parts

Set No.	A	B	C	D	E	F	Avg. Tensile strength (MPa)
1.	1	0.178	0.4064	0	0	0	25.67
2.	5	0.178	0.4064	0	0	0	28.95

It is evident from Table 3. 3 that addition of contour numbers to the specimen shifts the stress concentration zone towards the centre avoiding premature failure resulting in increase of strength due to uniform distribution of stress. The strength of the FDM built parts increases by 12.7% by addition of external perimeter to the specimen.

The effect of delta angle which plays a vital role in determining the anisotropic property of the built parts is studied. Generally, FDM build parts show anisotropic properties due to the raster fill pattern style in neighbouring layers. An attempt is made to decrease the anisotropic effect of the FDM build parts by changing the raster fill pattern style one over another. Previously some researchers (Ahn et al., 2002; Es Said et al., 2000; Rayegani et al., 2014; Lee et al., 2007; Sood et al., 2010; Wang et al., 2007) have focused on the study of the effect of raster orientation on the FDM build parts but no such experiments are conducted to decrease the anisotropic effect. The delta angle i.e. the angle between rasters in adjacent layers is modified and the effect is studied experimentally. The experimental investigation is given below in Table 3. 4 It is observed that change of delta angle to 30° (Figure 3. 4) from normal criss-cross pattern of delta angle of 90° causes an increase of 15% in average tensile strength due to enhancement of interlayer bond quality.

Table 3.4. Effect of delta angle on tensile strength

Set No.	A	B	C	D	E	F	Delta angle	Avg. Tensile strength (MPa)
1.	1	0.178	0.4064	0	0	0	30	25.67
2.	1	0.178	0.4064	0	0	0	90	22.25

In analysis of variance (ANOVA) table shown in Table 3. 5, the significant terms influencing the tensile strength of the FDM built parts can be identified at significance level of 0.05. However, raster width (C) is not a significant parameters but its interaction with other parameters exhibits significant influence. The coefficient of determination (R^2), which indicates the percentage of variation explained by the terms in the model to the total variation in the response is 0.9818 for tensile strength. It is to be noted from the table that lack of fit is not significant. Residual analysis has been carried out and found that residuals are normally distributed Figure 3. 12. The model for tensile strength involving important terms is shown in equation 3.14.

$$\begin{aligned}
 \text{Tensile Strength} = & 11.12055 - 0.34022 \times A + 131.87162 \times B + 6.47730 \times C - \\
 & 0.24266 \times D + 4.48923 \times 10^{-3} \times E - 234.63368 \times F + \\
 & 1.850 \times A \times C - 0.013333 \times A \times D - 4.09375 \times 10^{-3} \times A \times E + \\
 & 14.53002 \times A \times F - 9.47368 \times B \times C + 0.28618 \times B \times D - \\
 & 282.00114 \times B \times F + 0.12528 \times C \times E + 304.13386 \\
 & \times C \times F + 1.02361 \times 10^{-3} \times D \times E + 0.91043 \times D \times F - \\
 & 146.87624 \times B^2 - 1.02040 \times 10^{-3} \times E^2 \quad (\text{uncoded} \\
 & \text{form}) \quad (3.14)
 \end{aligned}$$

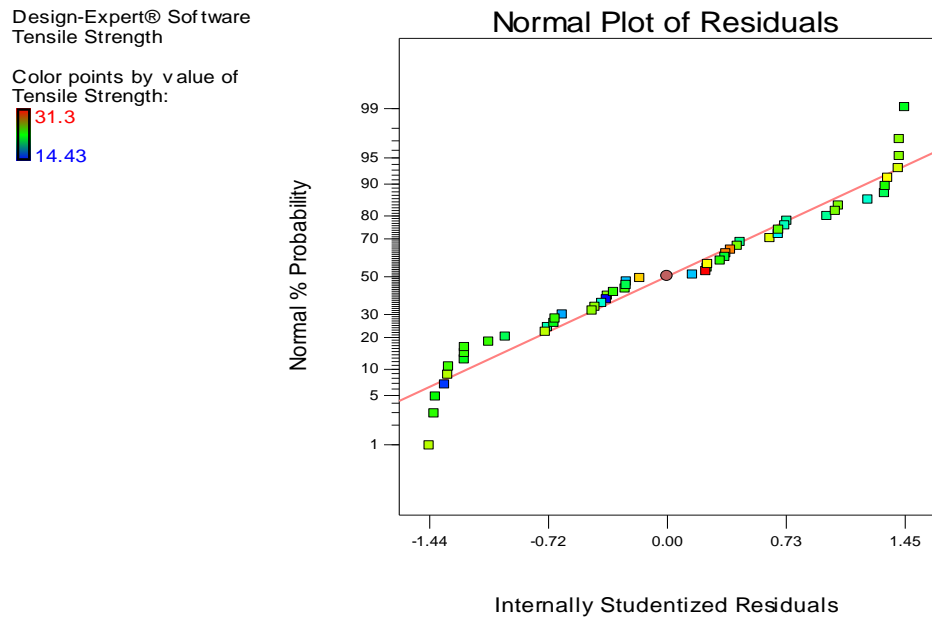
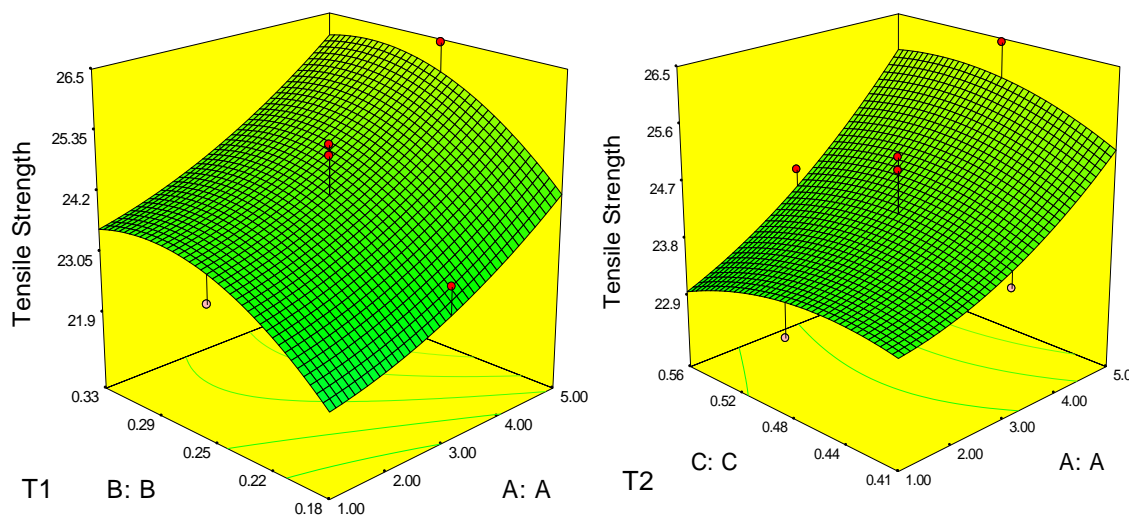


Figure 3.12. Normal probability plot of residual at 95% confidence interval for tensile strength

Table 3.5. ANOVA table for tensile strength

Source	Sum of Squares	df	Mean Square	F- Value	P-value Prob > F
Model	598.16	19	31.48	110.19	< 0.0001
A	48.41	1	48.41	169.44	< 0.0001
B	25.15	1	25.15	88.02	< 0.0001
C	0.12	1	0.12	0.41	0.5256
D	186.50	1	186.50	652.77	< 0.0001
E	1.35	1	1.35	4.73	0.0371
F	230.93	1	230.93	808.30	< 0.0001
AxC	2.46	1	2.46	8.63	0.0061
AxD	5.12	1	5.12	17.92	0.0002
AxE	1.93	1	1.93	6.76	0.0140
AxF	17.43	1	17.43	61.02	< 0.0001
BxC	8.32	1	8.32	29.13	< 0.0001
BxD	3.41	1	3.41	11.92	0.0016
BxF	9.48	1	9.48	33.19	< 0.0001
CxE	2.54	1	2.54	8.90	0.0054
CxF	10.74	1	10.74	37.60	< 0.0001
DxE	6.79	1	6.79	23.76	< 0.0001
DxF	3.85	1	3.85	13.48	0.0009
B ²	2.63	1	2.63	9.22	0.0047
E ²	3.09	1	3.09	10.80	0.0025
Residual	9.14	32	0.29		
Lack of Fit	5.53	25	0.22	0.43	0.9437
Pure Error	3.61	7	0.52		
Cor Total	607.30	51			

From response surface plots (Figure 3.13 T1-T5), it is observed that the tensile strength increases with increase in contour number (A) because increasing the contour number or offset contours in the build parts shifts the stress concentration zone towards the centre. In tensile loading, specimen fails prematurely due to shearing at stress concentration zone (Ahn et al., 2002). Therefore, shifting of stress concentration towards the centre of the part diminishes the chance of failure at the edge. Past research suggests that increasing the number of contours deposited around the specimen edge, both tensile strength and stiffness of the specimen increase (Croccolo et al., 2013). Figure 3. 13 T1, T6, T7 and T8 reveals that tensile strength increases as layer thickness (B) increases. Increase of layer thickness causes decrease in number of layers required for building the part. Consequently, it results in less number of interlayer bonds. As the strength of interlayer bonding depends on variations in the convective heat transfer coefficient and cooling temperature profile inside the chamber, less number of interlayer bonds is subjected to variations causing improvement in part strength. Figure 3. 13 T3 indicates that increase in part orientation angle (D) causes decrease in part strength. In fact, increase in part orientation angle results in increase in number of layers required for part building and subjected exposure to more heating-cooling cycles. As a result, the strength of the part decreases. Figure 3. 13 T5 and T8 shows that increase in air gap between rasters reduces the strength of the build parts due to voids and pores are resulted among layers. The voids and pores adversely influence the bond quality causing in decrease in strength. Zero air gap (rasters are just in contact with each other) exhibits good strength than that of any positive value of air gap.



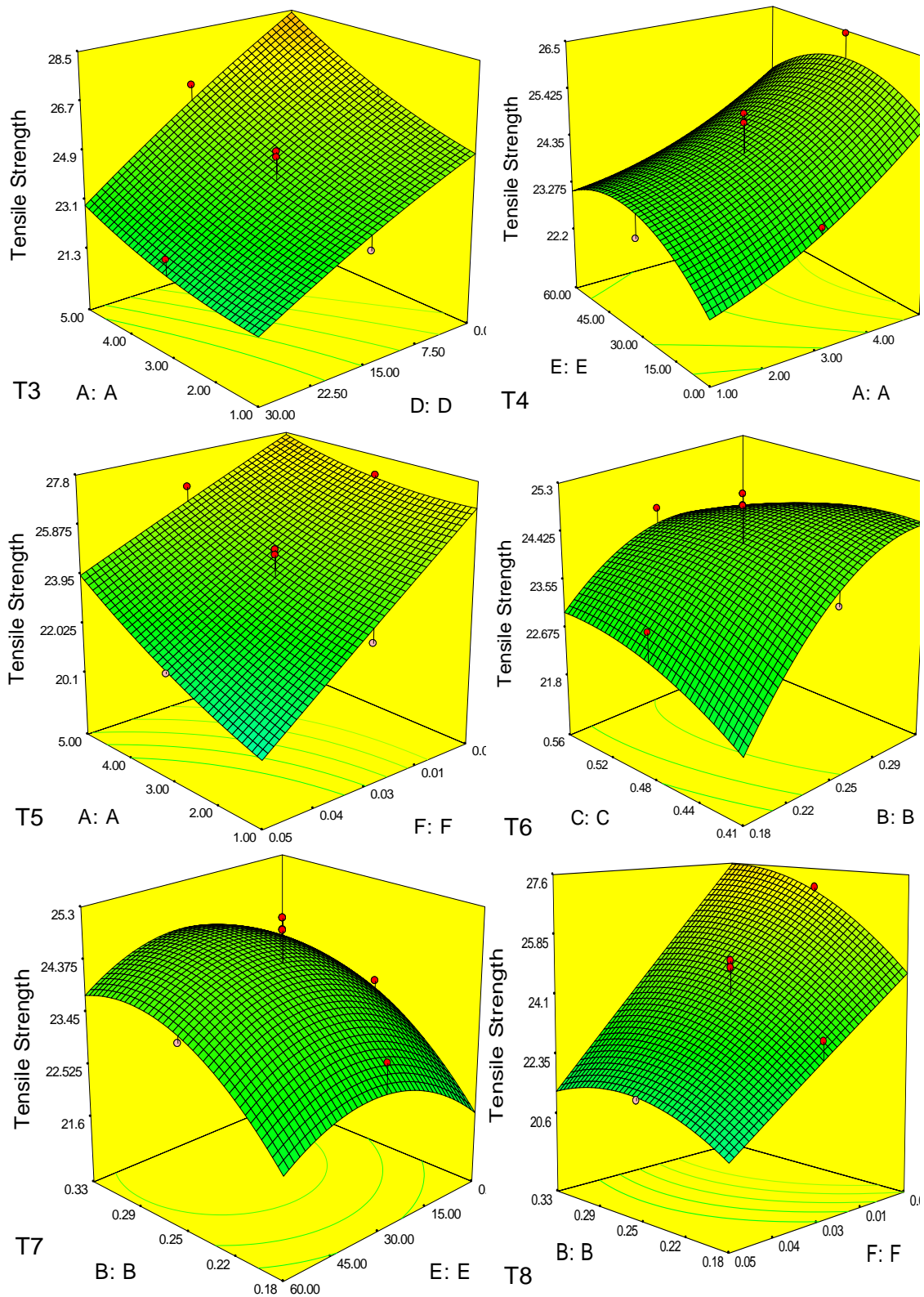


Figure 3.13. Surface plot for tensile strength

From the scanning electron microscope (SEM) micrograph (JEOL JSM-6480LV in the LV mode) shown in Figure 3. 14, it can be clearly seen that the failure of the specimens

are due to the tension and rupture in the rasters. Figure 3. 14 also exhibits the voids in the layers causing reduction in bond strength. The raster separation in a specimen occurs in a zigzag manner due to the overlaying raster orientation style which changes at an incremental angle with respect to its previous layer as can be clearly identified from the image shown in Figure 3. 15.

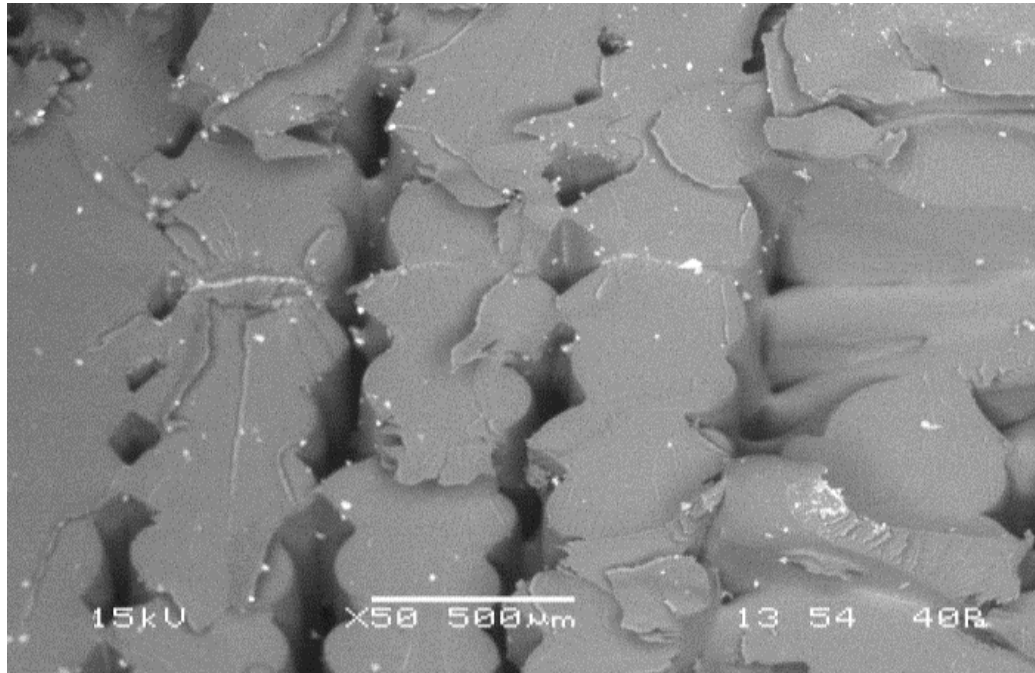


Figure 3.14. SEM image of part showing raster failure

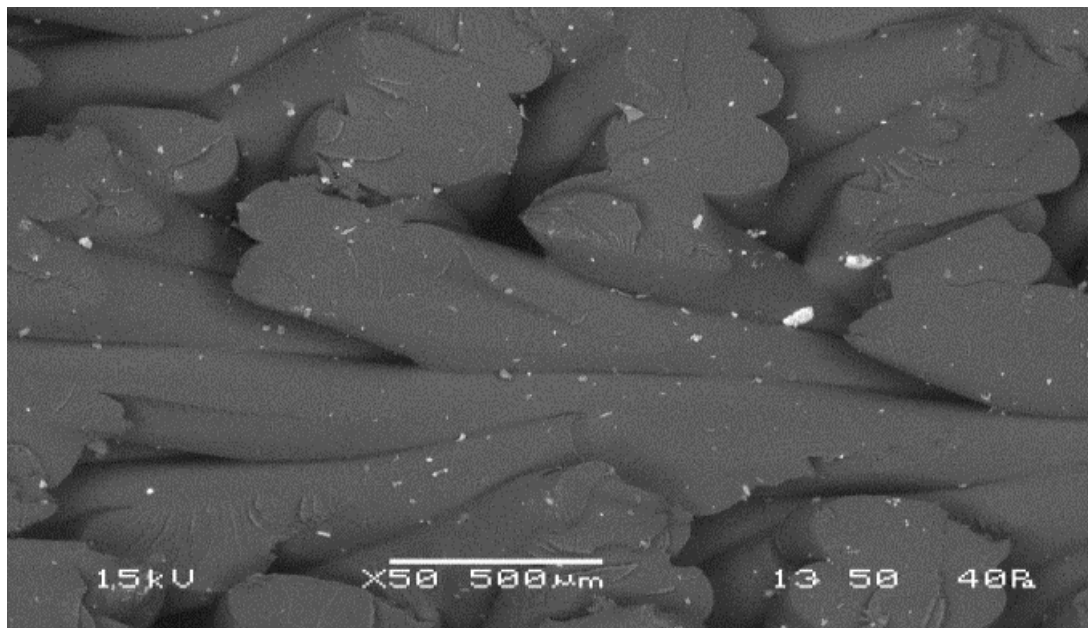


Figure 3.15. SEM image of overlaying raster orientation

The stress strain curve shown in Figure 3.16 indicates the brittle nature of the material. The staircase pattern in the graph shows that the force per unit area has reached a value at which material starts to deform and this staircase pattern repeats up to the fracture of the part. The failure starts from the weakest raster causing increase of stress on other rasters to get failure.

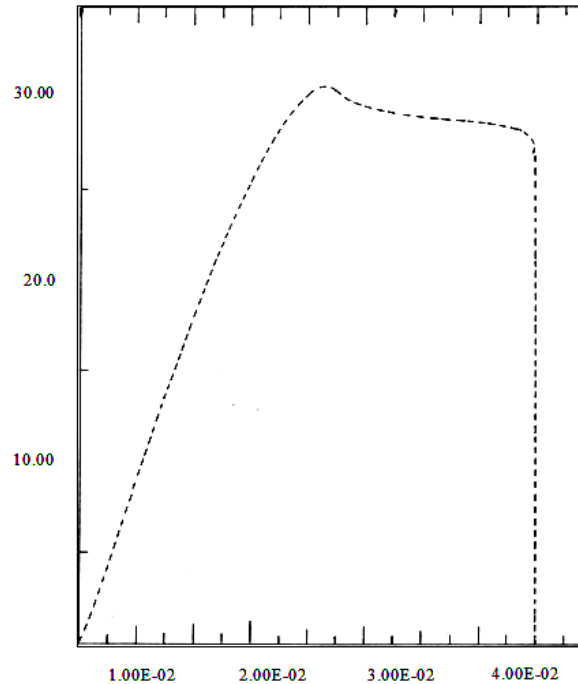


Figure 3.16. Stress strain curve for tensile strength

ANOVA table shown in Table 3. 6 depicts important terms influencing compressive strength of built parts. All the squared terms have less significance on compressive strength. The co-efficient of determination (R^2) which indicates the percentage of total variation explained by the terms in the model is 0.7945 for compressive strength. Residual analysis has been carried out and found that residuals are normally distributed Figure 3. 17. The empirical model for compressive strength is shown in equation 3. 15. This is to be noted that lack of fit is not significant.

$$\begin{aligned}
 \text{Compressive Strength} = & -30.86331-13.65788\times A+337.55929\times B+352.71315 \\
 & \times C+0.48073\times D-0.30815\times E-158.72989\times F+39.7624 \\
 & \times A\times B+0.24096\times A\times D-103.39321\times A\times F-987.83991 \\
 & \times B\times C-7.08037\times B\times D+2201.00109\times B\times F- \\
 & 1191.76509 \times C\times F+5.69939\times E\times F \\
 & \text{(uncoded form)}
 \end{aligned}
 \tag{3.15}$$

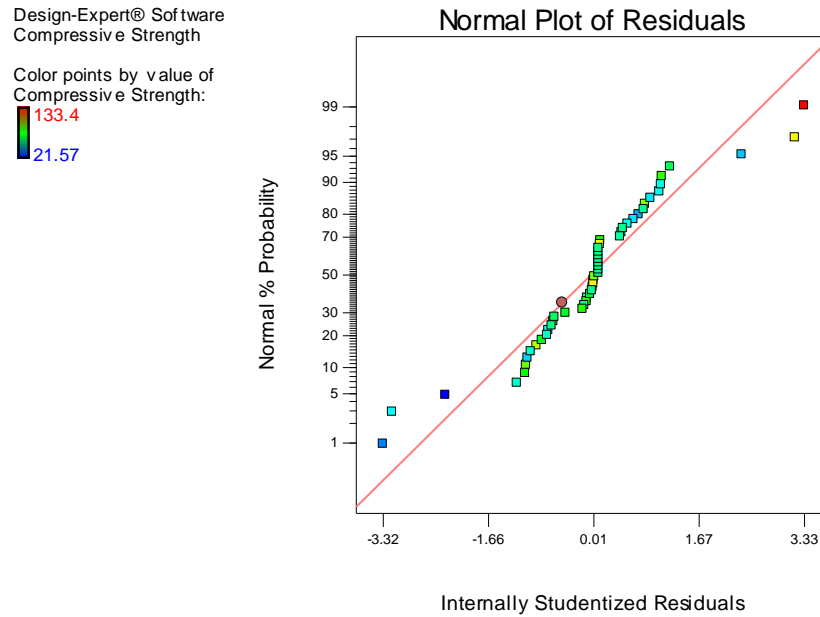


Figure 3.17. Normal probability plot of residual at 95% confidence interval for compressive strength

Table 3.6. ANOVA table for compressive strength

Source	Sum of Squares	df	Mean Square	F Value	p-value Prob > F
Model	16647.94	14	1189.14	37.08	< 0.0001
A-A	898.29	1	898.29	28.01	< 0.0001
B-B	934.98	1	934.98	29.15	< 0.0001
C-C	978.57	1	978.57	30.51	< 0.0001
D-D	2706.47	1	2706.47	84.39	< 0.0001
E-E	816.83	1	816.83	25.47	< 0.0001
F-F	2143.36	1	2143.36	66.83	< 0.0001
AxB	1168.91	1	1168.91	36.45	< 0.0001
AxD	1672.18	1	1672.18	52.14	< 0.0001
AxF	882.8	1	882.8	27.53	< 0.0001
BxC	1014.55	1	1014.55	31.64	< 0.0001
BxD	2084.84	1	2084.84	65.01	< 0.0001
BxF	577.68	1	577.68	18.01	0.0001
CxF	164.94	1	164.94	5.14	0.0293
ExF	603.56	1	603.56	18.82	0.0001
Residual	1186.59	37	32.07		
Lack of Fit	1110.7	30	37.02	3.41	0.0685
Pure Error	75.9	7	10.84		
Cor Total	17834.53	51			

The effect of part orientation (D) and air gap (F) have similar effect on compressive strength as on tensile strength. As contour number increases, compressive strength of the specimen also increases but its influence on compressive strength seems to be less as compared to tensile strength (Figure 3.18 T2 and 3.18 C1). The part orientation adversely affects the compressive strength because increase in part orientation increases the chance of shear failure between the rasters in adjacent layers (Lee et al., 2007). Hence, with an increase in part orientation (D), the compressive strength decreases (Figure 3.18 C1, C3 and C5). Decrease in the raster width increases the number of rasters in a layer which increases the involvement of rapid heating and cooling cycle producing distortions effect (Bellehumeue et al., 2008) Hence, with the increase in raster width (C) increases the compressive strength with involvement of less distortion effect (Figure 3.18 C2).

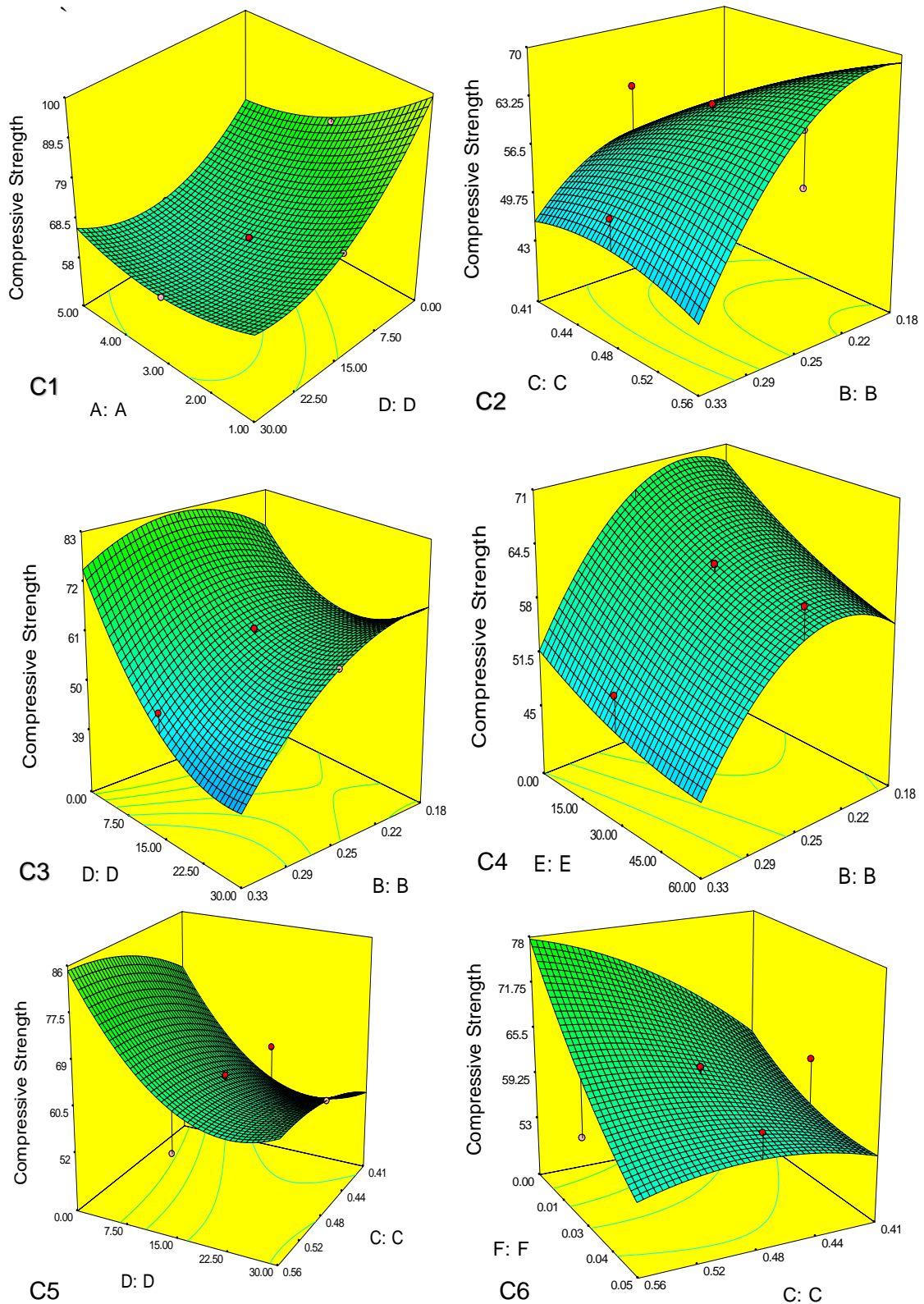


Figure 3.18. Surface plots for compressive strength

From the ANOVA table shown in Table 3.7, it is clear that all the input process parameters influence the flexural strength. The coefficient of determination (R^2) which indicates the percentage of variation explained by the model to the total variation in the response is 0.9850. It is to be noted that lack of fit is not significant. Residual analysis has been carried out and found that residuals are normally distributed (Figure 3.19). The empirical relation between flexural strength and process parameters is shown in equation 3.16.

$$\begin{aligned} \text{Flexural Strength} = & 51.41058 - 0.95826 \times A + 146.39257 \times B - 18.39720 \times C - \\ & 1.07898 \times D - 0.75614 \times E - 197.91936 \times F - 0.097313 \times A \times D \\ & + 0.017759 \times A \times E + 56.29699 \times A \times F - 179.43621 \times B \times C - \\ & 2.61379 \times B \times D + 0.77808 \times B \times E - 511.47168 \times B \times F + 1.59630 \\ & \times C \times E + 0.011116 \times D \times E + 2.68501 \times D \times F - 1.03896 \times E \times F \\ & + 0.025173 \times D^2 - 4.06978 \times 10^{-3} \times E^2 \quad (\text{uncoded form}) \quad (3.16) \end{aligned}$$

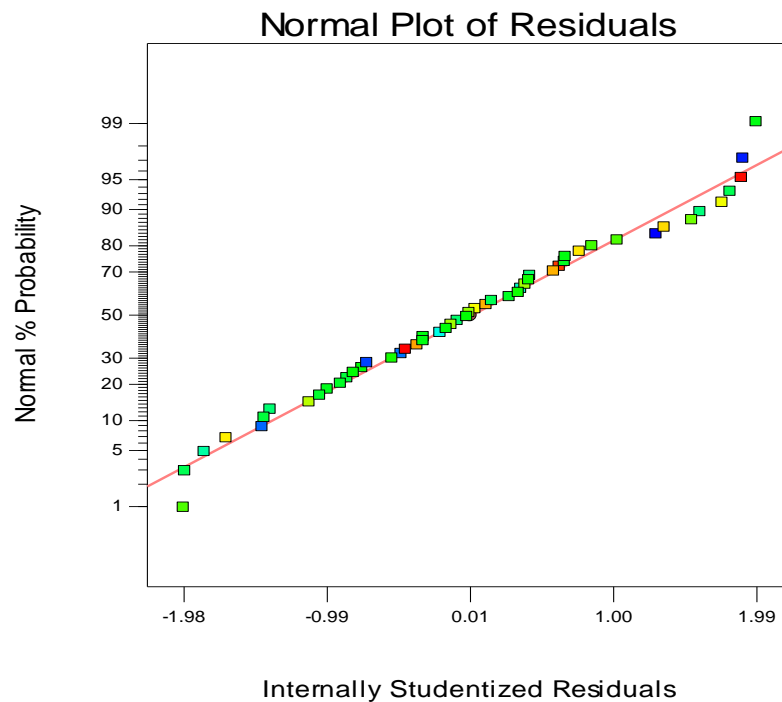


Figure 3.19. Normal probability plot of residual at 95% confidence interval for Flexural strength

Table 3.7. ANOVA table for flexural strength

Source	Sum of Squares	df	Mean Square	F-Value	P-value Prob>f
Model	9852.24	19	518.54	77.13	< 0.0001
A	28.18	1	28.18	4.19	0.0489
B	190.63	1	190.63	28.35	< 0.0001
C	49.48	1	49.48	7.36	0.0106
D	5896.44	1	5896.44	877.01	< 0.0001
E	777.53	1	777.53	115.65	< 0.0001
F	492.47	1	492.47	73.25	< 0.0001
AxD	272.73	1	272.73	40.57	< 0.0001
AxE	36.33	1	36.33	5.40	0.0266
AxF	261.73	1	261.73	38.93	< 0.0001
BxC	33.47	1	33.47	4.98	0.0328
BxD	284.12	1	284.12	42.26	< 0.0001
BxE	100.71	1	100.71	14.98	0.0005
BxF	31.20	1	31.20	4.64	0.0389
CxE	412.81	1	412.81	61.40	< 0.0001
DxE	800.76	1	800.76	119.10	< 0.0001
DxF	33.49	1	33.49	4.98	0.0328
ExF	20.06	1	20.06	2.98	0.0938
D ²	117.42	1	117.42	17.46	0.0002
E ²	49.10	1	49.10	7.30	0.0109
Residual	215.15	32	6.72		
Lack of Fit	200.18	25	8.01	3.74	0.0589
Pure Error	14.97	7	2.14		
Cor Total	10067.39	51			

It has been already established by previous reasearch work that air gap, raster angle, raster width and layer thickness significantly influence the performance of flexural strength of built parts (Lee et al., 2005). As observed, flexural strength increases on increasing layer thickness (B) because the number of layers decreases on increasing layer thickness as discussed previously (Figure 3. 20 F2 and F3). The flexural strength increases with decrease in the air gap (F) (Figure 3. 20 F4). Response surface plot between contour number (A) and part orientation (D) shows that flexural strength increases with decrease in part orientation but increases with contour number at low level of part orientation and decreases with contour number at high level of part orientation (Figure 3. 20 F1). In fact, bonding of rasters plays a significant role in determining the flexural strength of the part.

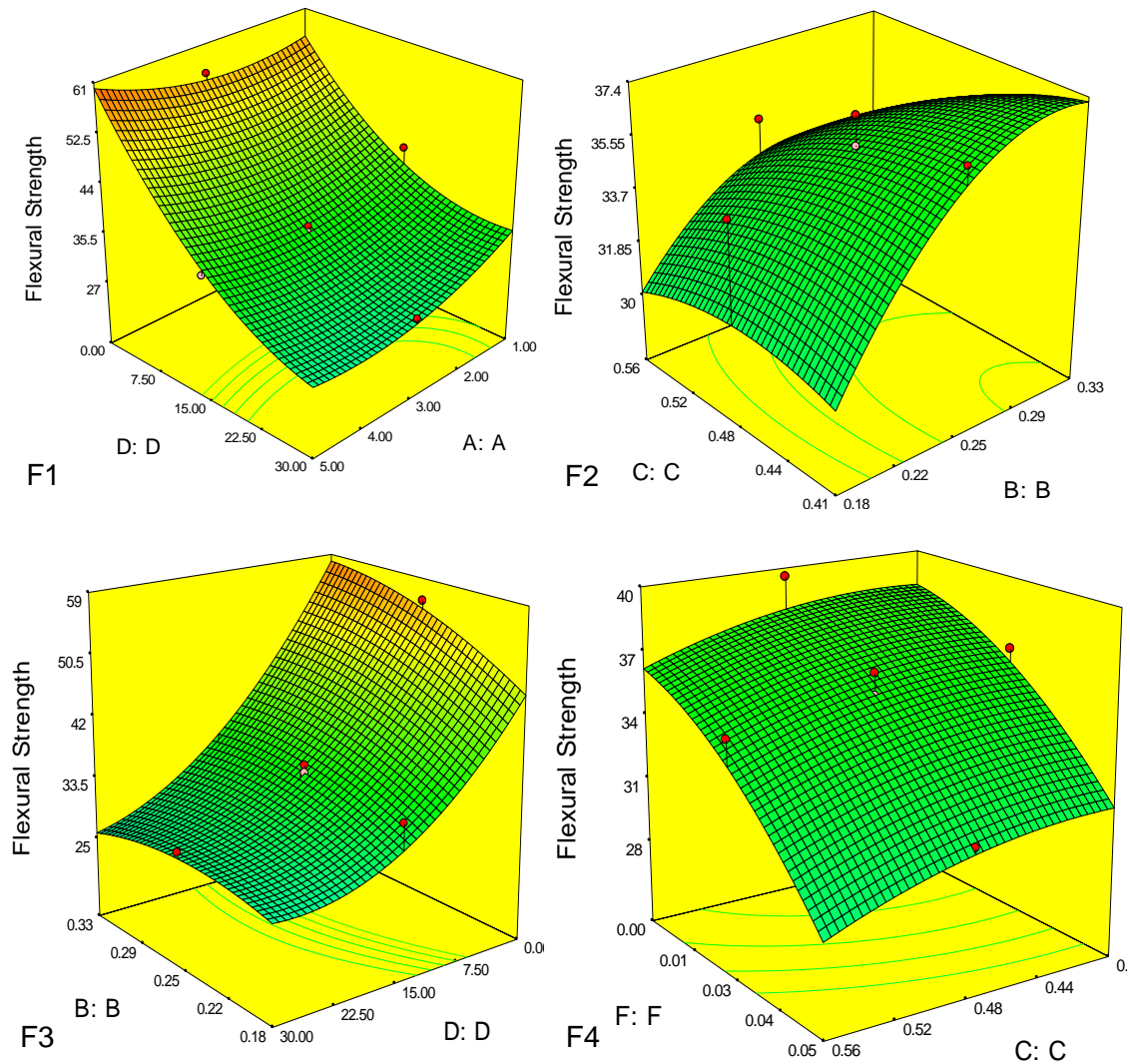


Figure 3.20. Surface plots for flexural strength

Close examination of specimens at fracture during testing, it is observed that the failure begins from the rasters which are under maximum tension. The flexural specimen is well connected by the unbroken rasters which are under compression side. The stress strain curve for flexural strength shown in Figure 3. 21 shows the stair case pattern indicating the breaking of individual rasters.

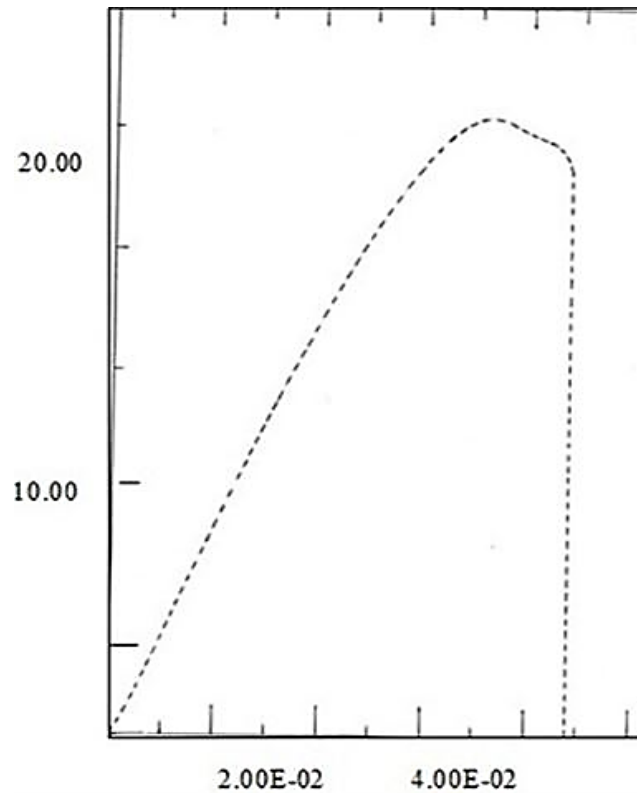


Figure 3.21. Stress strain curve for flexural strength

Analysis of variance shown in Table 3. 8, it can be observed that all the input process parameters influence the impact strength. The coefficient of determination (R^2) is 0.9755 for impact strength. Lack of fit is found to be insignificant. Residual analysis has been carried out and found that residuals are normally distributed (Figure 3. 22). The empirical relation relating impact strength with process parameters is shown in equation 3. 17.

$$\begin{aligned}
 \text{Impact Strength} = & 655.02749 - 15.73070 \times A - 75.13905 \times B - 1229.22270 \times C - \\
 & 12.96514 \times D + 0.37897 \times E - 6225.86933 \times F - 0.32843 \times A \times B + \\
 & 117.64323 \times A \times C - 0.96257 \times A \times D - 0.41130 \times A \times E + \\
 & 423.49748 \times A \times F + 1043.37993 \times B \times C - 7.42701 \times B \times D - \\
 & 10.88353 \times B \times E + 11539.26162 \times B \times F + 21.13715 \times C \times D + 13. \\
 & 80642 \times C \times E + 0.048893 \times D \times E + 37.60150 \times D \times F - 12.49539 \\
 & \times E \times F + 0.15193 \times D^2 - 0.043613 \times E^2 + 49112.39092 \times F^2
 \end{aligned}
 \tag{3.17}$$

(uncoded form)

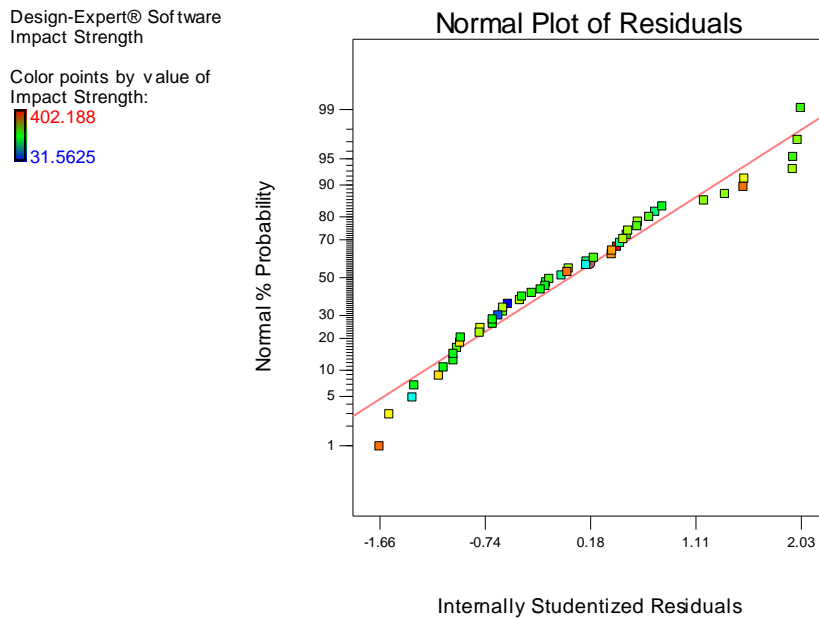


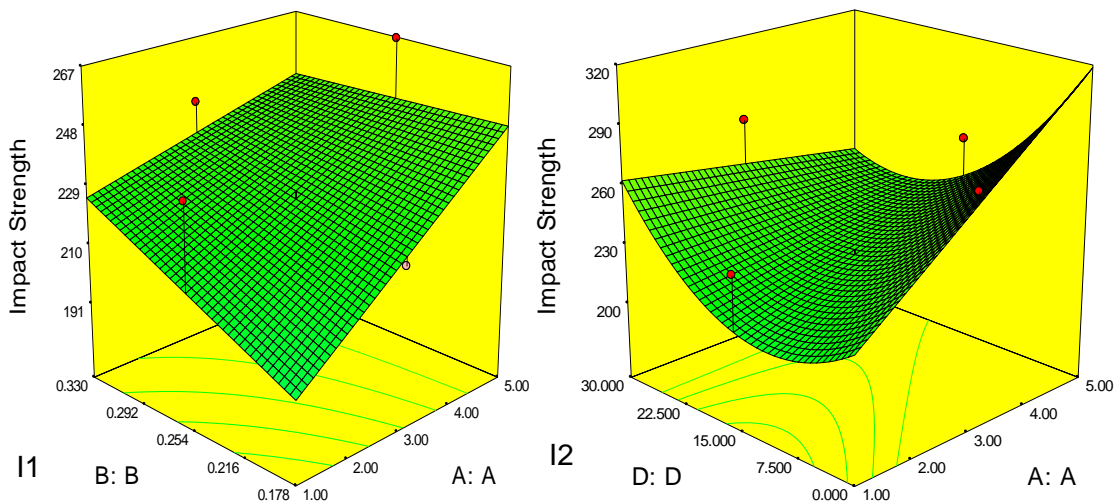
Figure 3.22. Normal probability plot of residual at 95% confidence interval for impact strength

Table 3.8. ANOVA table for Impact Strength

Source	Sum of Squares	df	Mean Square	F Value	p-value Prob>f
Model	2.512E+005	23	10920.50	48.43	< 0.0001
A	12426.47	1	12426.47	55.11	< 0.0001
B	2017.02	1	2017.02	8.95	0.0057
C	2752.88	1	2752.88	12.21	0.0016
D	2608.60	1	2608.60	11.57	0.0020
E	20892.14	1	20892.14	92.66	< 0.0001
F	9545.41	1	9545.41	42.34	< 0.0001
AxB	2690.80	1	2690.80	11.93	0.0018
AxC	9964.75	1	9964.75	44.20	< 0.0001
AxD	26684.11	1	26684.11	118.35	< 0.0001
AxE	19487.70	1	19487.70	86.43	< 0.0001
AxF	14810.82	1	14810.82	65.69	< 0.0001
BxC	1131.84	1	1131.84	5.02	0.0332
BxD	2293.97	1	2293.97	10.17	0.0035
BxE	19704.23	1	19704.23	87.39	< 0.0001
BxF	15878.18	1	15878.18	70.42	< 0.0001
CxD	18094.56	1	18094.56	80.25	< 0.0001
CxE	30880.01	1	30880.01	136.96	< 0.0001
DxE	15490.75	1	15490.75	68.70	< 0.0001
DxF	6567.65	1	6567.65	29.13	< 0.0001
ExF	2901.08	1	2901.08	12.87	0.0013

D ²	3397.40	1	3397.40	15.07	0.0006
E ²	4479.13	1	4479.13	19.87	0.0001
F ²	2918.66	1	2918.66	12.94	0.0012
Residual	6313.13	28	225.47		
Lack of Fit	6181.69	21	294.37	15.68	0.0605
Pure Error	131.43	7	18.78		
Cor Total	2.575E+005	51			

3-D surface plots shown in Figure 3. 23 indicate that impact strength of the FDM built parts increases with increase in the contour number (A) (Figure 3. 23 I1 and I2) because addition of contour number increases the stiffness by shifting the stress concentration zone towards the centre avoiding premature failure of the specimen (Ahn et al., 2002; Croccolo et al., 2013). Figure 3. 23 I3 shows that the impact strength increases with an increase in layer thickness (B) because increase in layer thickness decreases the number of layers resulting in less distortion effect (Wang et al., 2007). With an increase in part orientation (D), the impact strength decreases slowly (Figure 3. 23 I2). Figure 3. 23 I4 indicates that the impact strength increases with increase in raster width (C). This may be due to the fact that a wide raster offers more resistance to the impact blow than a narrow one.



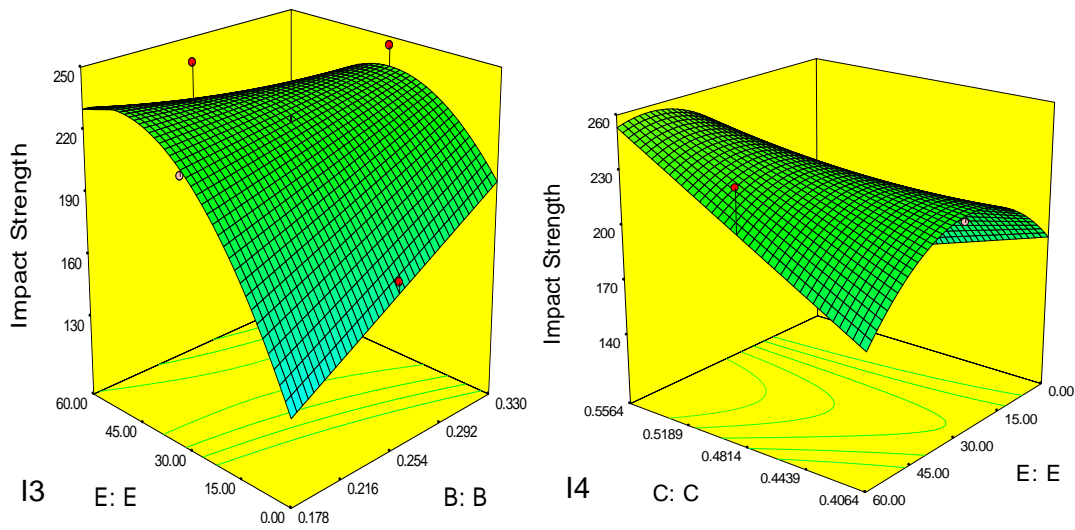


Figure 3.23. Surface plots for flexural strength

From the above discussion, it is concluded that FDM technology includes complex part building phenomenon. In many practical applications, more than one type of loading acts upon the built parts. The built part must be reasonably sustain various kinds of loading because FDM builds functional parts. The discussions on parametric analysis reveals that FDM parameters influence on various strengths in a different manner. Therefore, best parametric condition for improving tensile strength may not be adequate for all types of strengths. In order to determine best parameter setting that improves tensile, compressive, flexural and impact strength simultaneously is highly desirable from practical point of view. The methodology of combining desirability approach with fuzzy inference system is proposed to obtain a multi performance characteristic index (MPCI), which is nothing but a single performance index for all four types of strengths. The desirability approach is adopted applying higher the better criteria to normalise each response using equations 3.18 - 3.19 in order to bring all the strengths into same scale.

$$\text{If } \hat{y} \leq y_{min}, d_i = 0 \quad (3.18)$$

$$\text{If } y_{min} \leq \hat{y} \leq y_{max}, d_i = \left(\frac{\hat{y} - y_{min}}{y_{max} - y_{min}} \right)^r \quad (3.19)$$

$$\text{f } \hat{y} \geq y_{max}, d_i = 1 \quad (3.20)$$

where \hat{y} represents the value of the individual response. The term y_{min} and y_{max} denote lower and higher tolerance value of \hat{y} respectively. The individual desirability value and

desirability function index is represented as d_i and r respectively. The value of r is assigned accordingly to the requirement of the decision maker.

A fuzzy inference system is proposed to receive individual normalised values as input and deliver a single output known as MPCI, which is in crisp format. The normalised values of the responses (four types of strength) are treated as four inputs to FIS and the FIS is solved using the MATLAB 2014 software. For each input parameters, three fuzzy membership functions are considered viz. low (L), medium (M) and high (H) as shown in Figure 3. 24. Seven fuzzy sets have been assigned to the output (MPCI) viz. very low (VL), low (L), medium low (ML), medium (M), medium high (ML), high (H), very high (VH) as shown in Figure 3. 25. A total of 52 fuzzy rules are defined for this experimental controller.

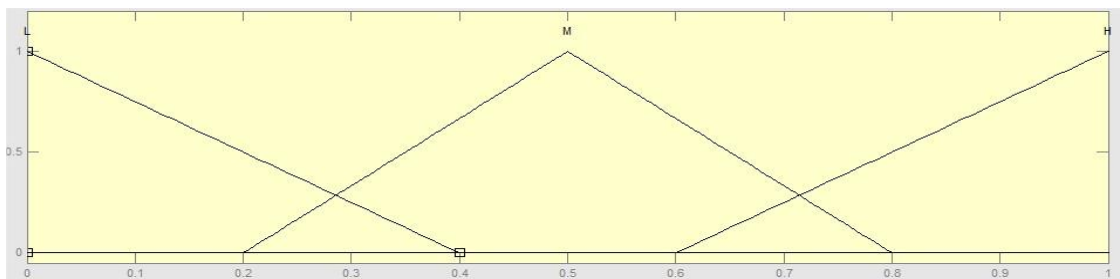


Figure 3.24. Membership function for each normalised response

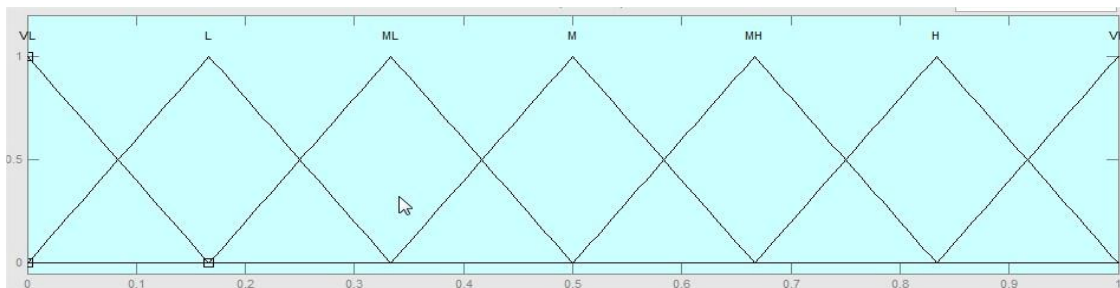


Figure 3.25. Membership function for MPCI

Table 3.9. Individual normalised values of responses with MPCI value

Sl. No.	Tensile Strength	Compressive Strength	Flexural Strength	Impact Strength	MPCI
1	0.6799	0.6871	0.8393	0.5717	0.6669
2	0.5495	0.0000	0.7436	0.8592	0.4445
3	0.3545	0.6597	0.7742	0.7277	0.6824
4	1.0000	0.6454	0.9899	0.7816	0.7665
5	0.3675	0.6040	0.4968	0.0000	0.5001
6	0.7967	0.7228	0.6470	0.6341	0.5560
7	0.7202	0.6221	0.7646	0.3710	0.6217
8	0.6337	0.4104	0.6824	1.0000	0.6953
9	0.0000	0.4038	0.3055	0.3904	0.5001
10	0.3284	0.5217	0.1132	0.2749	0.3333
11	0.6177	0.2658	0.3409	0.4115	0.4788

12	0.3397	0.2144	0.1017	0.7285	0.4055
13	0.2958	0.7505	0.2749	0.2749	0.5001
14	0.2958	0.3813	0.0654	0.5717	0.3332
15	0.0545	0.1728	0.0290	0.5717	0.3333
16	0.4778	0.4288	0.0000	0.3710	0.3333
17	0.2454	0.5484	0.3883	0.4705	0.5508
18	0.7481	0.2575	0.5770	0.6754	0.5045
19	0.8743	0.4675	0.9464	0.5717	0.6669
20	0.4784	0.3837	0.8269	0.6535	0.6669
21	0.6858	1.0000	0.7848	0.6669	0.7095
22	0.6402	0.2050	0.7369	0.7749	0.4387
23	0.3154	0.5370	0.6585	0.5717	0.5835
24	0.8743	0.5064	1.0000	0.6560	0.7004
25	0.4517	0.2979	0.5753	0.7546	0.5128
26	0.1660	0.2256	0.3784	0.5717	0.3604
27	0.1932	0.1286	0.3954	0.6619	0.4571
28	0.6420	0.2728	0.4672	0.0902	0.5001
29	0.1915	0.4688	0.4193	0.8895	0.5001
30	0.4191	0.6217	0.4432	0.8895	0.5564
31	0.5625	0.0949	0.6585	0.8423	0.4603
32	0.4173	0.2287	0.4672	0.8895	0.5210
33	0.5039	0.4591	0.6107	0.5540	0.5834
34	0.7119	0.3410	0.5207	0.6341	0.5331
35	0.5234	0.4424	0.4826	0.5008	0.5180
36	0.5625	0.2673	0.4729	0.5776	0.4803
37	0.5495	0.3558	0.5150	0.4958	0.5578
38	0.5886	0.4494	0.4853	0.5413	0.5235
39	0.6805	0.5324	0.8269	0.6619	0.7130
40	0.4713	0.3607	0.3954	0.6602	0.5610
41	0.5347	0.3698	0.4205	0.3710	0.5663
42	0.5430	0.3635	0.4996	0.5548	0.5626
43	0.7463	0.4037	0.5628	0.6332	0.6127
44	0.4256	0.3427	0.4193	0.6754	0.5491
45	0.6212	0.3690	0.4853	0.5034	0.5659
46	0.6331	0.4140	0.5141	0.4865	0.5657
47	0.5531	0.3859	0.4571	0.5135	0.5659
48	0.5424	0.3466	0.4916	0.5034	0.5659
49	0.6331	0.4028	0.4853	0.4764	0.5657
50	0.5483	0.3831	0.4628	0.4899	0.5659
51	0.6206	0.3618	0.4419	0.4924	0.5659
52	0.5483	0.3241	0.4972	0.4899	0.5659

The fourth run from the normalised experimental data shown in Table 3. 9 indicates best parameter setting because it exhibits highest MPCl value i.e. 0.7665. To achieve the optimum solution or to achieve the best parameter setting than suggested by the fuzzy inference system, a nature inspired metaheuristic known as firefly algorithm is applied. The objective function used in the firefly optimisation algorithm is empirically developed using non-linear regression analysis relating MPCl values shown in Table 3. 9 and process

parameters. The objective function used in the firefly algorithm is given below equation 3.21. R^2 -value of the fitted model is reasonably good.

$$\begin{aligned} \text{MPCI} = & - 1.31134 + 0.10366 \times A + 7.69170 \times B + 5.30274 \times C - 0.010161 \times D - \\ & 4.21988 \times 10^{-3} \times E - 3.23494 \times F + 0.25049 \times A \times B + 0.095792 \times A \times C - \\ & 1.98333 \times 10^{-4} \times A \times D + 1.16250 \times 10^{-4} \times A \times E + 0.076649 \times A \times F - \\ & 3.26864 \times B \times C - 0.030691 \times B \times D - 8.16886 \times 10^{-4} \times B \times E \\ & + 8.55716 \times B \times F + 3.71667 \times 10^{-3} \times C \times D + 9.10278 \times 10^{-3} \times C \times E - \\ & 2.79528 \times C \times F + 5.29722 \times 10^{-5} \times D \times E + 0.030003 \times D \times F - 6.97999 \times 10^{-3} \times E \times F \\ & - 3.03699 \times 10^{-3} \times A^2 - 12.33517 \times B^2 - 5.28853 \times C^2 \\ & + 2.960 \times 10^{-4} \times D^2 - 6.60886 \times 10^{-6} \times E^2 + 16.27818 \times F^2 \end{aligned}$$

(uncoded form) ($R^2 = 0.9486$ and $Adj. R^2 = 0.8907$) (3.21)

For the firefly algorithm, the values considered are: number of fireflies (n) = 10, number of iterations (N) = 50, attractiveness (β) = 0.9, randomisation (α) = 0.2 and absorption coefficient (γ) = 1. Hence, the total number of function evaluations is 500. The firefly algorithm provides a parameter setting to get optimum value of the MPCI as shown in Table 3.10. It is to be noted that maximum MPCI shown in the experimental data is 0.7665. Residual analysis has been carried out and found that residuals are normally distributed Figure 3.26.

Table 3.10. Optimum parameter setting to achieve the best MPCI

A	B	C	D	E	F	MPCI
1.4127	0.3096	0.4896	14.3139	43.3948	0.0449	0.8207

Design-Expert® Software
MPCI

Color points by value of
MPCI:

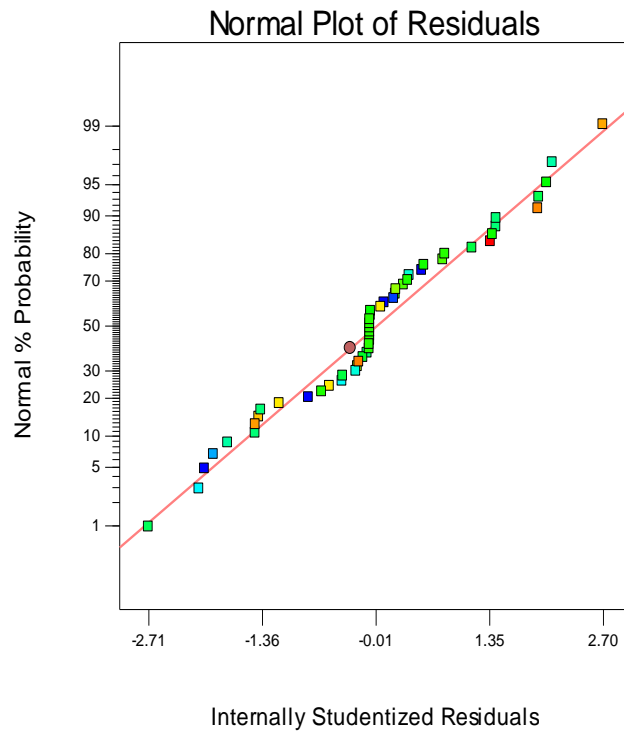


Figure 3.26. Normal distribution of residuals at 95% confidence interval for MPCI

In the present study, GP is applied to develop a model relating FDM process parameters with static strength of FDM build parts. From the experimental results, 80% data are taken are considered for training purpose and rest data are considered for testing purpose. Six input parameters such as contour number (x_1), layer thickness (x_2), raster width (x_3), part orientation (x_4), raster angle (x_5) and air gap (x_6) are considered for modelling purpose. The output parameter static strength is considered as the performance characteristic. The performance of GP model is measured in terms of MAPE. The diagram involving GP technique for the modelling of static strength of the FDM build part is shown in Figure 3.27.

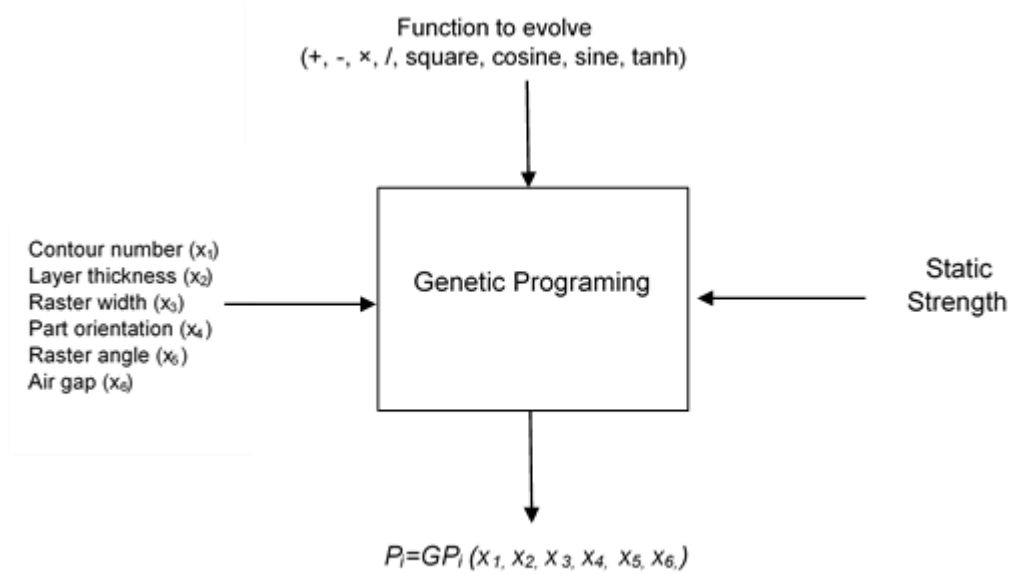


Figure 3.27. Diagram of GP formulation of mechanical strength of FDM built parts

The parameter setting for GP determined through several trial and experimental runs are shown below in Table 3.11.

Parameters	Value Assigned
Population size	65
Number of generations	1000
Maximum depth of tree	6
Maximum generation	50
Functional set	Multiply, plus, minus, divide, square, cosine, sine, tanh
Terminal set	($x_1, x_2, x_3, x_4, x_5, x_6, [-10,10]$)
Number of runs	110
Mutation rate	0.10
Crossover rate	0.85
Reproduction rate	0.05

The GP model with MAPE 0.024 and 4.31 on the training and testing data respectively signifies that it has efficiently generalise the data set. The relative percentage error between GP predicted value and experimental results of **mechanical strength** of the FDM build part are calculated. Using the GP technique, a model is developed relating six FDM process parameter with fatigue life of the build part and is given in equation 3.22.

$$\begin{aligned}
\text{Mechanical strength} = & 0.04414.xx(:,3) - 0.02477.xx(:,5) - 0.01813).xx(:,1) + \\
& (0.01057.xx(:,3) - 0.01183.xx(:,2) - 0.07376.xx(:,4) + \\
& 0.000738.xx(:,5) - 0.02588.xx(:,6) + 0.002422.xplog(- \\
& 8.067.xx(:,6))-0.02827.xtan(\text{square}(8.6))-0.1067.x \\
& \text{psqroot}(\text{psqroot}(x(:,2)))+0.03309.x\text{square}(\text{square}(x(:,4))) \\
& +2.973e-5.x\text{square}(\text{square}(x(:,5)))+0.03639.x\text{square} \\
& (x(:,1) + x(:,2)) + 0.006572.x\text{square}(x(:,3) + x(:,4)) + \\
& 0.005194.x\text{square}(x(:,2) + x(:,6)) - 0.004505.xtan(x(:,1) + \\
& x(:,2)) + 0.0922.x\text{cos}(x(:,1)) - 3.182e-15.xplog(x(:,3)) \\
& +0.01046.xplog(x(:,4))-0.03016.x\text{psqroot}(x(:,3)) \\
& +0.03309.x\text{psqroot}(x(:,4)) + 0.0001784.x\text{square}(x(:,5)) \\
& +0.00116.x\text{square}(x(:,6))-0.01226.xtan(x(:,3))- \\
& 0.001661.xtan(x(:,5))-0.01622.xx(:,2).xx(:,4)-0.0332.x \\
& x(:,2).xx(:,5)+0.004854.xx(:,3).xx(:,5)- 0.01046 .xx(:,3) \\
& .xx(:,6)-0.02131.xx(:,4).xx(:,6)+0.01986.xx(:,3).^2.xx(:,5) \\
& +0.0364.xx(:,2).x\text{square}(x(:,5)) + 0.2461); \tag{3.22}
\end{aligned}$$

Again, an artificial intelligent (AI) technique known as least square support vector machine (LS-SVM) is used for prediction purpose. The LS-SVM technique involves input training data followed by testing data. Around 80% of the experimental results are considered for training purpose while rest 20% are considered for testing purpose. Six important FDM process parameters such as contour number, layer thickness, part orientation, raster angle, raster width and air gap are considered as input parameters. The hyper parameters gamma (γ) and sig^2 (σ^2) are obtained as 59.5735 and 0.0543142 respectively. The formula used for calculation of relative error is given in equation 3.23.

$$\text{Relative error (\%)} = \frac{|M_i - Y_i|}{Y_i} \times 100 \tag{3.23}$$

where M_i is the predicted result by LS-SVM and Y_i is the actual value or experimental

Table 3.12 illustrates the relative error for GP model and LS-SVM model calculated with respect to the experimental value.

Table 3.12. Relative error (%) of the GP model and LS-SVM Model

Run Order	Experimental value	LS-SVM Model Prediction	Relative Error (%)	GP Prediction	Relative Error (%)
1	0.6669	0.6741	1.0779	0.6848	2.6796
2	0.4445	0.4829	8.6489	0.4438	0.1476
3	0.6824	0.6660	2.4065	0.6876	0.7613

4	0.7665	0.7097	7.4147	0.7446	2.8573
5	0.5001	0.5221	4.4080	0.5209	4.1543
6	0.556	0.5894	5.9984	0.5370	3.4173
7	0.6217	0.6456	3.8371	0.7210	15.9708
8	0.6953	0.5615	19.2452	0.7162	3.0095
9	0.5001	0.4610	7.8211	0.4630	7.4183
10	0.3333	0.3842	15.2666	0.3631	8.9490
11	0.4788	0.4900	2.3345	0.4951	3.3994
12	0.4055	0.4481	10.4954	0.4743	16.9697
13	0.5001	0.4829	3.4400	0.4964	0.7405
14	0.3332	0.3357	0.7408	0.3348	0.4660
15	0.3333	0.3695	10.8641	0.3312	0.6355
16	0.3333	0.4586	37.5852	0.4175	25.253
17	0.5508	0.6335	15.0110	0.5948	7.9960
18	0.5045	0.6097	20.8514	0.5110	1.2817
19	0.6669	0.6868	2.9794	0.6726	0.8557
20	0.6669	0.6659	0.1505	0.6678	0.1411
21	0.7095	0.6936	2.2429	0.6928	2.3540
22	0.4387	0.5672	29.3000	0.4972	13.3240
23	0.5835	0.5752	1.4242	0.5733	1.7528
24	0.7004	0.7132	1.8230	0.7256	3.5918
25	0.5128	0.5306	3.4641	0.5870	14.4781
26	0.3604	0.4065	12.7904	0.4054	12.4859
27	0.4571	0.5027	9.9761	0.4295	6.0429
28	0.5001	0.5004	0.0537	0.4858	2.8667
29	0.5001	0.5145	2.8856	0.5377	7.5204
30	0.5564	0.5372	3.4556	0.5331	4.1849
31	0.4603	0.4673	1.5303	0.4474	2.7952
32	0.521	0.4905	5.8488	0.5219	0.1823
33	0.5834	0.5738	1.6456	0.5853	0.3222
34	0.5331	0.5475	2.7069	0.5568	4.4419
35	0.518	0.5400	4.2547	0.4939	4.6602
36	0.4803	0.5206	8.3877	0.4897	1.9652
37	0.5578	0.5707	2.3143	0.5580	0.0304
38	0.5235	0.5474	4.5717	0.5086	2.8402
39	0.713	0.6492	8.9472	0.6889	3.3862
40	0.561	0.4864	13.2999	0.5704	1.6827
41	0.5663	0.5343	5.6480	0.5425	4.2038
42	0.5626	0.5881	4.5392	0.5717	1.6170
43	0.6127	0.5911	3.5235	0.5487	10.4394
44	0.5491	0.5324	3.0475	0.5342	2.7095
45	0.5659	0.5643	0.2754	0.5710	0.9065
46	0.5657	0.5643	0.2402	0.5710	0.9422
47	0.5659	0.5643	0.2754	0.5710	0.9065
48	0.5659	0.5643	0.2754	0.5710	0.9065
49	0.5657	0.5643	0.2402	0.5710	0.9422
50	0.5659	0.5643	0.2754	0.5710	0.9065
51	0.5659	0.5643	0.2754	0.5710	0.9065
52	0.5659	0.5643	0.2754	0.5710	0.9065

The comparison graph between GP and LS-SVM technique predicted value shows that the relative error for the GP model is comparatively less (Figure 3.28). Therefore, it can be said that GP model predicts static strength of FDM build parts adequately than LS-SVM model.

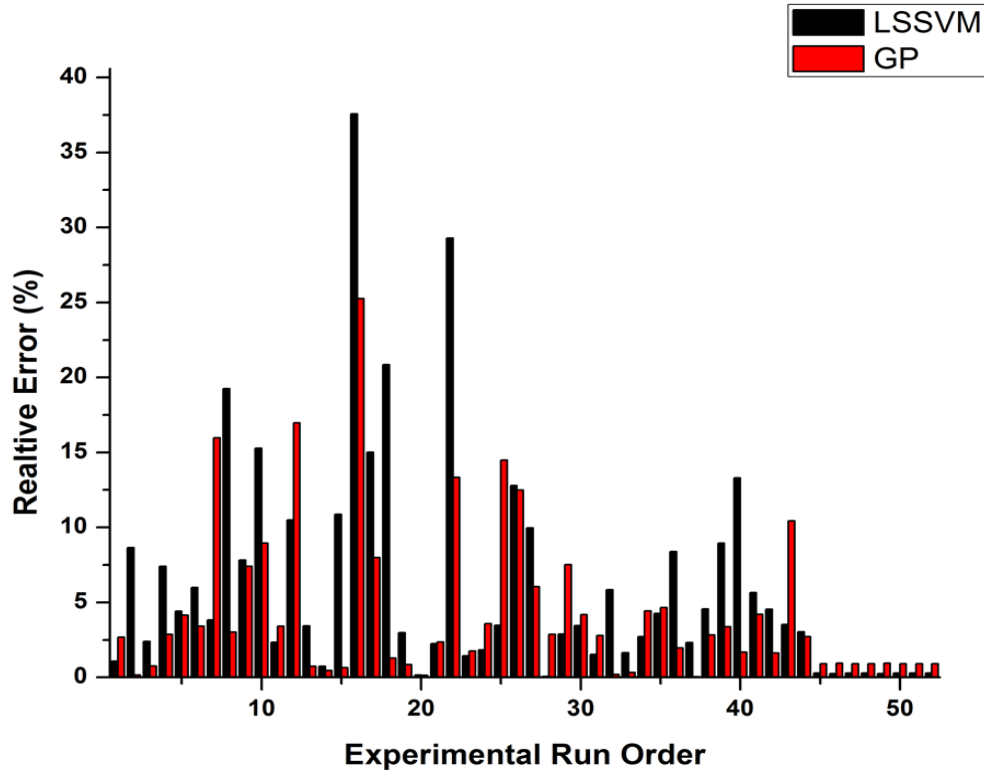


Figure 3.28. Relative error comparison between GP and LS-SVM models for static strength

3.8. Conclusion

This chapter primarily attempts to study the effect of contour number and raster fill pattern on mechanical strength of FDM built specimen along with other controllable parameters viz. layer thickness, raster width, part orientation, raster orientation and air gap. A comparative study is made between the injection moulded ABS parts with the ABS parts manufactured by the FDM route. Generally, the strength of the ABS built parts manufactured by injection moulding process is greater than the parts manufactured by FDM routes due to the absence of voids during injection moulding. The strength values of injection moulded parts are collected from the plastics international data sheet (<http://www.plasticsintl.com/datasheets/ABS.pdf>). The deviation of the strengths from

injection moulded parts to FDM parts considering highest strength in Table 3. 2 is presented in Table 3.13.

Table 3.13. Comparison of strength of injection moulded parts with FDM parts

Sl. No.	Strength	Units	Injection Moulded Parts	FDM Parts (Present study)	Improvement/Decrement in percentage
1.	Tensile	MPa	42	31.3	25.48 (↓)
2.	Compressive	MPa	52	106.8	105.3(↑)
3.	Flexural	MPa	72	66.5	7.6 (↓)

It is observed that flexural of the FDM built parts closely approach to the strengths of the injection moulded parts due to the modification in contour number and raster orientation style resulting in the improvement of bond quality. The compressive strength of the FDM build parts is two times greater than the strength of the moulded parts due to the presence of voids in between rasters resulting in absorption of more energy than the solid parts. The results of the previous research work (Sood et al., 2010) are compared with the current experimental results and the findings are shown in Table 3.14.

Table 3.14. Comparison of results of present study with previous research work

SL. No.	Strength	Units	Sood et al. (2010)	Present study	Improvement in percentage
1.	Tensile	MPa	18.09	31.3	73.02 (↑)
2.	Compressive	MPa	74.4	106.8	43.50 (↑)
3.	Flexural	MPa	39.24	66	68.19 (↑)

It can be observed from Table 3.14 that tensile strength, compressive strength and flexural strength significantly improve from previous study (Sood et al., 2010) simply by modifying contour number and raster fill pattern instead of using default values. Since the FDM process is complex one, it is really challenging to derive the functional relationship between process parameters and mechanical strength using response surface methodology. The surface plots have been analysed exhaustively and following observations have been made:

- Among the six controlling process parameters, contour number seems to be a significant parameter for improving tensile, flexural and the impact strength of specimen built through FDM build route. Addition of contour number (offset contour) to build parts shifts the stress concentration zone towards the centre of the specimen from the outer edge surface resulting in evading premature failure of the built parts.

- An attempt is made to decrease the anisotropic nature of FDM build parts by changing the raster fill pattern in adjacent layers. The raster orientation changes at certain incremental angle with respect to its previously placed raster on the layer below resulting in a strong bond between the rasters.
- Negative air gap between rasters increases the strength but it decreases the part quality and surface quality of the build part. Use of positive air gap between the rasters increases the heat removal by convection process but decreases the mechanical strength due to the generation of voids inside the part. Zero air gap increases the diffusion between rasters and increases the cooling area resulting in a stronger bond which increases the strength and the part quality.
- The involvement of layer number depends on the layer thickness and part orientation. With an increase in the number of layers, the involvement of rapid heating and cooling cycles increases causing decrease in the part strength. The increase in part orientation angle develops a staircase effect resulting in the deterioration of part quality.
- In order to reduce the experimental cost and time, genetic programming and least square support vector machine have been adopted for prediction of static strength of the FDM build parts. A relative error of 4.31% and 6.16% has been obtained respectively

The study also proposes a best parametric combination for simultaneously improving four types of strengths such as tensile, compressive, flexural and impact strength using a recently proposed meta-heuristic known firefly algorithm. The effective search in the optimization landscape is made using exploration and exploitation capability of the algorithm. The study can be extended to analyse thermos-residual stress developed during the sequential deposition of rasters and its impact on mechanical strength.

Chapter 4

Parametric assessment of fatigue life of FDM build parts

4.1. Introduction

The RP process, also known as additive manufacturing (AM) process, is finding its technical ability to face the batch production requirements of manufacturing industries. RP process has been successfully used in last two decades with the prime objective of manufacturing models for design verifications, visualisation and functionality testing of the assembly parts. Among all RP processes, fused deposition modelling (FDM) is widely appreciated for its ability to build 3D complex geometry with reasonable strength directly from computer aided design (CAD) file saved in .stl (stereo lithography) format. Due to the layer-by-layer build mechanism, the FDM process parameters have significant effect on the strength of the build parts (Sood et al., 2010; Croccolo et al., 2013; Onwubolu and Rayegani, 2004). While used as an end use part, FDM build parts are subjected to static as well as dynamic loading. The parametric assessment of static strength has been already explored in the previous chapter (Chapter 3). The behaviour of RP build parts under repetitive cyclic (dynamic) loading resulting in fatigue needs to be established because it affects functionality as well as the durability (Ziemian et al., 2015; Lee and Huang, 2013). Normally, fatigue occurs due to repetitive cyclic loading of the specimen where the loading is just below the static strength of the material. The fatigue of the material is characterised by the rate of failure which is a function of amplitude and frequency of the stress intensity factor. The fatigue life is measured under strain, stress and energy controlled mode (Kallrath et al., 1999; Tao and Xia, 2007b). The fatigue life of acrylonitrile butadiene styrene (ABS) build part has been investigated under stress controlled mode by Ziemian et al. (2015) considering the part orientation as a major process parameter. Since the life cycles of the FDM build parts are below 10^5 cycles, low cycle fatigue (LCF) test are carried out under strained controlled mode for better characterisation of the FDM build parts (ASTM E606). In this direction, present research work focuses on the better understanding of the influence of FDM process parameters on the fatigue life of build parts when subjected to repetitive cyclic loads

Foregoing discussions reveal that static strength of FDM parts have been widely investigated by the researchers (Sood et al., 2010; Gurralla et al., 2014; Wang et al., 2007; Ahn et al., 2002; Croccolo et al., 2013). But estimation of fatigue life is not adequately addressed to assess the long term durability and sustainability of the FDM build parts. Therefore, in this chapter, experiments are conducted based on face centred central composite design (FCCCD) of response surface methodology (RSM) considering six FDM process parameters namely contour number, layer thickness, raster width, part orientation, raster angle and air gap to evaluate the fatigue life of the build specimen. Effect of cyclic loading, like failure of rasters, rapture of adhesive bond between rasters, formation of crack and crack propagation inside the build part are analysed from the scanning electron microscope (SEM) micrographs and broken samples. In order to establish a clear relationship between process parameters and fatigue life of the FDM build part, a statically valid empirical model is developed. From analysis of variance (ANOVA) table, the significance of process parameters is analysed. Finally, a nature inspired meta-heuristic known as firefly algorithm is applied to obtain a best parametric combination for the improvement of fatigue life of the FDM build part. To predict the Fatigue life, two latest artificial intelligence techniques known as genetic programming (GP) and least square support vector machine (LS-SVM) have been adopted. The prediction model enables to predict the performance measures with reasonable accuracy so that costly experimental time can be minimized.

4.2. Experimental plan

The durability and life span of the build part depends upon the type of loading and on the material quality. While used as a functional part, the life span of the build part is badly affected by the induced fatigue strain. The fatigue mechanism states that the fatigue occurs due to the application repetitive or cyclic stresses on a body. Fatigue is also known as progressive fracture mechanism because when a crack is initiated it goes on increases further with the number of cycle. Normally, material loading is classified in to two types i.e. monotonic and cyclic. Both monotonic and cyclic tests are used to characterise the mechanical properties of metal, composites and polymers. The cyclic test apply oscillating loads until the fracture of the specimen occurs. The cyclic load may include either cyclical tension, compression or a combination of both. In case of fatigue test, the applied load should be low enough so that the specimen will not break at a single cycle. The fatigue test is divided into two type such as low cycle and high cycle considering the sustainable

life cycle of the specimen. Materials having life cycle above 10^5 is known as high cycle fatigue (HCF) and below known as low cycle fatigue (LCF). Since the plastics, composites and polymer cannot sustain more than 10^5 cycles, LCF test are conducted to characterise the material properties. So far as LCF tests are concerned, it gives better results when it is operated in strain control mode. In the strain controlled fatigue test, result plays a vital role in the field of mechanical design, material research, product development and failure analysis. Before experimentation, the static tensile strength of the material should be measured. Considering the ASTM D638 standard, five sets specimens of each experimental runs are tested to measure the average stress at break. The frequency for plastic must be limited to about 3 Hz in order to prevent premature failure due to heat built up inside the specimen (Driscoll, 2004). All fatigue test are conducted according to the ASTM E606 (standard test method for strain controlled fatigue testing) standard procedure. All tests are conducted at zero strain ratio (R) means the specimen are subject to tension followed by relaxation. The term R is the ratio between mean strain (ϵ_m) and strain amplitude (ϵ_a). The area under stress strain curve during loading is defined as the strain energy per unit volume induced into the specimen. Subsequently, the area under the unloading curve is the energy released by the specimen (Ziemian et al., 2015). These two stress strain curves and the respective areas are equal for perfectly elastic material and more complex for non-perfectly elastic material. These loading and unloading curves between stress and strain give rise to the formation hysteresis loop. Considering six FDM process parameters, specimens are manufactured according to ASTM D638 standard using a face centred central composite design (Table 3.2) approach and tensile tests are conducted. The experimental data on tensile test reveals that tensile strength of the FDM build parts largely depends on input process parameters setting. It is clear from the table that tensile strength lies between 14.56- 31.34 MPa (Table 4.2). This indicates the material property of the specimen is severely influenced by input parameters due to FDM build mechanism for static tensile strength. It is corroborated that variation of input process parameter may also affect the fatigue life of the FDM build part. Therefore, Low cycle fatigue test under fully reversed strain controlled mode is selected to determine the fatigue life of the build parts manufactured in adherence to parameter setting suggested by face centred central composite design of design of experiment (DOE) approach. Among all experimental runs, run order 18 and 23 having tensile strength 26.92 and 19.62 MPa are chosen for analysis of fatigue life of the FDM build part.

For accurate prediction of fatigue life of the FDM build part, a suitable damage parameter is needed. The relation between fatigue life and damage parameter can be expressed as suggested by Tao and Xia (2007a) (equation 4.1).

$$\Psi = k.(N_f)^\gamma + \Psi_0 \quad (4.1)$$

where Ψ denotes the damage parameter and N_f represents the total number of cycles undergone before failure. The terms k and γ are material constants. The fatigue limit is denoted by Ψ_0 . Normally, the fatigue test are classified into three categories i.e. stress based, strain based and energy based approach depending upon the type damage parameter considered for experimentation (Ellyin, 1997). One common stress/strain function is introduced including the damage parameter for the evolution of stress/strain effect. The mean stress function in the form of power law for epoxy resin proposed by Kujawski and Ellyin (1995) and Tao and Xia (2007b) is given below (equation 4.2).

$$f\left(\frac{\sigma_m}{\sigma_a}\right) = \left(1 + \eta \frac{\sigma_m}{\sigma_a}\right)^n \quad (4.2)$$

where σ_m and σ_a represents the mean stress and stress amplitude. The term η and n are material constants. Similarly, the mean strain function can be written as

$$f\left(\frac{\varepsilon_m}{\varepsilon_a}\right) = \left(1 + \eta \frac{\varepsilon_m}{\varepsilon_a}\right)^n \quad (4.3)$$

where ε_m and ε_a represents the mean strain and strain amplitude. The equivalent damage parameter (Ψ) including the mean strain function is defined in equation 4. 4.

$$\varepsilon_{eq} = \left(1 + \eta \frac{\varepsilon_m}{\varepsilon_a}\right)^n \varepsilon_a \quad (4.4)$$

For fully reverse cycles i.e. tension followed by compression loading the mean strain is equal to zero ($\varepsilon_m = 0$). Thus, equation 4. 4 becomes $\varepsilon_{eq} = \varepsilon_{-1}$, here the subscript -1 represents fully reversed cycle test. In case of strain approach, the equivalent damage parameter can be clearly understood if the tests are conducted under fully reversed mode. No mean strain effect exists in the fully reversed fatigue tests. Using statistical software Systat version 12, a nonlinear equations are developed relating strain amplitude (ε_a) and fatigue life (N_f). The equation are generated by the regression analyses of the best fitting curve (Figure 4.7 and Figure 4.8) drawn for the run order 18 and 23 having R -square value 0.861 and 0.993 respectively.

$$\varepsilon_{eq} = 0.584.N_f^{-0.051} + 0.5\% \quad (\text{For run order 18}) \quad (4.5)$$

$$\varepsilon_{eq} = 2.071.N_f^{-0.432} + 0.5\% \quad (\text{For run order 23}) \quad (4.6)$$

It can be observed from equation 4. 6 and 4. 7 that the equivalent strain (ε_{eq}) of the build part varies along with the selection set of parameter setting. Hence, the material properties of FDM build parts vary along with the selection set of parameters setting. For the test within mean strain, the equation 4. 5 can be written as:

$$\frac{\varepsilon_a}{\varepsilon_{eq}} = \frac{1}{f\left(\frac{\varepsilon_m}{\varepsilon_a}\right)} \quad (4.7)$$

FDM is one of the proficient RP processes that produces 3D complex models by depositing heated filament one over another. Materials from the extruded nozzle are placed accordingly as defined by the machining software (Insight 10.2). The semi-melted plastic rapidly solidifies to chamber temperature (95°C), which develops thermos-residual stress inside the build part causing adverse effect on build part. Since FDM is a parametric controllable process, the strength and part quality are severely influenced by the process parameters. Among all FDM parameters, six controllable process parameters such as contour number, layer thickness, raster width, part orientation, raster angle and air gap are considered to study their effect on FDM build parts experimentally. Other process parameters such as part fill style, contour width, shrinkage factor, part interior style, delta angle and perimeter to raster gap are kept constant. The process parameters considered for experimental purpose are selected as described in Table 3.1.

FDM build part exhibits anisotropic effect when rasters are placed in a single direction. To decrease the anisotropic effect to some extent, filaments are deposited in a crisscross manner known as default raster fill pattern style. Furthermore, the potentiality of the machine is explored in this research to modify the raster fill pattern so as to decrease the anisotropic effect. The raster fill pattern controlled by delta angle is modified in such a manner that the raster angle will change at an incremental angle of 30° to its previously placed rasters in the adjacent layer (Figure 3. 4). By changing the raster orientation at an incremental angle, FDM will place the rasters on the build platform in all direction with respect to the z- axis.

In order to develop an empirical model for fatigue life of the FDM build parts, experiments are conducted based on face centred central composite design (FCCCD) of response surface methodology (RSM). 11. Parameters and their levels are considered as shown in Table 3.1 for experimental purpose. For determining the fatigue life of FDM build parts, specimens are manufactured in accordance with ASTM D638 standard (Figure 4.1). Specimens are fabricated using FDM FORTUS 400mc (manufactured by Stratasys, USA)

for the fatigue life measurement of the FDM build parts (Figure 3. 10). Specimens are designed using CATIA V5 R21 software and saved in .stl format for importing to the machine. The .stl file then imported to FDM machine software i.e. insight 10. 2 to set the controllable machining parameter. The material used for fabrication of test specimen is acrylonitrile butadiene styrene (ABS). ABS is a widely used plastic for manufacturing of low cost and end use parts having high strength and stiffness. Further, ABS plastic can be used for production of prototypes due to its exceptional dimensional stability and reasonable strength. ABS is a combination of monomeric chemical acrylonitrile butadiene and styrene in presence of carbon hydrogen and nitrogen. ABS is a carbon chain copolymer and belongs to styrene ter-polymer chemical family. It is made by dissolving butadiene-styrene copolymer in a mixture of acrylonitrile and styrene monomers and then polymerizing the monomers with free-radical initiators. Its three structural units provide a balance of properties with the acrylonitrile providing heat resistance, butadiene imparting good impact strength and the styrene gives the copolymer its rigidity. All tests are conducted using a temperature controlled servo hydraulic testing machine manufactured by Bangalore Integrated System Solutions, India (BISS) (Figure 4.2). For strain controlled fatigue, the setup is listed below:

Parameter	Setting	Parameter	Setting
Gauge length	57mm	Strain Amplitude	0.5%
Modulus	4.463 GPa	Minimum Strain	0
Poisson's ratio	0.33	Frequency	2 Hz
Gauge Section	91 mm ²	Warm up stress	1 MPa

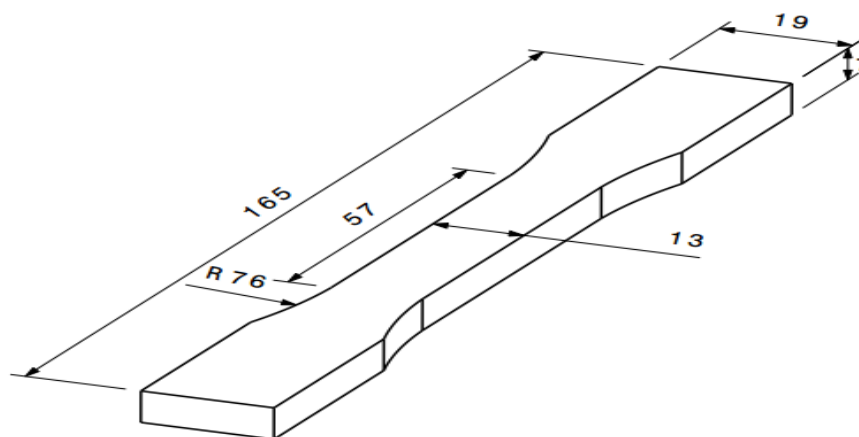


Figure 4.1. ASTM standard specimen for strain controlled fatigue test



Figure 4.2. BISS machine (Bangalore Integrated System Solutions)

4.3. Results and Discussions

All tests are carried out at normal ambient temperature 23 ± 2 °C and relative humidity $50 \pm 10\%$ as per ASTM D618 standard. For each experimental run, three samples have been tested and the average values are listed below in Table 4. 1.

Table 4.1. Experimental results

Sl. No.	Factors in Coded Form						Static Loading	Dynamic Loading				
	A	B	C	D	E	F	Tensile Strength (MPa)	Mean strain (ϵ_m) %	Strain amplitude (ϵ_a) %	Mean Strain ratio (R_m)	Stress amplitude (σ_a) MPa	Number of Cycles (N f)
1	-1	-1	-1	-1	-1	-1	25.77	0.01	0.48	0	0.20	21804
2	1	-1	-1	-1	-1	1	23.57	0.01	0.50	0	-2.33	16990
3	-1	1	-1	-1	-1	1	20.28	0.01	0.48	0	-2.25	8353
4	1	1	-1	-1	-1	-1	31.34	0.00	0.49	0	-2.78	29570
5	-1	-1	1	-1	-1	1	20.50	0.00	0.50	0	0.05	6678
6	1	-1	1	-1	-1	-1	27.74	0.00	0.50	0	2.84	17012
7	-1	1	1	-1	-1	-1	26.45	0.00	0.50	0	0.77	13532
8	1	1	1	-1	-1	1	24.99	0.00	0.49	0	0.57	8811
9	-1	-1	-1	1	-1	1	14.56	0.01	0.47	0	-3.71	6394
10	1	-1	-1	1	-1	-1	19.84	0.00	0.50	0	0.36	26472
11	-1	1	-1	1	-1	-1	24.72	-0.01	0.49	0	9.69	17585
12	1	1	-1	1	-1	1	20.03	-0.01	0.45	0	1.80	16287
13	-1	-1	1	1	-1	-1	19.29	0.00	0.50	0	-0.35	5761
14	1	-1	1	1	-1	1	19.29	0.00	0.45	0	0.06	7159
15	-1	1	1	1	-1	1	15.22	0.00	0.50	0	0.28	3525
16	1	1	1	1	-1	-1	22.36	0.03	0.49	0	1.45	18347
17	-1	-1	-1	-1	1	1	18.44	0.00	0.50	0	2.33	19011
18	1	-1	-1	-1	1	-1	26.92	0.00	0.50	0	1.33	10624
19	-1	1	-1	-1	1	-1	29.05	0.01	0.49	0	2.74	7576
20	1	1	-1	-1	1	1	22.37	0.00	0.50	0	0.22	9278

21	-1	-1	1	-1	1	-1	25.87	0.00	0.50	0	-0.92	11973
22	1	-1	1	-1	1	1	25.10	0.00	0.50	0	-1.13	15281
23	-1	1	1	-1	1	1	19.62	0.00	0.49	0	0.37	12085
24	1	1	1	-1	1	-1	29.05	0.00	0.50	0	-0.18	6172
25	-1	-1	-1	1	1	-1	21.92	0.02	0.47	0	-2.12	8333
26	1	-1	-1	1	1	1	17.10	0.00	0.50	0	2.01	6369
27	-1	1	-1	1	1	1	17.56	0.01	0.50	0	-3.44	8319
28	1	1	-1	1	1	-1	25.13	0.02	0.44	0	-1.99	3343
29	-1	-1	1	1	1	1	17.53	0.00	0.50	0	0.32	10264
30	1	-1	1	1	1	-1	21.37	0.00	0.50	0	-0.55	3341
31	-1	1	1	1	1	-1	23.79	0.01	0.50	0	-0.67	3343
32	1	1	1	1	1	1	21.34	0.00	0.50	0	0.18	3342
33	-1	0	0	0	0	0	22.80	0.00	0.50	0	2.39	3344
34	1	0	0	0	0	0	26.31	0.02	0.49	0	-1.33	3345
35	0	-1	0	0	0	0	23.13	0.00	0.50	0	0.20	3340
36	0	1	0	0	0	0	23.79	0.01	0.48	0	-7.78	3343
37	0	0	-1	0	0	0	23.57	0.00	0.50	0	-0.34	4630
38	0	0	1	0	0	0	24.23	0.00	0.49	0	0.47	2445
39	0	0	0	-1	0	0	25.78	0.00	0.50	0	-2.96	5836
40	0	0	0	1	0	0	22.25	0.00	0.50	0	0.15	3439
41	0	0	0	0	-1	0	23.32	0.01	0.49	0	-2.26	6151
42	0	0	0	0	1	0	23.46	0.00	0.50	0	1.85	3330
43	0	0	0	0	0	-1	26.89	0.00	0.50	0	-0.09	4418
44	0	0	0	0	0	1	21.48	0.00	0.50	0	2.92	3367
45	0	0	0	0	0	0	24.78	0.00	0.50	0	1.57	3127
46	0	0	0	0	0	0	24.98	0.00	0.45	0	0.80	3170
47	0	0	0	0	0	0	23.63	0.00	0.49	0	0.22	3120
48	0	0	0	0	0	0	23.45	0.00	0.48	0	0.16	2961
49	0	0	0	0	0	0	24.98	0.01	0.49	0	1.10	3084
50	0	0	0	0	0	0	23.55	0.02	0.46	0	0.34	3181
51	0	0	0	0	0	0	24.77	0.00	0.49	0	1.09	3285
52	0	0	0	0	0	0	23.55	0.01	0.48	0	0.37	3296

Figure 4.3 shows that the failure of FDM build specimen after static tensile test. From the Figure, it can be clearly observed that the failure of raster is in a single plane perpendicular to the applied force. However, in case of dynamic loading the failure occurs in a zig-zag manner because failure of rasters leads to the formation of crack and it propagates with the increase in the number of cycles (Figure 4.4)

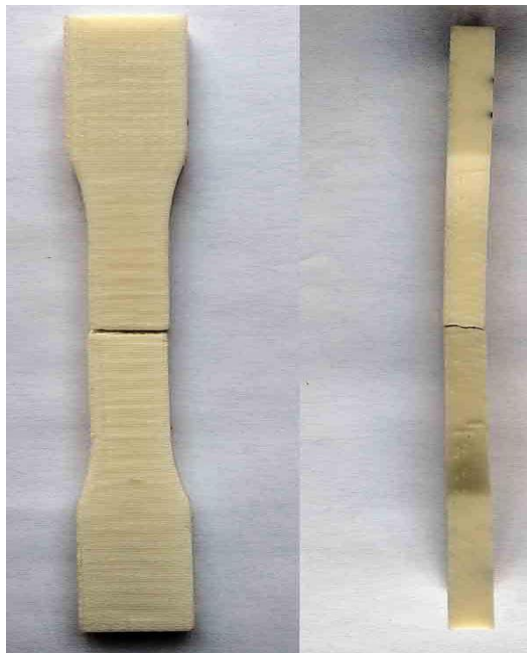


Figure 4.3. Failure of FDM build parts under static loading

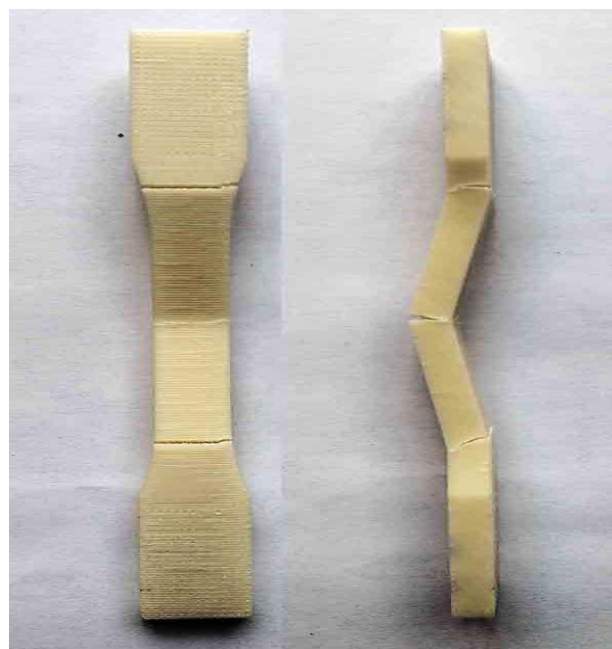


Figure 4.4 Failure of FDM build parts under dynamic loading

For strain controlled fatigue testing, the plot between strain amplitude and life cycles for run order 18 and 23 show that the strain amplitude decreases gradually with an increase in number of cycles (Figure 4.5 and Figure 4.6). Similar curves have been obtained for other experimental run order. The empirical model shown in the Figure varies with experimental run order because parametric setting is different in each run order. It can be observed that the strain amplitude decreases rapidly with respect to the load cycles at the beginning of the experiment but after some cycles, the strain amplitude remains constant due to softening of the material. All the experiments are conducted below the plastic limit of the material to avoid the failure at a single cycle.

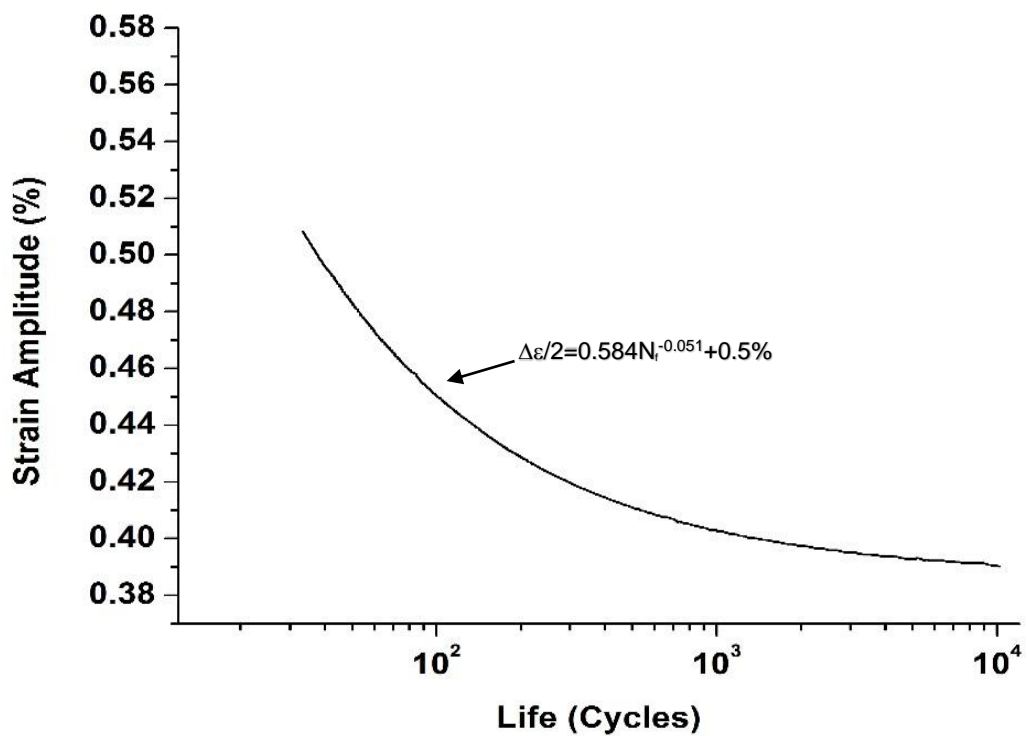


Figure 4.5. Strain amplitude vs fatigue life curve for strain controlled fatigue test (ϵ -Nf) for run order 18

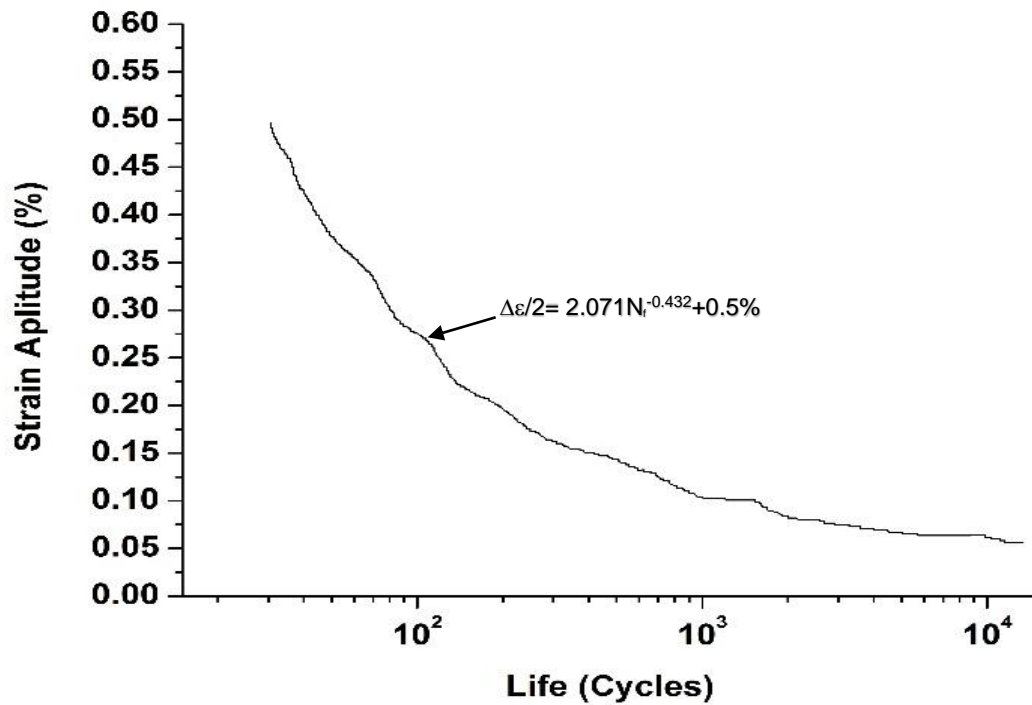


Figure 4.6. Strain amplitude vs fatigue life curve for strain controlled fatigue test (ϵ -Nf) for run order 23

From the stress-strain (hysteresis loop) curves, it can be concluded that the specimen suffers enough damage which leads to its failure (Figure 4.7 and Figure 4.8). During the cyclic loading, the material suffers both plastic and elastic strain. The total sum of these two strains is referred as total strain. The area under the stress strain curve up to fracture is termed as modulus of toughness, which is the energy needed to completely fracture the material (Roylance, 2001). Generally, when the plastic or polymers are stressed, a light colour or greyish region is generated known as crazing effect. The crazing effect occurs when the plastic deformation of a region is generated in a direction perpendicular to the applied force, which results in the formation of micro voids (Zhang et al., 2009).

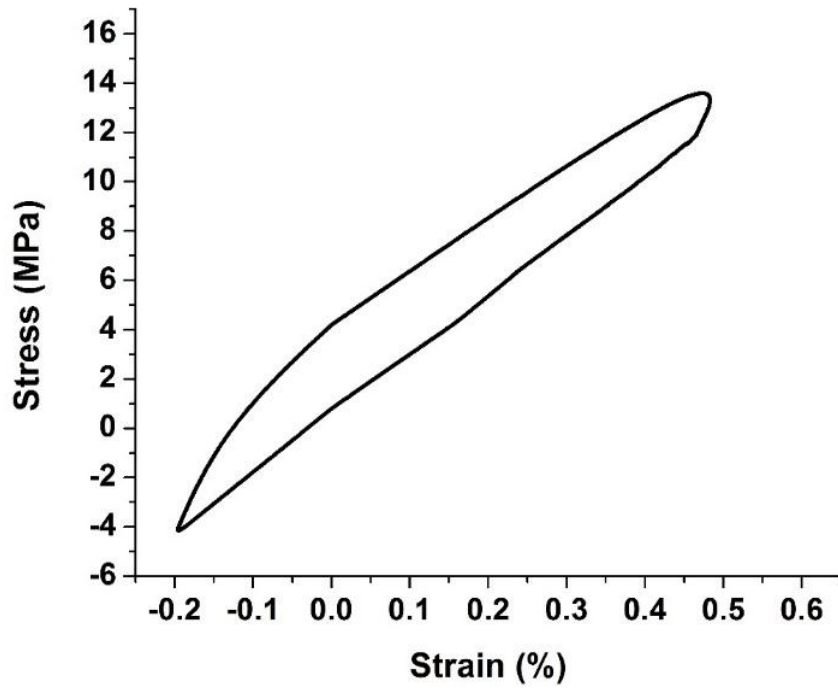


Figure 4.7. Stress strain-curve for fatigue test for run order 18

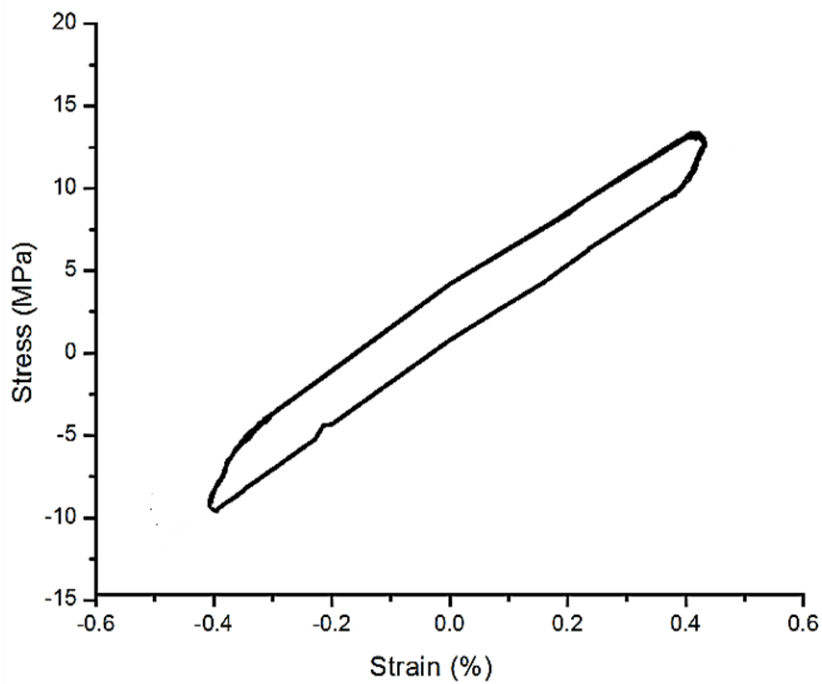


Figure 4.8. Stress strain-curve for fatigue test for run order 23

Due to the complexity of the problem, a full quadratic model is attempted for suitably explaining the performance of fatigue life. In this present context, experimental data obtained using FCCCD design runs are fitted with following empirical model (equation 4.8).

$$y = \beta_0 + \sum_{i=1}^k \beta_i x_i + \sum_{i=1}^k \beta_{ii} x_i^2 + \sum_{i < j} \beta_{ij} x_i x_j \quad (4.8)$$

where y is the performance measure and x_i and x_j are i^{th} and j^{th} factor respectively, k is the total number of factors. Analysis of variance (ANOVA) is conducted as shown in Table 4.2 and the parameters, their interactions and square terms having p value less than 0.05 are considered as significance. The significant terms are contour numbers (A), layer thickness (B), raster width (C), part orientation (D), raster angle (E), air gap (F), interactions between contour number and raster angle (A×E), layer thickness and part orientation (B×D), layer thickness and raster angle (B×E), raster width and raster angle (C×E), raster width and air gap (C×F), part orientation and raster angle (D×E), raster angle and air gap (E×F) and square of part orientation (D^2) and raster angle (E^2). The coefficient of determination (R^2), which indicates the percentage of variation explained by the terms in the model to the total variation in the response is 0.9766 for fatigue life. Residual analysis has been carried out and found that residuals are normally distributed (Figure 4.9). It is to be noted from the Table 4.2 that lack of fit is not significant. The model for fatigue life involving all the terms is shown in equation 4.9.

$$\begin{aligned} \text{Fatigue life} = & 96555.64410 + 1113.72479 \times A - 96780.16583 \times B - \\ & 2.41144 \times 10^5 \times C - 472.80392 \times D - 429.83562 \times E - \\ & 3.84238 \times 10^5 \times F + 1604.02961 \times A \times B - 1927.91667 \times A \times C \\ & + 8.76042 \times A \times D - 41.75521 \times A \times E - 9895.42323 \times A \times F + \\ & 40427.63158 \times B \times C + 657.73026 \times B \times D - 541.0910 \times B \times E - \\ & 1.99020 \times 10^5 \times B \times F - 176.61111 \times C \times D + 771.91667 \times C \times E + \\ & 3.60400 \times 10^5 \times C \times F - 1.67542 \times D \times E - 253.44488 \times D \times F + \\ & 4311.43373 \times E \times F + 212.92164 \times A^2 + 1.46933 \times 10^5 \times B^2 + \\ & 1.85722 \times 10^5 \times C^2 + 9.53194 \times D^2 + 2.49743 \times E^2 \\ & + 2.16952 \times 10^6 \times F^2. \end{aligned} \quad (\text{Uncoded form}) \quad (4.9)$$

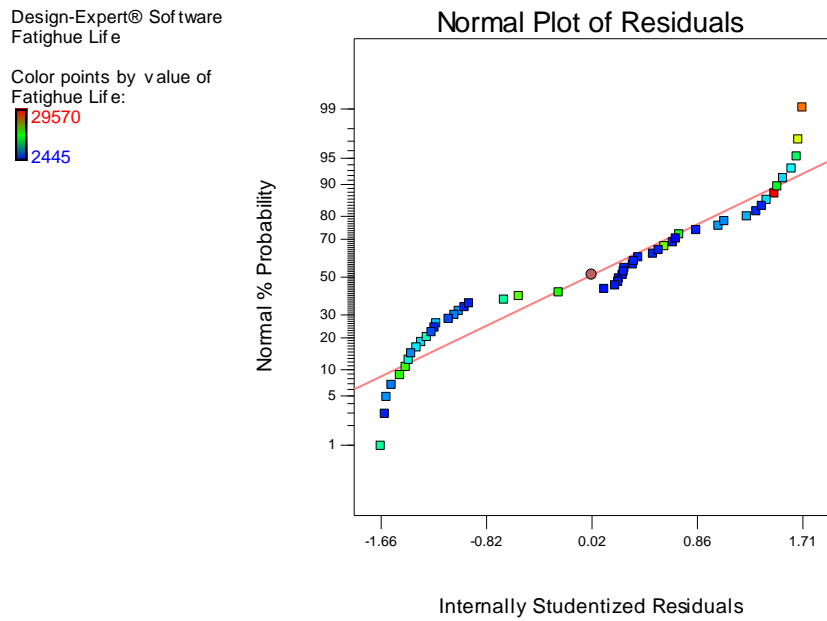


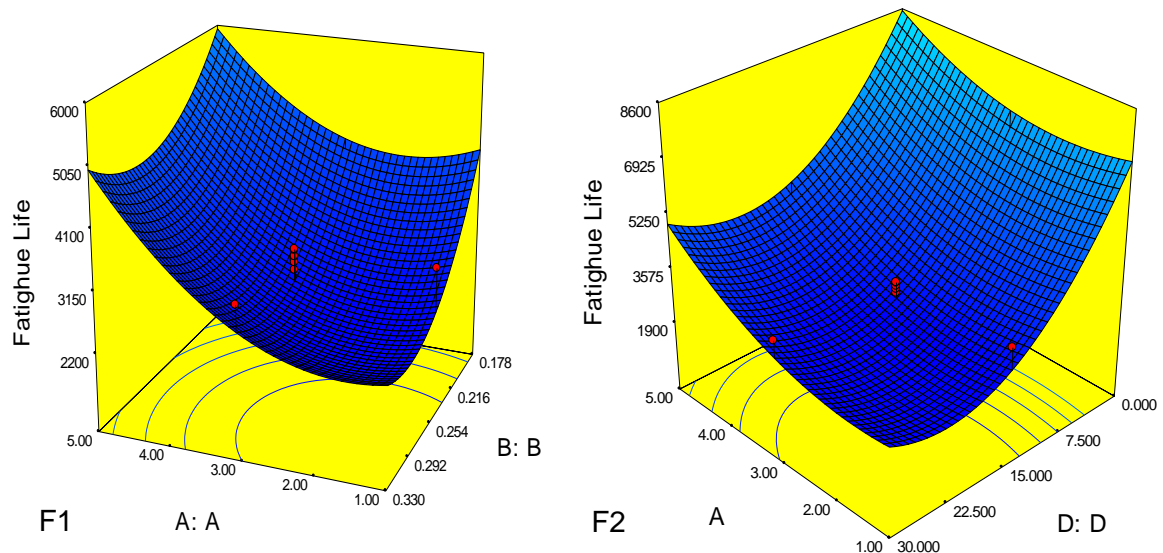
Figure 4.9 Normal probability plot of residual at 95% confidence interval for fatigue life

Table 4.2. ANOVA for fatigue life

Source	Sum of Squares	df	Mean Square	F Value	p-value Prob > F
Model	2.15E+09	27	79456475	37.16871	< 0.0001
A	3.37E+07	1	33726552	15.77685	0.0006
B	1.69E+07	1	16934118	7.921562	0.0096
C	1.52E+08	1	1.52E+08	71.06051	< 0.0001
D	1.40E+08	1	1.4E+08	65.43372	< 0.0001
E	2.30E+08	1	2.3E+08	107.6305	< 0.0001
F	6.69E+07	1	66900654	31.29526	< 0.0001
AxB	1.90E+06	1	1902225	0.889836	0.3549
AxC	2.68E+06	1	2676141	1.251864	0.2743
AxD	2.21E+06	1	2210253	1.033928	0.3194
AxE	2.01E+08	1	2.01E+08	93.95546	< 0.0001
AxF	8.09E+06	1	8086231	3.782635	0.0636
BxC	1.70E+06	1	1699246	0.794885	0.3815
BxD	1.80E+07	1	17991001	8.415958	0.0078
BxE	4.87E+07	1	48703515	22.78288	< 0.0001
BxF	4.72E+06	1	4723201	2.209453	0.1502
CxD	1.26E+06	1	1263255	0.590934	0.4496
CxE	9.65E+07	1	96528565	45.15482	< 0.0001
CxF	1.51E+07	1	15083778	7.055997	0.0138
DxE	1.82E+07	1	18189496	8.508812	0.0076
DxF	2.98E+05	1	298378.1	0.139577	0.7120
ExF	3.45E+08	1	3.45E+08	161.5666	< 0.0001

A ²	1.73E+06	1	1729475	0.809026	0.3773
B ²	1.72E+06	1	1717313	0.803337	0.3790
C ²	2.60E+06	1	2602117	1.217237	0.2808
D ²	1.10E+07	1	10966863	5.130157	0.0328
E ²	1.20E+07	1	12045539	5.634748	0.0260
F ²	4.67E+06	1	4671070	2.185066	0.1524
Residual	5.13E+07	24	2137725		
Lack of Fit	5.12E+07	17	3013121	256.168	< 0.0801
Pure Error	8.23E+04	7	11762.29		
Cor Total	2.20E+09	51			

From the surface plots (Figure 4.10 F1-F3), it can be observed that the fatigue life increases with an increase in contour number (A) because increase in the contour number shifts the stress concentration zone from outer edge to the centre of the specimen resulting increase in strength and stiffness of the build part (Ahn et al., 2002; Croccolo et al., 2013). Figure 4.10 F2 and F4 reveal that the fatigue life increases with decrease in part orientation (D). In fact, increase in part orientation angle (D) results an increase in number of layer required for part building. Simultaneously involvement of number of heating and cooling cycle increases resulting an increase in residual stress inside the build part. Accumulation of residual stress inside the build part adversely affects the strength. With an increase of air gap (F), the fatigue life of the build part decreases (Figure 4.10 F3 and F4) because an increase in air gap give rises to the formation of voids inside the build part resulting a decrease in part strength (Sood et al., 2010).



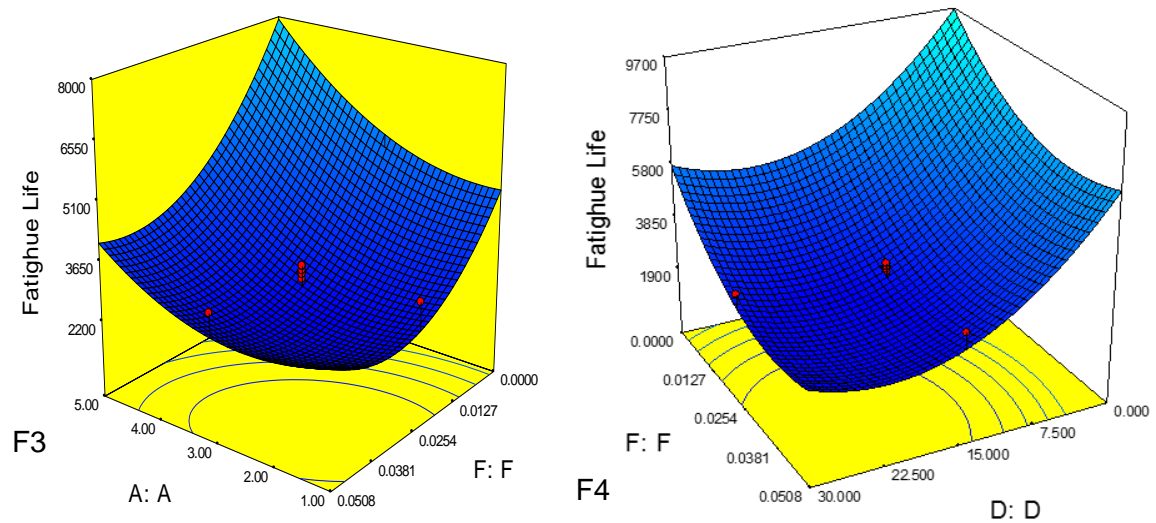


Figure 4.10 Surface plots for fatigue life

Generally, the fatigue life is influenced by four factors such as microstructure of the material, particle size, surface roughness and frequency. The microstructure and particle size hardly influence fatigue life because homogenous material like ABS plastic has been used throughout the experimentation. However, surface roughness of the FDM build part is affected by part orientation and layer thickness. The surface roughness of the build part increases with an increase in part orientation (D) and layer thickness (B) because increase in these process parameters increase the staircase effect on the build part (Mahapatra et al., 2012). The stress concentration increases in the build part due to the stair case effect and results decrease in the fatigue life. Therefore, fatigue life increases when parts are built with setting of minimum value of layer thickness and part orientation. Increase in cycling frequency increase the heat accumulation inside the build part. In order to avoid premature failure of the FDM build parts, the frequency is limited to 3Hz throughout the experimentation (Driscoll, 2004).

From scanning electron microscope (SEM) images (Figure 4.11-4.14), the failure of rasters can be clearly observed. Under static loading condition, the failure occurs at a plane perpendicular to the applied load (Figure 4.11) but the failure occurs in a zigzag manner in cyclic loading due to rupture of weakest raster (Figure 4. 12). In case of static loading conditions, the rasters are subjected to uniaxial tension but rasters are subjected to both tension and compression in case of repetitive cycle loading giving rise to residual stresses. The residual stress accumulates near the raster and leads to rupture. Rupturing of rasters weaken the raster bonds between inter- and intra-layer rasters (Figure 4.13).

Rupture of rasters create cracks inside the build part and propagates with an increase in the number of cycles (Figure 4.14).

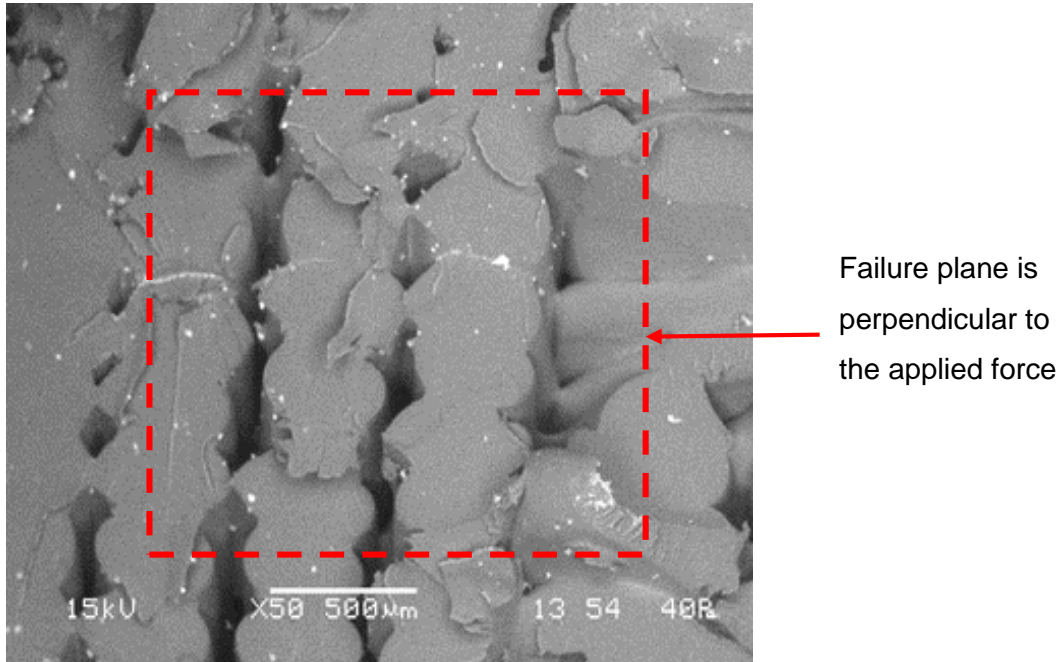


Figure 4.11. Raster failure during static loading

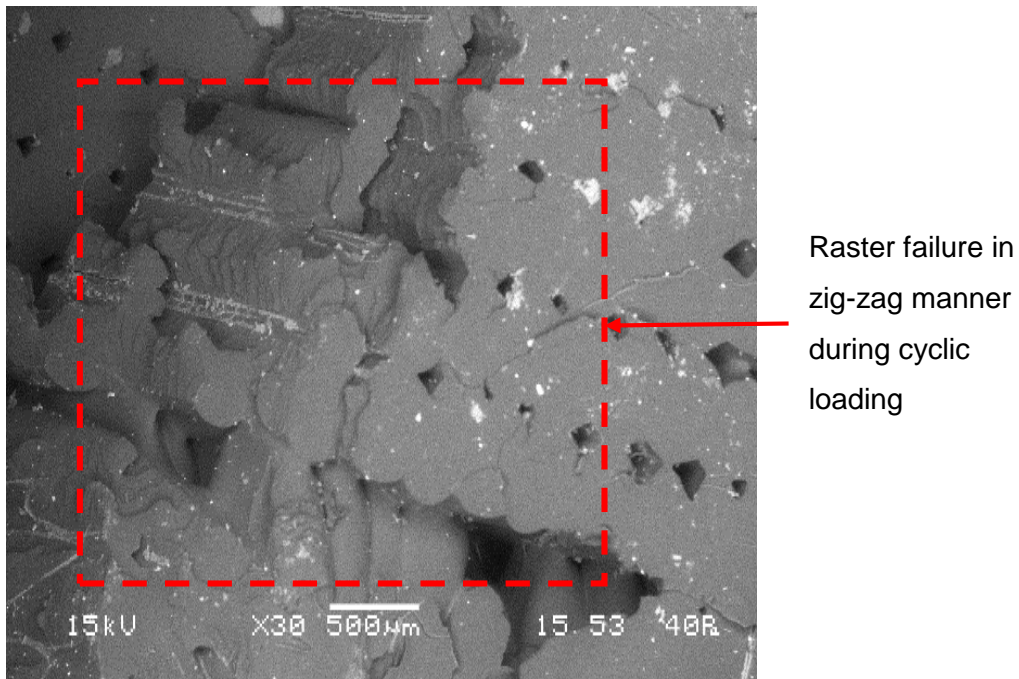


Figure 4.12 Raster failure in zig-zag manner during cyclic loading

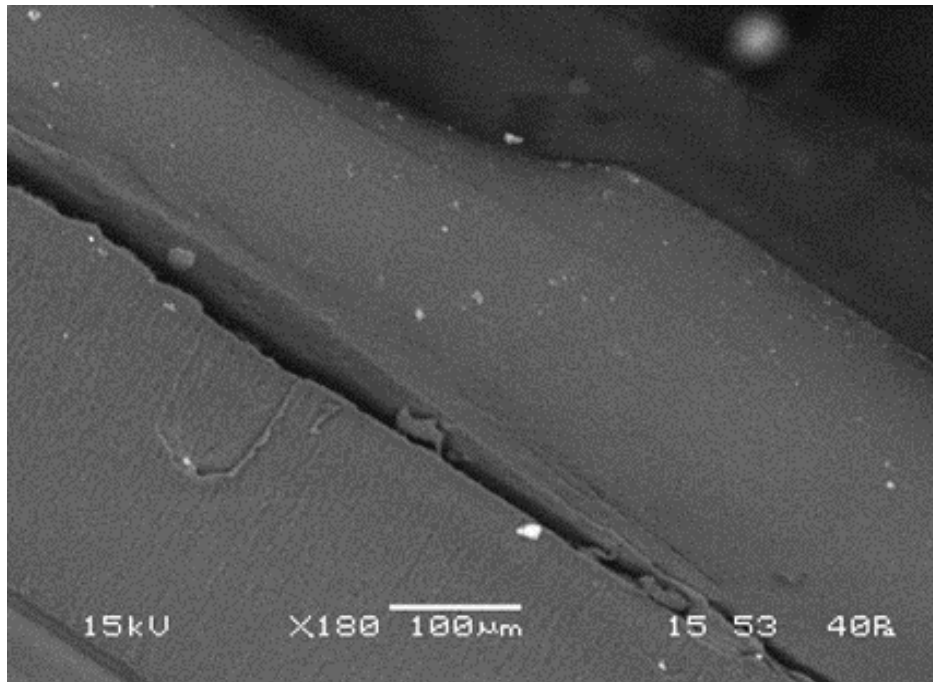


Figure 4.13 Rupture of adhesive bond during cyclic loading

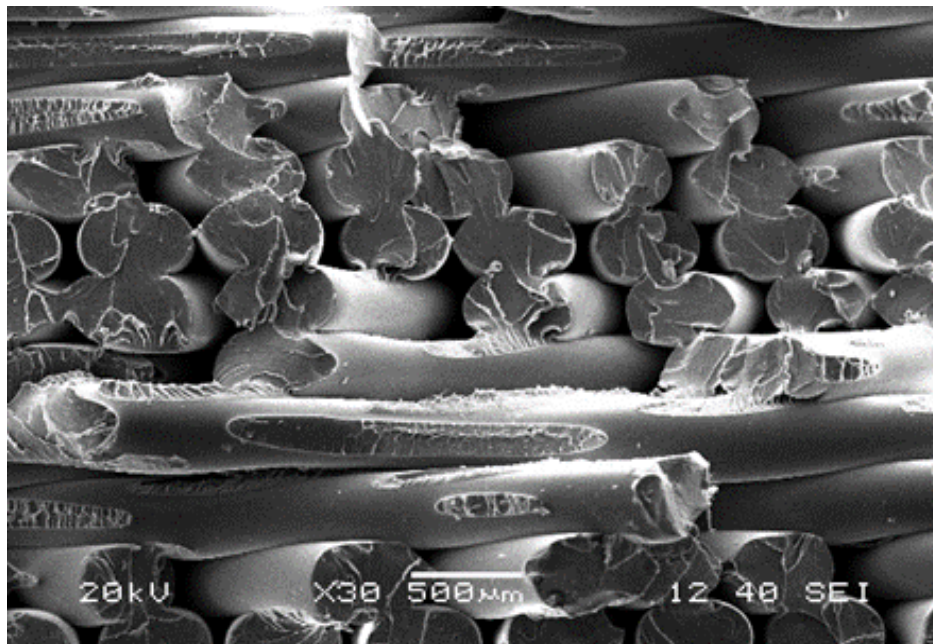


Figure 4.14 Crack formation during cyclic loading

To achieve the optimum solution or to achieve the best parameter setting, a nature inspired metaheuristic known as firefly algorithm is applied. The objective function used in the firefly optimisation algorithm is empirically developed using non-linear regression analysis relating fatigue life values shown in Table 4. 1 and process parameters. The

objective function used in the firefly algorithm is the empirical models developed using regression analysis, relating process parameters and fatigue life. (equation 4.9).

For the firefly algorithm, the values considered are: number of fireflies (n) = 20, number of iterations (N) = 50, attractiveness (β) = 0.9, randomisation (α) = 0.2 and absorption coefficient (γ) = 1. Hence, the total number of function evaluations is 1000. The firefly algorithm provides a parameter setting to get optimum value of the fatigue life as shown in Table 4.3.

Table 4.3. Optimum parameter setting to achieve the best fatigue life

A	B	C	D	E	F	Fatigue Life (N)
4.82	0.192	0.4124	1.267	4.317	0.0012	33287

In the present study, GP is applied to develop a model relating FDM process parameters with fatigue life. From the experimental results, 80% data are taken are considered for training purpose and rest data are considered for testing purpose. Six input parameters such as contour number (x_1), layer thickness (x_2), raster width (x_3), part orientation (x_4), raster angle (x_5) and air gap (x_6) are considered for modelling purpose. The output parameter fatigue life is considered as the performance characteristic. The performance of GP model is measured in terms of MAPE. The diagram involving GP technique for the modelling of fatigue life of the FDM build part is shown in Figure 4. 15.

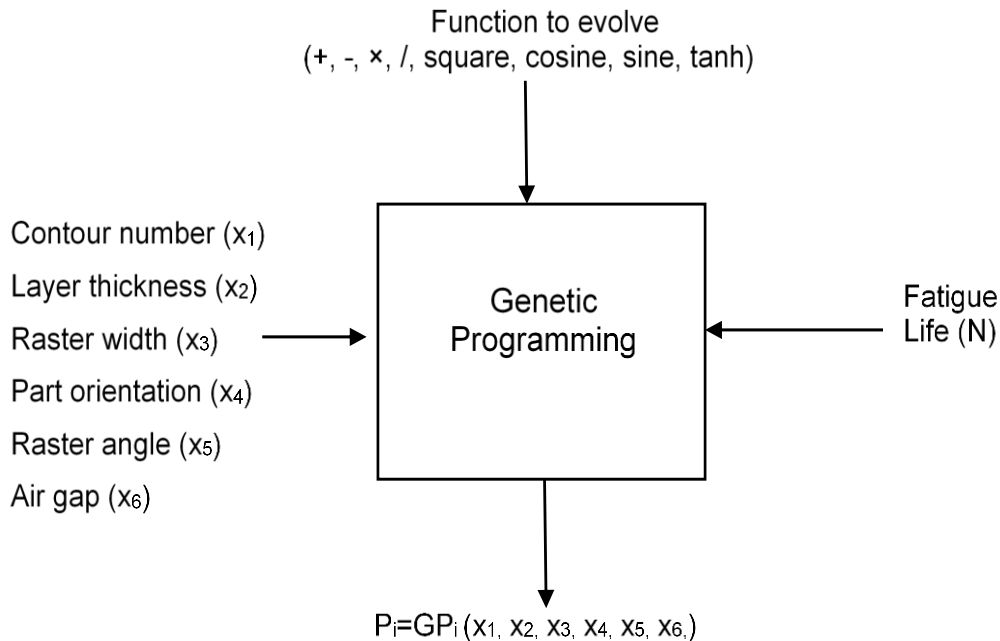


Figure 4.15. Diagram of GP formulation of Wear of FDM built parts

The parameter setting for GP determined through several trail and experimental runs are shown below in Table 4. 4.

Table 4.4. Parameter setting for genetic programming	
Parameters	Value Assigned
Population size	50
Number of generations	1000
Maximum depth of tree	5
Maximum generation	45
Functional set	Multiply, plus, minus, divide, square, cosine, sine, tanh
Terminal set	($x_1, x_2, x_3, x_4, x_5, x_6, [-10,10]$)
Number of runs	100
Mutation rate	0.10
Crossover rate	0.85
Reproduction rate	0.05

The GP model with MAPE 0.06 and 6.29 on the training and testing data respectively signifies that it has efficiently generalise the data set. The relative percentage error between GP predicted value and experimental results of fatigue life cycle of the FDM build part are calculated. Using the GP technique, a model is developed relating six FDM process parameter with fatigue life of the build part and is given in equation 4. 10.

$$\begin{aligned}
 \text{Fatigue Life} = & 604.3 \times x(:,4) - 47788.0 \times x(:,2) - 46733.0 \times x(:,3) - 10255.0 \times x(:,1) - \\
 & 1439.0 \times x(:,5) - 1.212e5 \times x(:,6) + 528.3 \times \cos(x(:,1) - x(:,4)) + \\
 & 3551.0 \times \log(x(:,5) - x(:,1)) - 18144 \times \text{square}(x(:,3) - x(:,2)) + \\
 & 37200.0 \times \tanh(x(:,2) - x(:,5)) - 85288.0 \times \tanh(\text{psqroot}(x(:,1))) - \\
 & 13266.0 \times \tanh(\text{psqroot}(x(:,6))) - 33077.0 \times \cos(x(:,1) \times x(:,5)) - \\
 & 4729.0 \times \cos(x(:,3) \times x(:,4)) - 28588.0 \times \sin(x(:,1) + x(:,6)) - \\
 & 366.8 \times \text{square}(x(:,1) \times x(:,3)) - 320.3 \times \tan(x(:,3) \times x(:,5)) - \\
 & 3430.0 \times \tanh(x(:,4) \times x(:,5)) + 20.29 \times \tan(x(:,4) + x(:,5)) + \\
 & 4509.0 \times \text{psqroot}(x(:,1)) + 532.5 \times \text{psqroot}(x(:,4)) - 21477.0 \\
 & \times \text{psqroot}(x(:,1)) \times \tanh(x(:,6)) + 4870.0 \times x(:,1) \times x(:,2) - \\
 & 150.9 \times x(:,2) \times x(:,4) - 1750.0 \times x(:,3) \times x(:,4) + 532.5 \times x(:,3) \times \\
 & (x(:,5) + 3.316e5 \times x(:,3) \times x(:,6)) - 10111.0 \times x(:,4) \times x(:,6) + 4509.0 \\
 & \times x(:,5) \times x(:,6) + 4.015 \times x(:,3) \times \text{square}(x(:,5)) - 5.345e5 \times \\
 & x(:,2) \times \tanh(x(:,6)) + 389.6 \times \text{psqroot}(x(:,1)) \times x(:,5) - \tag{4.10}
 \end{aligned}$$

$$x(:,6))+38800.0 \times x(:,2) \times x(:,4) \times x(:,6)+1753.0 \times x(:,2) \\ \times x(:,5) \times x(:,6)-1.969 \times x(:,4) \times x(:,5) \times x(:,6)+1.751 \times 10^5$$

Table 4.5 illustrates the relative error for GP model and LS-SVM model with respect to the experimental value and are listed below.

Table 4.5. Relative error (%) of the GP model and LS-SVM Model

Run Order	Experimental value	LS-SVM Model Prediction	Relative Error (%)	GP Predication	Relative Error (%)
1	21804	21138.09	3.054	21736.38	0.310
2	16990	16819.58	1.003	16936.50	0.315
3	8353	8587.221	2.804	8282.62	0.843
4	29570	28660.98	3.074	29520.31	0.168
5	6678	6862.22	2.759	6605.17	1.091
6	17012	16114.25	5.277	16960.10	0.305
7	13532	13401.67	0.963	13462.86	0.511
8	8811	9015.332	2.319	8755.72	0.627
9	6394	6594.111	3.130	6329.71	1.005
10	26472	25408.33	4.018	26421.03	0.193
11	17585	16413.19	6.664	18421.03	4.754
12	16287	15864.62	2.593	17082.53	4.884
13	5761	6001.788	4.180	6178.52	7.247
14	7159	6940.435	3.053	6587.49	7.983
15	3525	3598.948	2.098	3313.66	5.995
16	18347	16845.97	8.181	18293.75	0.290
17	19011	17126.87	9.911	18992.76	0.096
18	10624	10940.26	2.977	10609.16	0.140
19	7576	7919.539	4.535	7558.93	0.225
20	9278	9153.22	1.345	9260.86	0.185
21	11973	12121.5	1.240	11953.80	0.160
22	15281	14905.85	2.455	15261.70	0.126
23	12085	11715.77	3.055	12064.44	0.170
24	6172	6160.826	0.181	6155.14	0.273
25	8333	8182.6	1.805	8315.60	0.209
26	6369	7060.49	10.857	6358.64	0.163
27	8319	7458.599	10.343	8308.06	0.132
28	3343	3547.957	6.131	3327.26	0.471
29	10264	10557.83	2.863	9386.12	8.553
30	3341	3321.431	0.586	3322.66	0.549
31	3343	3473.304	3.898	3028.61	9.404
32	3342	3525.863	5.502	3564.50	6.658
33	3344	2978.804	10.921	3517.30	5.183
34	3345	3781.75	13.057	3132.04	6.366
35	3340	3682.256	10.247	3598.51	7.740
36	3343	3799.575	13.658	3052.56	8.688
37	4630	5110.349	10.375	4598.78	0.674
38	2445	2330.281	4.692	2411.26	1.380
39	5836	6160.955	5.568	5801.91	0.584
40	3439	3173.996	7.706	3407.71	0.910
41	6151	6802.193	10.587	6085.79	1.060
42	3330	2950.208	11.405	3310.76	0.578

43	4418	4860.932	10.026	4384.85	0.750
44	3367	3002.858	10.815	3336.30	0.912
45	3127	2924.972	6.461	3230.00	3.294
46	3170	2924.972	7.730	3230.00	1.893
47	3120	2924.972	6.251	3230.00	3.526
48	2961	2924.972	1.217	3230.00	9.085
49	3084	2924.972	5.157	3230.00	4.734
50	3181	2924.972	8.049	3230.00	1.540
51	3285	2924.972	10.960	3230.00	1.674
52	3296	2924.972	11.257	3230.00	2.002

The comparison graph between GP and LS-SVM technique predicted value shows that the relative error for the GP model is comparatively less (Figure 4.16). The relative error obtained from the LS-SVM and GP model are 2.3% and 1.65% respectively. Therefore, it can be said that GP mode predicts fatigue life of FDM build parts adequately than the LS-SVM model. The formula used for calculation of relative error is given in equation 4.11.

$$\text{Relative error (\%)} = \frac{|M_i - Y_i|}{Y_i} \times 100 \quad (4.11)$$

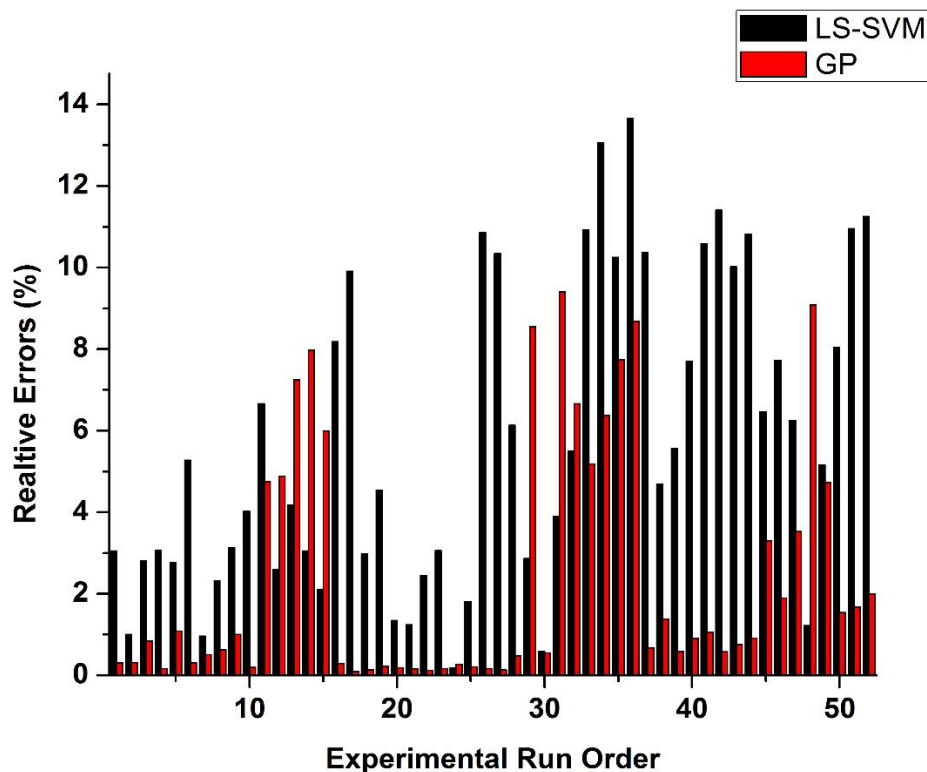


Figure 4.16. Relative error comparison between GP and LS-SVM models for fatigue life

4.4. Conclusion

The effect of low cycle fatigue under fully reversed strain controlled mode on the FDM build parts are experimentally studied and analysed. Influence of six FDM build parameters such as contour number, raster angle, part orientation, air gap, raster width and layer thickness on the fatigue life have been analysed using analysis of variance (ANOVA). The contour number seems to be more important than other parameters since it shifts the stress concentration zone from outer boundary to the centre of the specimen avoiding premature failure of the build parts and helps to improve the stiffness and strength. The raster fill pattern changes at an incremental angle of 30° to its previously placed raster fill pattern in the adjacent layers which is helpful to reduce the anisotropic effect of the build parts in comparison to the default raster fill pattern. Generally, build part having low surface roughness exhibits high fatigue life. An increase in part orientation and layer thickness increases the surface roughness of the build part due to the staircase effect. Therefore, efforts must be made to reduce the staircase effect through controlling part orientation and layer thickness in order to enhance fatigue life of build parts. Increase in layer thickness and part orientation leads to residual stresses to be accumulated near the rasters due to increase in number of cooling and heating cycle leading to failure of weak rasters and rupturing of bond between rasters. Failure of bonds between rasters initiate formation cracks inside the build part. Consequently, the crack propagates in a zigzag manner and increases with an increase in the number of strain cycles. Since FDM process is a complex one, it is difficult to develop a model relating fatigue life with the process parameters. Using response surface methodology (RSM), a relation between process parameters with the fatigue life is established. Using one nature inspired metaheuristic known as firefly algorithm optimum parameter is suggested to improve the fatigue life of the build parts. In order to improve the prediction capability, genetic programming (GP) and least square support vector machine (LS-SVM) techniques are successfully adopted. Finally, the predictive relations of GP and LS-SVM approaches are compared. It is observed that GP predicts fatigue life in an accurate manner as compared to LS-SVM approach.

Chapter 5

Parametric assessment of wear behaviour of FDM build parts

5.1. Introduction

Among all RP process, fused deposition modelling (FDM) is considered as the proficient technology due to its ease of operation, reasonable durability of build parts and less product development cycle (Dunne et al., 2004; Cheah et al., 2004; Pham and Gault, 1998). Since FDM is an additive manufacturing process, it offers a cost and time advantage over conventional manufacturing processes (Upcraft and Fletcher, 2003; Chua et al., 1999). However, due to the inherent build mechanism, performance characteristics are largely influenced by the process parameters. In order to increase the reliability of the FDM build parts, it is more essential to understand the effect of individual process parameters on the performance characteristics. In this direction, previous chapters focus on the assessment of static strength (Chapter 3) and assessment of fatigue life of the FDM build parts (Chapter 4). These above said works reveal that properties of build part varies with the selection of process parameters and can be improved by proper selection of parameters. The effect of FDM process parameters such as layer thickness, raster angle, air gap, raster width, model temperature and colour on strength have been extensively studied (Ahn et al., 2002; Es said et al., 2000; Rayegani and Onwubolu, 2014; Sood et al., 2010). The durability of the build part depends on the wear resistance offered during sliding wear test. Less articles have been published addressing the wear behaviour of the RP processed part (Sood et al., 2012; Singh and Singh 2015; Ramesh and Shrinivas, 2009; Kumar and Kurth, 2008). To fill this research gap, present research work is focused on the sliding wear behaviour of FDM build part and its relationship with the process parameters. Since FDM process is complex one, it is really challenging to develop empirical models which will help for ease understanding of the relation between process parameters and wear behaviour. This analysis may be useful where sliding contact of mating surface occurs such as gears, journal bearings, cams etc. when conventional parts are replaced by FDM parts due to light weight and reasonable strength.

In order to assess the effect of process parameters on the wear behaviour of the FDM build parts, six controllable process parameters such as contour number, layer thickness, part orientation, raster width, raster angle and air gap are considered for experimental purpose. Standard test specimens are manufactured using the Fortus 400mc (FDM machine supplied by Stratasys) and tested according to ASTM G99-05 (standard test method for wear testing with pin-on-disk apparatus) standards. Experiments have been conducted based on face centred central composite design (FCCCD) of response surface methodology (RSM) in order to standardise the experimental runs and to extract maximum information from less experimental run orders. Sliding wear tests are conducted using pin on disk apparatus and wear volumes are measured. The wear amount is calculated for each build part by dividing the wear volume with the sliding distance (Sood et al., 2012) Using analysis of variance (ANOVA) table the significance level of each process parameter is checked. Using the surface plots, influence of process parameters on the wear behaviour are analysed and discussed. From the SEM micrographs the failure criteria of rasters, formation of pit and crack propagation inside the build part are analysed. Finally, a nature inspired meta-heuristic known as firefly algorithm is applied to obtain a best parametric combination for the improvement of wear behaviour of the FDM build part. To predict the wear behaviour, two latest artificial intelligence techniques known as genetic programming (GP) and least square support vector machine (LS-SVM) have been adopted. The prediction model enables to predict the performance measures with reasonable accuracy so that costly experimental time can be minimized.

5.2. Experimental Details

Fused deposition modelling manufacturing process is a parametric dependant process. Some process parameters have large influence over the mechanical properties of the FDM build parts. While used as an end use product, the wear (sliding) behaviour adversely affects the durability of the FDM build part. Therefore, present research work is devoted to study the effect of some important controllable process parameters (layer thickness, contour number, contour width, raster angle, air gap and part orientation) on the wear behaviour of the FDM build parts. Other supplementary parameter such as part interior style, shrinkage factor, perimeter to raster gap etc. are kept at default levels. The process parameters considered for experimental purpose are selected as defined in Table 3.1. To study the wear behaviour of the FDM build part, tests are conducted using the parametric suggestion of central composite design (Table 3.2). After that, specimens are

manufactured according to the ASTM G99 standard as shown in Figure 5. 1. The specimens are fabricated using FDM FORTUS 400mc (supplied and manufactured by Stratasys Inc. USA, Figure 3. 10). Acrylonitrile butadiene styrene (ABS) material has been used for the preparation of the specimen. The main advantage of ABS is its high heat resistance, rigidity and impact resistance properties as compared to other plastics. It is a combination of acrylonitrile, butadiene and styrene. Wear tests are conducted using pin on disk apparatus (Figure 5. 2) with an rpm of 300 and time period of 5 minutes. The sliding distance is calculated by multiplying the rpm with time. The contact path diameter is 60mm. To make perfect contact between disk and specimen, 20 N load is applied parallel to the specimen. The disk is made of EN 31 steel (hardened) having hardness RC 62 and roughness (Ra) 0.32-0.35. The wear volume is determined in mm^3 by multiplying the cross sectional area with the decrease in height after sliding. At initial state, some foreign particles are present on the surface of the specimen. Therefore, initial readings are not taken into account. After removal of this foreign particle completely, contact between disk and specimen is confirmed.

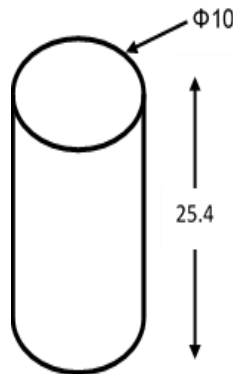


Figure 5.1 ASTM standard specimen for wear test (all dimensions are in mm)



Figure 5.2. Pin on disk wear testing machine

5.3. Results and Discussions

All experiments are conducted according to ASTM D618 standard i.e. at ambient temperature 23 ± 2 °C and humidity 45 ± 5 . For each run order, three test specimens are considered and the average wear is listed in the table below.

Table 5.1. Experimental results

Exp. No.	A	B	C	D	E	F	Wear (mm^3/m)
1	-1	-1	-1	-1	-1	-1	0.0198
2	1	-1	-1	-1	-1	1	0.0190
3	-1	1	-1	-1	-1	1	0.0210
4	1	1	-1	-1	-1	-1	0.0198
5	-1	-1	1	-1	-1	1	0.0220
6	1	-1	1	-1	-1	-1	0.0183
7	-1	1	1	-1	-1	-1	0.0239
8	1	1	1	-1	-1	1	0.0198
9	-1	-1	-1	1	-1	1	0.0215
10	1	-1	-1	1	-1	-1	0.0185
11	-1	1	-1	1	-1	-1	0.0231

12	1	1	-1	1	-1	1	0.0204
13	-1	-1	1	1	-1	-1	0.0209
14	1	-1	1	1	-1	1	0.0204
15	-1	1	1	1	-1	1	0.0245
16	1	1	1	1	-1	-1	0.0194
17	-1	-1	-1	-1	1	1	0.0229
18	1	-1	-1	-1	1	-1	0.0184
19	-1	1	-1	-1	1	-1	0.0232
20	1	1	-1	-1	1	1	0.0210
21	-1	-1	1	-1	1	-1	0.0220
22	1	-1	1	-1	1	1	0.0203
23	-1	1	1	-1	1	1	0.0220
24	1	1	1	-1	1	-1	0.0216
25	-1	-1	-1	1	1	-1	0.0224
26	1	-1	-1	1	1	1	0.0208
27	-1	1	-1	1	1	1	0.0250
28	1	1	-1	1	1	-1	0.0209
29	-1	-1	1	1	1	1	0.0231
30	1	-1	1	1	1	-1	0.0196
31	-1	1	1	1	1	-1	0.0230
32	1	1	1	1	1	1	0.0228
33	-1	0	0	0	0	0	0.0199
34	1	0	0	0	0	0	0.0187
35	0	-1	0	0	0	0	0.0201
36	0	1	0	0	0	0	0.0207
37	0	0	-1	0	0	0	0.0201
38	0	0	1	0	0	0	0.0198
39	0	0	0	-1	0	0	0.0196
40	0	0	0	1	0	0	0.0219
41	0	0	0	0	-1	0	0.0203
42	0	0	0	0	1	0	0.0201
43	0	0	0	0	0	-1	0.0189
44	0	0	0	0	0	1	0.0188
45	0	0	0	0	0	0	0.0188
46	0	0	0	0	0	0	0.0187
47	0	0	0	0	0	0	0.0189
48	0	0	0	0	0	0	0.0187
49	0	0	0	0	0	0	0.0188
50	0	0	0	0	0	0	0.0189
51	0	0	0	0	0	0	0.0189
52	0	0	0	0	0	0	0.0188

From the analysis of variance (ANOVA) table, the significant terms (0.05 significance level) influencing the wear are identified and listed in Table 5. 2. It is observed that raster width (C) is not significant term as far as sliding wear of test specimen is concerned. The coefficient determination (R^2) is 0.9002 and the value of adjusted R^2 value is 0.8062. It is to be noted that the value of lack of fit is insignificant. The residual analysis has been done and found that the residuals are normally distributed. The RSM model for the wear involving the parameters is given below in equation 5. 1.

$$\begin{aligned} \text{Wear} = & 0.040135 - 3.37233e-004 \times A - 0.059777 \times B - 0.060071 \times C - 1.14319e- \\ & 004 \times D + 1.32759e-005 \times E + 0.076645 \times F - 1.43914e-004 \times A \times B + \\ & 1.87500e-004 \times A \times C - 2.18750e-006 \times A \times D + 1.51042e-006 \times A \times E \\ & + 2.64518e-003 \times A \times F - 3.83772e-003 \times B \times C + 6.30482e-005 \times B \times D - \\ & 2.05592e-005 \times B \times E - 0.13760 \times B \times F - 1.02778e-004 \times C \times D - 8.75000e- \\ & 005 \times C \times E + 0.01148 \times C \times F + 7.63889e-008 \times D \times E + 7.95604e-004 \times D \\ & \times F + 7.79199e-005 \times E \times F - 6.52919e-005 \times A^2 + 0.14523 \times B^2 + 0.069126 \\ & \times C^2 + 5.28370e-006 \times D^2 + 7.09814e-007 \times E^2 - 1.01021 \times F^2 \end{aligned}$$

(uncoded form) (5.1)

Table 5.2. ANOVA table for wear

Source	Sum of Squares	df	Mean Square	F Value	p-value Prob > F
Model	0.000138	27	5.12E-06	7.87E+00	< 0.0001
A	4.82E-05	1	4.82E-05	7.42E+01	< 0.0001
B	1.44E-05	1	1.44E-05	2.21E+01	< 0.0001
C	9.22E-07	1	9.22E-07	1.42E+00	0.2452
D	5.44E-06	1	5.44E-06	8.37E+00	0.0080
E	8.01E-06	1	8.01E-06	1.23E+01	0.0018
F	3.96E-06	1	3.96E-06	6.09E+00	0.0211
AxB	1.53E-08	1	1.53E-08	2.36E-02	0.8793
AxC	2.53E-08	1	2.53E-08	3.89E-02	0.8452
AxD	1.38E-07	1	1.38E-07	2.12E-01	0.6493
AxE	2.63E-07	1	2.63E-07	4.04E-01	0.5309
AxF	5.78E-07	1	5.78E-07	8.89E-01	0.3552
BxC	1.53E-08	1	1.53E-08	2.36E-02	0.8793
BxD	1.65E-07	1	1.65E-07	2.54E-01	0.6186
BxE	7.03E-08	1	7.03E-08	1.08E-01	0.7451
BxF	2.26E-06	1	2.26E-06	3.47E+00	0.0746
CxD	4.28E-07	1	4.28E-07	6.58E-01	0.4252
CxE	1.24E-06	1	1.24E-06	1.91E+00	0.1799
CxF	1.53E-08	1	1.53E-08	2.36E-02	0.8793
DxE	3.78E-08	1	3.78E-08	5.82E-02	0.8115

D×F	2.94E-06	1	2.94E-06	4.52E+00	0.0439
E×F	1.13E-07	1	1.13E-07	1.74E-01	0.6807
A ²	1.63E-07	1	1.63E-07	2.50E-01	0.6215
B ²	1.68E-06	1	1.68E-06	2.58E+00	0.1212
C ²	3.6E-07	1	3.60E-07	5.55E-01	0.4637
D ²	3.37E-06	1	3.37E-06	5.18E+00	0.0320
E ²	9.73E-07	1	9.73E-07	1.50E+00	0.2330
F ²	1.21E-06	1	1.21E-06	1.86E+00	0.1858
Residual	1.56E-05	24	6.50E-07		
Lack of Fit	1.56E-05	17	9.147E-07	131.3542	< 0.085
Pure Error	4.87E-08	7	6.964E-09		
Cor Total	0.000154	51			

From the surface plots, it can be observed that wear is dependent upon the FDM build parameters. The wear decreases with an increase in contour number (A) of the build part because an increase in contour number moves the stress concentration from outer corner to centre of the specimen exhibiting uniform distribution of stress and avoiding premature failure of the specimen (Ahn et al., 2002) (Figure 5. 3 I, II, III). Normally, the layer number depends upon the layer thickness (B) and the part orientation (D) of the build part. During part building, layers are deposited in a sequential manner as programmed by the machine software. Since, the newly deposited filament temperature is higher than the previously deposited filaments, heat transfer occurs. So local re-melting and diffusion between inter as well as intra layer rasters takes place resulting a strong adhesive bond. These strong adhesive bonds between rasters decrease the wear at the part interface and increases durability. Therefore, with the decrease of layer thickness, the wear decreases favourably (Figure 5. 3 I, IV). The air gap (F) adversely affects the wear of the build part. Increase in air gap increases the possibility of increase in the pit formation during sliding wear test and results in failure of part (Figure 5. 3 III, IV).

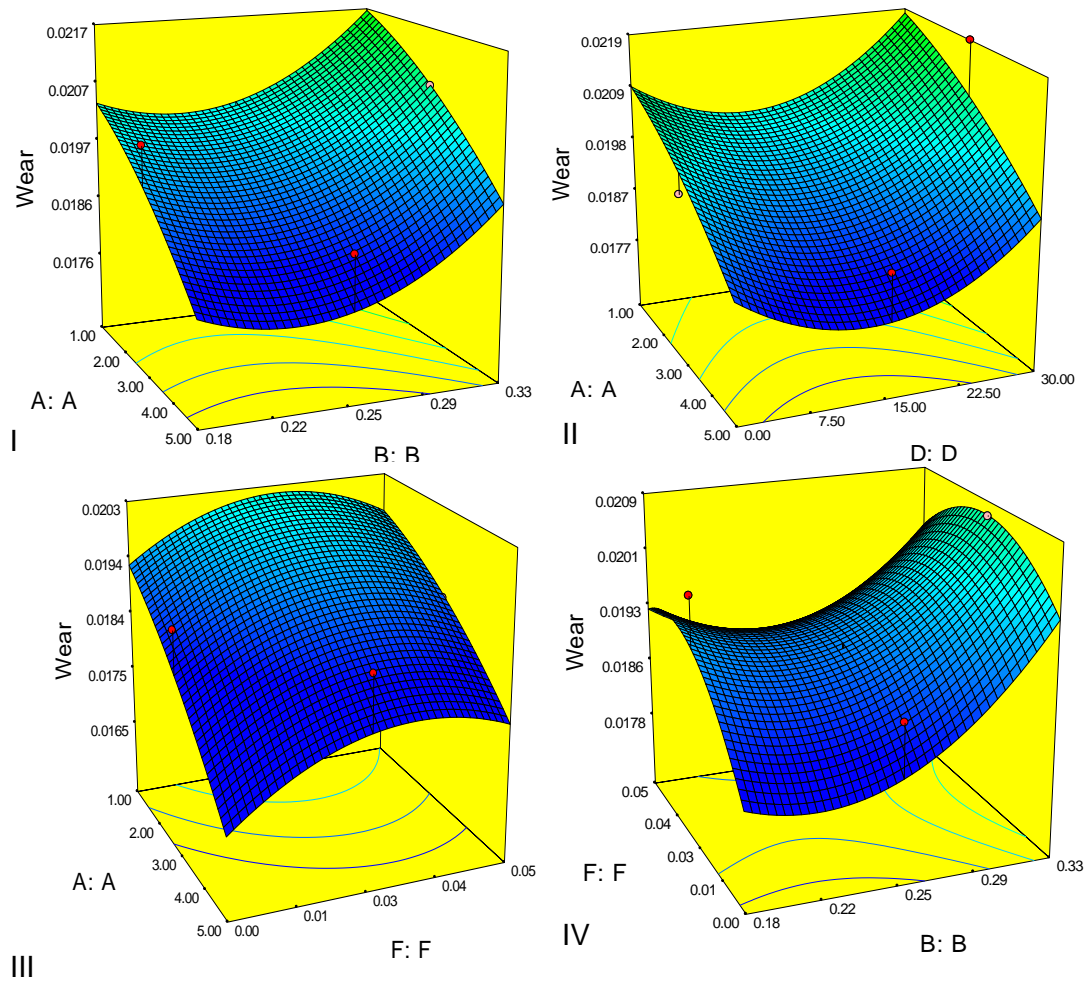


Figure 5.3. Response surface plots for wear

Due to the relative motion between specimen and disk with a constant compressive force, heat is generated at the interface and develops internal strain in the build part. Excessive generation of heat at the interface decreases the bond strength between rasters and give rise to the formation of cracks in the build part. These crack propagation gives rise to the formation of small pits on the interface and increases the material removal rate. Wear surfaces having small crack propagation can be clearly seen from the micrographs Figure 5. 4 a, b. Normally, positive air gaps between rasters are responsible for the generation of voids in the build part. During wear testing, these voids increase the wear rate and develop pits in the build parts (Figure 5. 4 c, d).

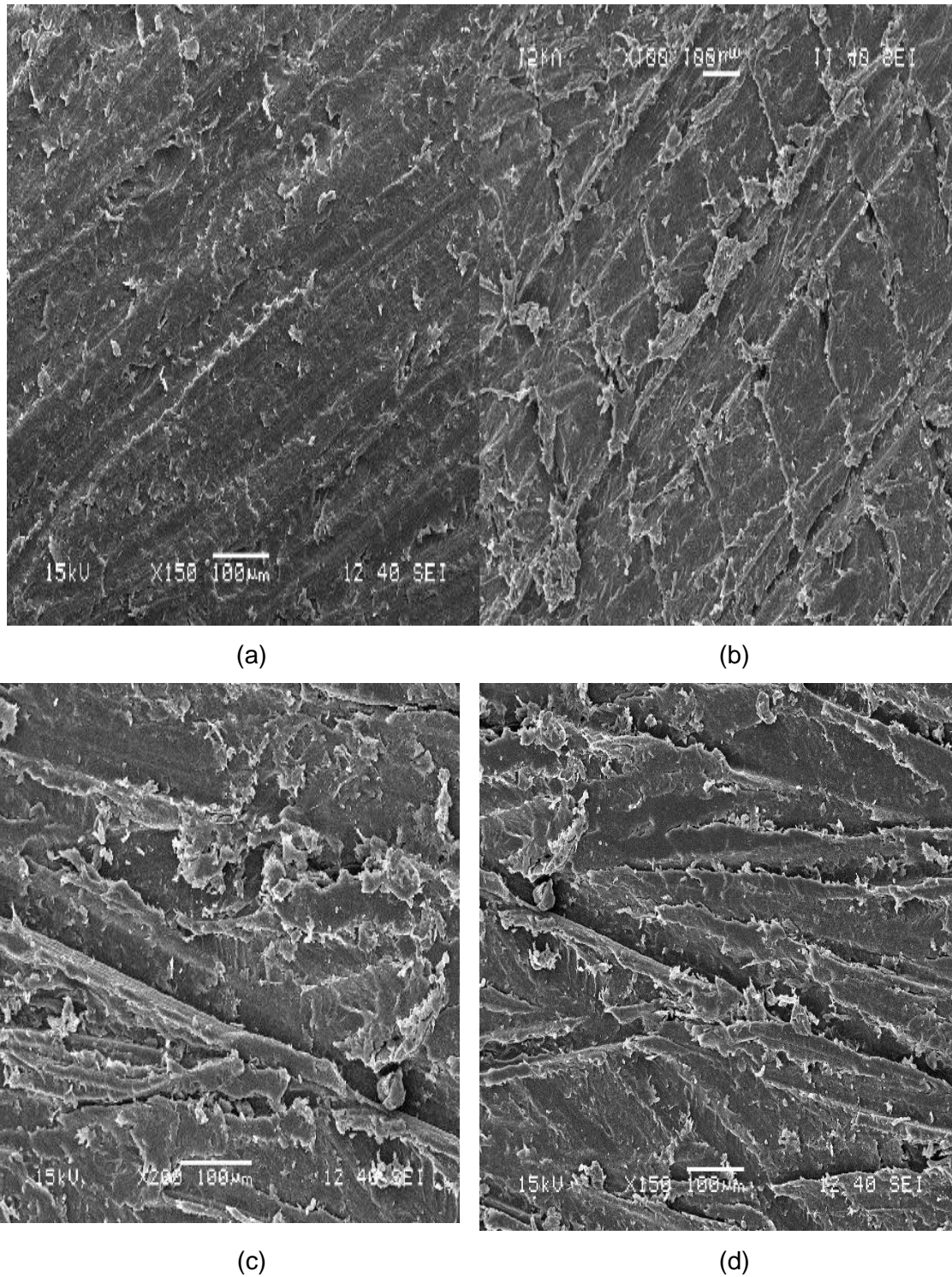


Figure 5.4. SEM plots of the FDM specimen after wear testing

Figure 5. 5 shows the plot between wear volume with the sliding distance covered by the specimen during experimentation. The plot between the coefficient of friction and the sliding distance (Figure 5. 6) illustrates that it is not stable throughout the test. At the beginning, coefficient of friction increases rapidly due to the presence of foreign particle in

the surface and become stable when there is a perfect contact between the disk and specimen. Similar types of graphs are observed for all run order.

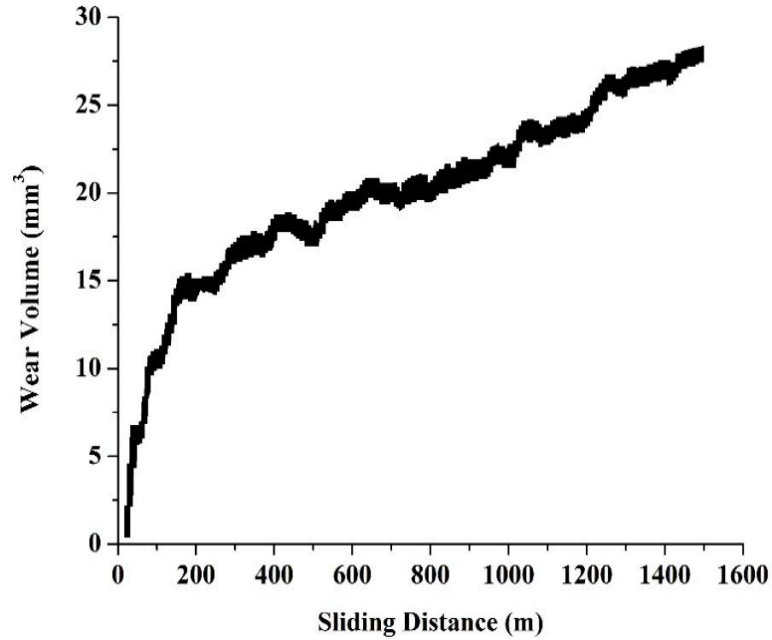


Figure 5.5. Wear volume with sliding distance

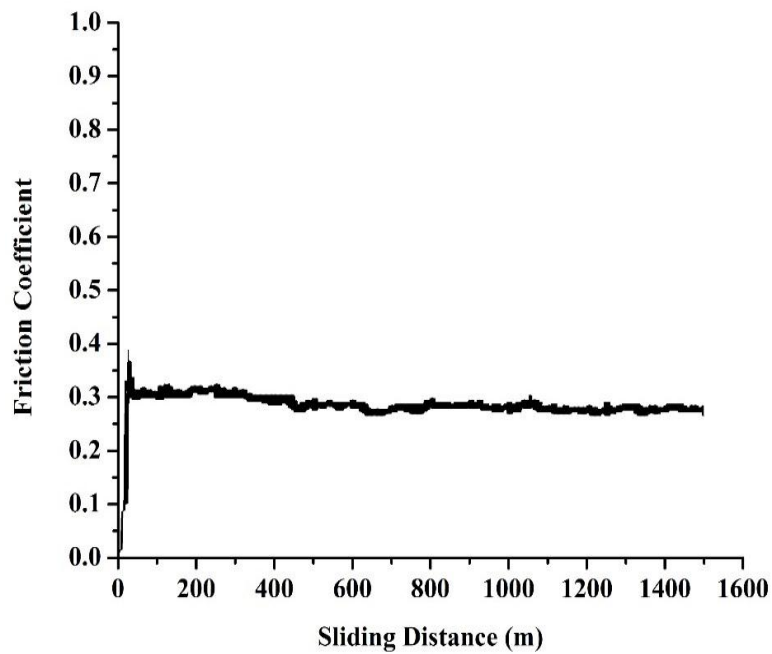


Figure 5.6. Friction coefficient with sliding distance

To achieve the optimum solution or to achieve the best parameter setting, a nature inspired metaheuristic known as firefly algorithm is applied. The objective function used in the firefly optimisation algorithm has been empirically developed using non-linear regression analysis relating wear values and process parameters shown in Table 5. 1.

For the firefly algorithm, the values considered are: number of fireflies (n)=10, number of iterations (N) = 50, attractiveness (β) = 0.9, randomisation (α) = 0.19 and absorption coefficient (γ) = 1. Hence, the total number of function evaluations is 500. The firefly algorithm provides a parameter setting to get optimum value of the wear as shown in Table 5.3.

Table 5.3. Optimum parameter setting to achieve the best wear behaviour

A	B	C	D	E	F	Wear
4.76	0.183	0.5184	3.16	41.65	0.0017	0.0178

In the present study, GP is applied to develop a model relating FDM process parameters with fatigue life. From the experimental results, 80% data are taken are considered for training purpose and rest data are considered for testing purpose. Six input parameters such as contour number (x_1), layer thickness (x_2), raster width (x_3), part orientation (x_4), raster angle (x_5) and air gap (x_6) are considered for modelling purpose. The output parameter fatigue life is considered as the performance characteristic. The performance of GP model is measured in terms of MAPE. The diagram involving GP technique for the modelling of fatigue life of the FDM build part is shown in Figure 5.7.

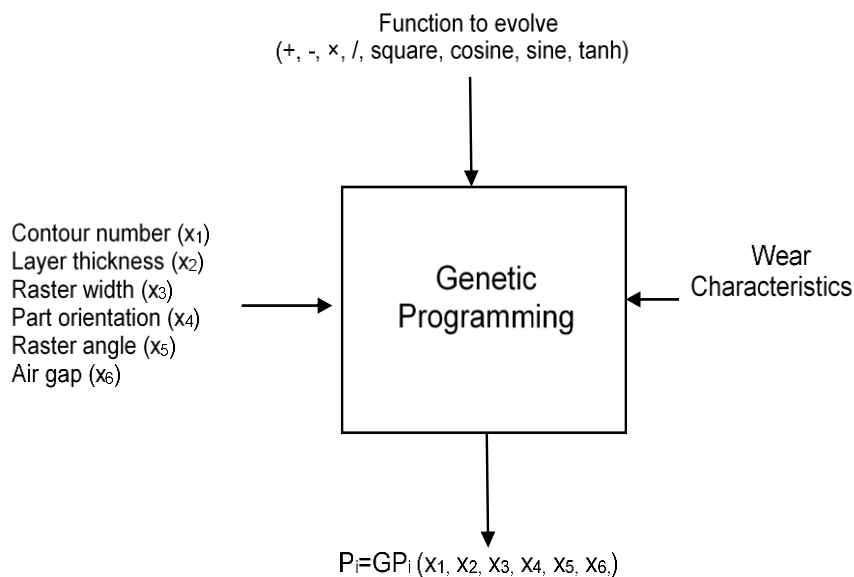


Figure 5.7. Diagram of GP formulation of wear of FDM built parts

The parameter setting for GP determined through several trial and experimental runs are shown below in Table 5. 4.

Parameters	Value Assigned
Population size	50
Number of generations	700
Maximum depth of tree	6
Maximum generation	45
Functional set	Multiply, plus, minus, divide, square, cosine, sine, tanh
Terminal set	($x_1, x_2, x_3, x_4, x_5, x_6, [-10,10]$)
Number of runs	100
Mutation rate	0.10
Crossover rate	0.85
Reproduction rate	0.05

The GP model with MAPE 0.021% and 3.29% on the training and testing data respectively signifies that it has efficiently generalise the data set. The relative percentage error between GP predicted value and experimental results of fatigue life cycle of the FDM build part are calculated. Using the GP technique, a model is developed relating six FDM process parameter with fatigue life of the build part and is given in equation 5.2.

$$\begin{aligned}
 \text{Wear} = & 0.000364.xx(:,2)-0.0003049.xx(:,1)+0.000133.xx(:,3)+ 0.0004924 \\
 & .xx(:,4)-4.139e-5.xx(:,5)+0.0001713.x\tan(x(:,1)-x(:,6))- \\
 & 0.0002122.xsquare(-2.372)+0.003456.x\cos(\text{psqroot}(x(:,3)))- \\
 & 0.001529.x\sin(\cos(x(:,1)))+.0003639.x\sin(\tan(x(:,2))) +7.937e- \\
 & 5.x\exp(\text{square}(-2.372))-0.000309.x\tanh(x(:,3)).xx(:,4)+ \\
 & 0.000229.x\tan(x(:,3) + x(:,4)) - 0.004242.x\cos(x(:,4)) -1.648e- \\
 & 17.x\text{plog}(x(:,3))+0.0014.x\text{psqroot}(x(:,5))+0.000214.x\text{psqroot} \\
 & (x(:,6))-6.966e-5.x\sin(x(:,5))-0.0004749.x\tan(x(:,1))+0.0001934 \\
 & x\tan(x(:,4)) -0.0001752. x\tanh(x(:,6))+0.0001933.xx(:,1).xx(:,3)- \\
 & 0.0005948xx(:,2)xx(:,6)+0.0002138.xx(:,4).x x(:,5)+0.0003493. \\
 & xx(:,4).xx(:,6)+0.0004319x\text{psqroot}(x(:,4))x(x(:,3)+x(:,5)) \\
 & +0.0001725.xx(:,6).x\exp(x(:,3))-0.000164.x(x(:,1)-x(:,6))x \\
 & (x(:,2)-x(:,6))+ 0.000539.xx(:,2).xx(:,4).xx(:,6) + 2.855e-7; \tag{5.2}
 \end{aligned}$$

Again an artificial intelligent (AI) technique known as LS-SVM is used for prediction purpose. The SVM technique involves input training data followed by testing data. Around 80% of the experimental results are considered for training purpose while rest 20% are considered for testing purpose. Six important FDM process parameters such as contour

number, layer thickness, part orientation, raster angle, raster width and air gap are considered as input parameters. The hyper parameters gamma (γ) and sig² (σ^2) are obtained as 43.945 and 0.06574 respectively. The formula used for calculation of relative error is given in equation 5.3

$$\text{Relative error (\%)} = \frac{|M_i - Y_i|}{Y_i} \times 100 \quad (5.3)$$

where M_i is the predicted results by and GP and LS-SVM and Y_i is the actual value or experimental value of the wear test. The relative errors obtained from the LS-SVM and GP model are 2.3% and 1.65% respectively. Predicted results by LS-SVM and RSM along with their relative errors are listed below in Table 5. 5.

Table 5.5. Relative error of LS-SVM model and RSM model.

Run Order	Experimental value	GP Prediction	Relative Error (%)	LS-SVM Predication	Relative Error (%)
1	0.0198	0.1547	3.3892	0.0199	0.3026
2	0.0188	1.1366	2.7841	0.0190	0.0273
3	0.0208	0.8471	2.1603	0.0211	0.2535
4	0.0200	1.2527	1.3182	0.0198	0.0331
5	0.0221	0.4405	1.6685	0.0220	0.0191
6	0.0181	1.3008	2.5590	0.0184	0.4160
7	0.0239	0.1590	3.1341	0.0238	0.5525
8	0.0199	0.3249	2.0246	0.0198	0.2105
9	0.0217	1.0627	3.2714	0.0215	0.0413
10	0.0185	0.0541	3.5746	0.0185	0.2226
11	0.0229	0.8344	0.5569	0.0225	2.6852
12	0.0209	2.3465	1.8201	0.0199	2.6249
13	0.0207	0.9252	1.6777	0.0214	2.3064
14	0.0205	0.4184	0.0028	0.0199	2.6789
15	0.0239	2.4236	3.1297	0.0239	2.4093
16	0.0195	0.7281	4.9926	0.0194	0.0043
17	0.0222	2.9949	4.0439	0.0229	0.0678
18	0.0172	6.4300	4.3984	0.0185	0.7496
19	0.0238	2.5437	0.1808	0.0231	0.2164
20	0.0199	5.1982	1.4672	0.0209	0.3443
21	0.0207	6.0234	1.4944	0.0220	0.0288
22	0.0209	3.0166	0.8432	0.0203	0.2042
23	0.0222	0.8056	3.1991	0.0220	0.1235
24	0.0214	1.0858	3.0594	0.0216	0.0512
25	0.0224	0.1398	1.5998	0.0225	0.4113
26	0.0206	0.8369	3.8057	0.0208	0.1564
27	0.0248	0.7200	1.7030	0.0249	0.4733
28	0.0205	1.9487	1.9597	0.0209	0.0384
29	0.0230	0.4439	1.3139	0.0231	0.1331
30	0.0197	0.6189	2.0976	0.0197	0.2707
31	0.0234	1.5885	2.4849	0.0236	2.5948
32	0.0229	0.5302	2.7568	0.0221	2.9863

33	0.0200	0.7496	1.3009	0.0205	2.8243
34	0.0185	1.1032	4.9384	0.0192	2.4708
35	0.0198	1.4709	3.3951	0.0199	1.1219
36	0.0195	5.8009	0.0863	0.0202	2.4167
37	0.0189	6.0051	3.2193	0.0195	2.8325
38	0.0187	5.6956	0.0884	0.0193	2.7506
39	0.0198	1.0204	2.1312	0.0196	0.1147
40	0.0213	2.8706	4.9420	0.0219	0.0707
41	0.0201	1.1264	4.5201	0.0203	0.0538
42	0.0190	5.2286	1.2587	0.0201	0.0708
43	0.0186	1.6210	3.8277	0.0190	0.5887
44	0.0188	0.1525	0.3130	0.0190	0.8136
45	0.0188	0.1525	2.2812	0.0190	0.9118
46	0.0188	0.3815	2.8282	0.0190	1.4514
47	0.0188	0.6808	1.7401	0.0190	0.3779
48	0.0188	0.3815	2.8282	0.0190	1.4514
49	0.0188	0.1525	2.2812	0.0190	0.9118
50	0.0188	0.6808	1.7401	0.0190	0.3779
51	0.0188	0.6808	1.7401	0.0190	0.3779
52	0.0188	0.1525	2.2812	0.0190	0.9118

Figure 5. 8 compares the relative error between GP predicted values with LS-SVM predicted values for the wear of the FDM build parts. The boxplot illustrates the relative error (%) for the GP and LS-SVM model. From the graph, it can be seen that the relative error of the GP model is less as compared to the LS-SVM model. Hence, the GP model is acceptable with less relative error.

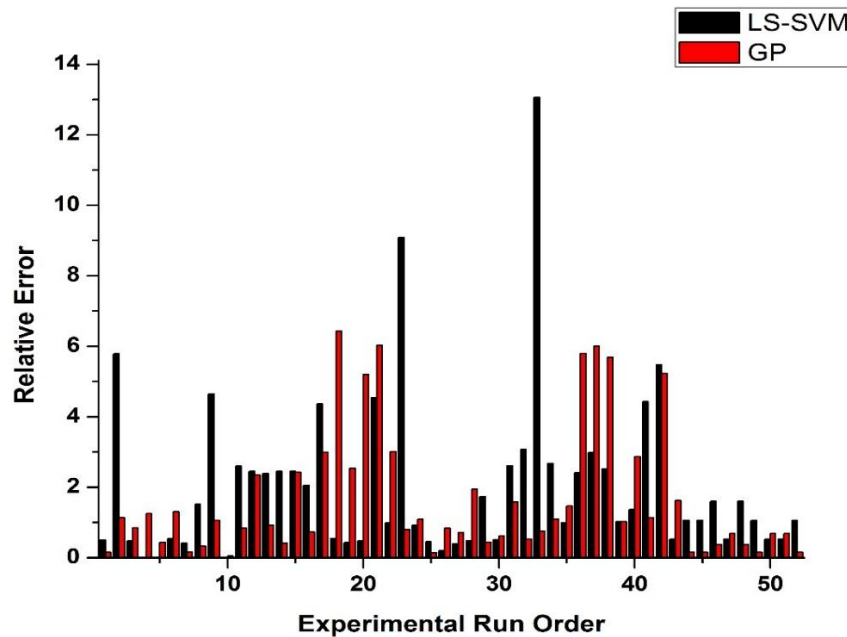


Figure 5.8. Relative error comparison between LS-SVM and GP models for wear behaviour

5.4. Conclusion

Effect of six controllable process parameters viz. contour number, raster orientation, raster angle, layer thickness, air gap and raster width on the wear of the FDM build part is studied. An increase in contour number decreases the wear rate by shifting the stress concentration zone from outer edge to the centre of the specimen and decreases the chance of premature failure of the build part. The air gap, which generates voids inside the build parts, increases the material removal rate due to the formation of pits. The bond strength between rasters decreases due to the generation of excess heat at the interface and increases the material removal rate. A functional relationship between the FDM process parameters and wear using response surface methodology is developed. Significance of each process parameter on the wear has been studied using ANOVA. One nature inspired Metaheuristic algorithm known as firefly algorithm is adopted to get optimum parameter setting for the improvement of wear behaviour. In order to improve the prediction capability, genetic programming (GP) and least square support vector machine (LS-SVM) techniques are successfully adopted. Finally, the predictive relations of GP and LS-SVM approaches are compared. It is observed that GP predicts wear behaviour in an accurate manner as compared to LS-SVM approach.

Chapter 6

Executive Summary and Conclusion

6.1. Introduction

Fused deposition modelling has the ability to build 3D complex geometry with reasonable accuracy using layer-by-layer build mechanism in a temperature controlled environment within a stipulated time. FDM process has significant advantages over conventional manufacturing process in terms of avoidance in the preparation of jigs and fixtures, flexibility in design modifications, less human intervention and capability of producing complex shapes. Specifically, FDM has major advantage over conventional manufacturing process in terms of time and cost. Since FDM process is a parametric dependent process, process parameters largely influence the mechanical strength, part quality and durability of the build parts. In this direction, the present research work emphasises on the improvement of part strength under both static and cyclic loading through selection of proper process parameters.

6.2. Summary of findings

Findings gathered from the current research work attempts to explain not only the complex build mechanism of FDM process but also the effect of FDM process parameters on the output performance characteristics.

- Among six controlling process parameters, contour number happens to be the significant parameter for improving mechanical strength, fatigue life and wear resistance of FDM build part because existence of contour numbers shifts the stress concentration zone from outer edge to inner surface. The delta angle is set at 30° to change the raster fill pattern to its previously placed rasters so that anisotropic behaviour of build part can be decreased to some extent.
- Since the part building mechanism in FDM is a complex process, it is challenging to develop analytical or numerical model to predict the performance measures. Therefore, statistically valid empirical models have been proposed in this study to relate process parameters with mechanical strength, fatigue life and wear resistance. Latest evolutionary algorithm like firefly algorithm is adopted to obtain

optimum parameter settings for various performance measures so that effective search can be made in optimization landscape.

- The tensile strength of the specimen obtained at optimal parameter setting is 32.72 MPa which is almost 77.92% of the specimen produced through injection moulding process. Interestingly, it is 73.02% above the previous study (Sood et al. 2010). The optimal compressive strength (108.38 MPa) is two times greater than the strength (52 MPa) of the injection moulded specimen due to the hollow structure produced inside the build part resulting from air gap. Further, it is 45.6% higher than the previous study (Sood et al. 2010). The optimal flexural strength of the FDM specimen closely approaches to that of the injection moulded specimen (96%). An improvement of 76.5% is observed in flexural strength over the previous study (Sood et al. 2010) due to modification in contour number and raster fill pattern style.
- An increase in part orientation and layer thickness increases the surface roughness of the build part due to the presence of staircase effect. A build part having with high surface roughness exhibits low fatigue life under strain controlled mode. Therefore, efforts must be made to reduce the staircase effect through selection of suitable process parameters in order to enhance fatigue life of build parts.
- Increase in layer thickness and part orientation leads to residual stresses to be accumulated near the rasters due to increase in number of cooling and heating cycle leading to failure of weak rasters and rupturing of bond between rasters. Failure of bonds between rasters initiates crack formation inside the build part. Subsequently, this crack propagates in a zigzag manner and increases with an increase in number of strain cycles as observed in fatigue test.
- In order to reduce the experimental cost and time, genetic programming and least square support vector machine have been adopted for prediction of performance measures. A relative error of 5.24% and 6.71% has been reported with respect to experimental value for GP and LS-SVM respectively for multi-performance characteristics index (MPCI) an equivalent measure for tensile, compressive, flexural and impact strength.
- In the FDM process, the molten is extruded to the build platform at a temperature of 230°C while the temperature of the build platform is maintained at 95°C. This sudden cooling of the filament from high temperature to low temperature gives rise

to the formation of thermo-residual stresses inside the build part resulting in decrease in part strength. This is to be noted that increase in layer numbers (due to increase in part orientation or decrease in layer thickness) causes increase in number of involvement of heating and cooling cycles during part building. This phenomenon results in increase in residual stresses within the build part and decreases the mechanical strength.

- Accumulation of residual stresses near the rasters leads to failure of weak rasters resulting in rupture of bonds between adjacent rasters. Failure of bonds between rasters initiate formation cracks inside the build part. Consequently, this crack propagates in a zigzag manner and increases with an increase in the number of strain cycles.
- Zero air gap means that rasters are placed in contact with each other. Zero air gap increases the bond strength resulting an increase in load bearing capacity. If negative air gap is maintained, rasters will be placed one over another on a single layer and part geometry will be affected. Positive air gap increases the generation of voids inside the build part resulting a decrease in part strength. It also observed that generation of voids inside the build part increases the material removal rate during sliding wear test. The bond strength between rasters decreases due to the generation of excess heat at the interface and increases material removal rate when FDM build part subjected to sliding wear.

6.3. Contribution of the research work

- The effect of contour number on the strength of FDM build part has been studied under static and dynamic loading conditions. Among all process parameters, contour number seems to be more important than other controllable process parameter since it shifts the stress concentration towards the centre of the specimen from outer edge surface resulting in avoidance of premature failure during static and dynamic loading.
- An effort has been made to decrease the anisotropic effect of the FDM build part by changing the raster fill pattern style.
- Understandings generated in this research work explain the complex build mechanism of FDM process and explain the effect of process parameters on the output responses using surface plots and micrographs.

- An empirical model has been developed relating process parameter with the mechanical strength of FDM build parts. Optimum parameter setting has been suggested using a nature inspired firefly algorithm and is experimentally validated.
- The work can be seen as the first attempt to study the effect of process parameter on the fatigue life of FDM part under strain controlled mode.
- In order to improve the prediction capability, genetic programming (GP) is adopted to develop an empirical model relating the process parameters with the fatigue life of the FDM build parts.
- An attempt is made to study the sliding wear mechanism of FDM build parts.
- For prediction purpose, least square support vector machining (LS-SVM) is adopted to assess the wear behaviour of the FDM build parts.

6.4. Limitation of the study

In spite of all these advantages obtained from the research work, following limitation has been noticed and addressed below.

- The work extensively studies the fatigue life of the FDM build parts under strain controlled mode but fatigue life under stress control mode needs to be assessed.
- Present work is focused on the study of sliding wear behaviour of the FDM build parts but other type of mechanical wear such as fretting, abrasive and erosive wear behaviour needs to be analysed for FDM build parts.
- Effect of process parameters on the shape (cylinder, cone, prism, cuboid, hexagonal pyramid) of the FDM build part need to be highlight.
- Present work uses only ASTM standards for preparing the specimens. In order to enhance the practical implication of FDM build parts experiments may be conducted using the real end use parts manufactured through FDM route
- In this research work, empirical models have been developed using various statistical tools but mathematical or numerical approaches may be developed to study the effect of process parameters on performance measures.

6.5. Scope for future work

Present research work provides ample opportunity for the investigation of usefulness of FDM process. Some scopes for future research have been given below.

- Effects of environmental variables like temperature and humidity on the part quality may be explored.
- Research on increase of build space and provision of multiple nozzles for part deposition in FDM process needs to be explored to cater to the needs of medium or large batch manufacturer.
- FDM process specific CAD modelling and analysis tools need to be developed.
- Option of depositing multiple materials in a single setting needs to be explored.
- Possibility of using different materials or modification in the present material composition may be explored.
- Furthermore, research can be extended to study the effect of process parameters on circularity of inner holes in FDM build parts.

Bibliography

- Ahn, S. H., Montero, M., Odell, D., Roundy, S., and Wright, P. K. (2002). Anisotropic material properties of fused deposition modeling ABS. *Rapid Prototyping Journal*, 8(4), 248-257.
- Ajoku, U., Saleh, N., Hopkinson, N., Hague, R., and Erasenthiran, P. (2006). Investigating mechanical anisotropy and end-of-vector effect in laser-sintered nylon parts. *Proceedings of the Institution of Mechanical Engineers, Part B: Journal of Engineering Manufacture*, 220(7), 1077-1086.
- Allahverdi, M., Danforth, S. C., Jafari, M., and Safari, A. (2001). Processing of advanced electroceramic components by fused deposition technique. *Journal of the European Ceramic Society*, 21(10), 1485-1490.
- Anitha, R., Arunachalam, S., and Radhakrishnan, P. (2001). Critical parameters influencing the quality of prototypes in fused deposition modelling. *Journal of Materials Processing Technology*, 118(1), 385-8.
- ASTM D256-93A. Standard Test Methods for Determining the Izod Pendulum Impact Resistance of Plastics, ASTM International, West Conshohocken, PA 19428-2959.USA.
- ASTM D638-10. Standard Test Method for Tensile Properties of Plastics. Annual Book of ASTM Standards, ASTM International, West Conshohocken, PA 19428-2959.USA.
- ASTM D695-10. Standard Test Method for Compressive Properties of Plastics. Annual Book of ASTM Standards, ASTM International, West Conshohocken, PA 19428-2959.USA.
- ASTM D790-10. Standard Test Methods for Flexural Properties of Unreinforced and Reinforced Plastics and Electrical Insulation Materials. Annual Book of ASTM Standards, ASTM International, West Conshohocken, PA 19428-2959.USA.
- ASTM E606-12. Standard test method for strain controlled fatigue testing. Annual Book of ASTM Standards, ASTM International, West Conshohocken, PA 19428-2959.USA.
- ASTM G99-05 (2010). Standard Test Method for Wear Testing with a Pin-on-Disk Apparatus, Annual Book of ASTM Standards, ASTM International, West Conshohocken, PA 19428-2959. USA.
- Baziar, M. H., Jafarian, Y., Shahnazari, H., Movahed, V., and Tutunchian, M. A. (2011). Prediction of strain energy-based liquefaction resistance of sand-silt mixtures: an evolutionary approach. *Computers and Geosciences*, 37(11), 1883-93.
- Behera, A., Behera, S., Tripathy, R. K., and Mishra, S. C. (2012). Least square support vector machine alternative to artificial neural network for prediction of surface roughness and porosity of plasma sprayed copper substrates, 4(12), 399-404.
- Bernard, A., and Fischer, A. (2002). New trends in rapid product development. *CIRP Annals-Manufacturing Technology*, 51(2), 635-52.

- Berry, E., Brown, J. M., Connell, M., Craven, C. M., Efford, N. D., Radjenovic, A., and Smith, M. A. (1997). Preliminary experience with medical applications of rapid prototyping by selective laser sintering. *Medical Engineering and physics*, 19(1), 90-6.
- Bibb, R., Taha, Z., Brown, R., and Wright, D. (1999). Development of a rapid prototyping design advice system. *Journal of Intelligent Manufacturing*, 10(3-4), 331-9.
- Bose, S., Suguira, S., and Bandyopadhyay, A. (1999). Processing of Controlled Porosity Ceramic structures via fused deposition. *Scripta Materialia*, 41(9), 1009-14.
- Braglia, M., and Petroni, A. (1999). A management-support technique for the selection of rapid prototyping technologies. *Journal of Industrial Technology*, 15(4), 2-6.
- Byun, H. S., and Lee, K. H. (2005). A decision support system for the selection of a rapid prototyping process using the modified TOPSIS method. *The International Journal of Advanced Manufacturing Technology*, 26(11-12), 1338-47.
- Campbell, R. I., and Bernie, M. R. N. (1996). Creating a database of rapid prototyping system capabilities. *Journal of Materials Processing Technology*, 61(1), 163-67.
- Campbell, R. I., Martorelli, M., and Lee, H. S. (2002). Surface roughness visualisation for rapid prototyping models. *Computer-Aided Design*, 34(10), 717-25.
- Çaydaş, U., and Ekici, S. (2012). Support vector machines models for surface roughness prediction in CNC turning of AISI 304 austenitic stainless steel. *Journal of Intelligent Manufacturing*, 23(3), 639-50.
- Chang, D. Y., and Huang, B. H. (2011). Studies on profile error and extruding aperture for the RP parts using the fused deposition modelling process. *The International Journal of Advanced Manufacturing Technology*, 53(9-12), 1027-37.
- Chang, P. C., Hieh, J. C., and Liao, T. W. (2005). Evolving fuzzy rules for due-date assignment problem in semiconductor manufacturing factory. *Journal of Intelligent Manufacturing*, 16(4-5), 549-57.
- Cheah, C. M., Chua, C. K., Lee, C. W., Feng, C., and Totong, K. (2005). Rapid prototyping and tooling techniques: a review of applications for rapid investment casting. *The International Journal of Advanced Manufacturing Technology*, 25(3-4), 308-20.
- Cheah, C. M., Chua, C. K., Lee, C. W., Lim, S. T., Eu, K. H., and Lin, L. T. (2002). Rapid sheet metal manufacturing. Part 2: direct rapid tooling. *The International Journal of Advanced Manufacturing Technology*, 19(7), 510-5.
- Cheah, C. M., Fuh, J. Y. H., Nee, A. Y. C., Lu, L., Choo, Y. S., and Miyazawa, T. (1997). Characteristics of photopolymeric material used in rapid prototypes Part II. Mechanical properties at post-cured state. *Journal of Materials Processing Technology*, 67(1), 46- 9.
- Chockalingam, K., Jawahar, N., Chandrasekar, U., and Ramanathan, K. N. (2008). Establishment of process model for part strength in stereolithography. *Journal of Materials Processing Technology*, 208(1), 348-365.

- Chockalingam, K., Jawahar, N., Ramanathan, K. N., and Banerjee, P. S. (2006). Optimization of stereolithography process parameters for part strength using design of experiments. *The International Journal of Advanced Manufacturing Technology*, 29(1-2), 79-88.
- Chowdary, B. V. (2007). Back-propagation artificial neural network approach for machining centre selection. *Journal of Manufacturing Technology Management*, 18(3), 315-332.
- Chua, C. K., Hong, K. H., and Ho, S. L. (1999). Rapid tooling technology. Part 1. A comparative study. *The International Journal of Advanced Manufacturing Technology*, 15(8), 604-608.
- Chua, C. K., Teh, S. H., and Gay, R. K. L. (1999). Rapid prototyping versus virtual prototyping in product design and manufacturing. *The International Journal of Advanced Manufacturing Technology*, 15(8), 597-603.
- Colombo, G., Filippi, S., Rizzi, C., and Rotini, F. (2010). A new design paradigm for the development of custom-fit soft sockets for lower limb prostheses. *Computers in Industry*, 61(6), 513-23.
- Croccolo, D., De Agostinis, M., and Olmi, G. (2013). Experimental characterization and analytical modelling of the mechanical behaviour of fused deposition processed parts made of ABS-M30. *Computational Materials Science*, 79, 506-18.
- Czyżewski, J., Burzyński, P., Gawęł, K., and Meisner, J. (2009). Rapid prototyping of electrically conductive components using 3D printing technology. *Journal of Materials Processing Technology*, 209(12), 5281-5.
- Ding, Y., Lan, H., Hong, J., and Wu, D. (2004). An integrated manufacturing system for rapid tooling based on rapid prototyping. *Robotics and computer-integrated manufacturing*, 20(4), 281-8.
- Dong, B., Qi, G., Gu, X., and Wei, X. (2008). Web service-oriented manufacturing resource applications for networked product development. *Advanced Engineering Informatics*, 22(3), 282-95.
- Driscoll, S. B. (2004). *The basics of testing plastics*. ASTM, West Conshohocken.
- Dunne, P., Soe, S. P., Byrne, G., Venus, A., and Wheatley, A. R. (2004). Some demands on rapid prototypes used as master patterns in rapid tooling for injection moulding. *Journal of Materials Processing Technology*, 150(3), 201-7.
- Edwards, P., and Ramulu, M. (2014). Fatigue performance evaluation of selective laser melted Ti-6Al-4V. *Materials Science and Engineering: A*, 598, 327-37.
- Ellyin, F. (1997). *Fatigue damage, crack growth and life prediction*. Springer Science and Business Media.
- Espalin, D., Arcaute, K., Rodriguez, D., Medina, F., Posner, M., and Wicker, R. (2010). Fused deposition modeling of patient-specific polymethylmethacrylate implants. *Rapid Prototyping Journal*, 16(3), 164-73.

- Es-Said, O. S., Foyos, J., Noorani, R., Mendelson, M., Marloth, R., and Pregger, B. A. (2000). Effect of layer orientation on mechanical properties of rapid prototyped samples. *Materials and Manufacturing Processes*, 15(1), 107-22.
- Garg, A., Rachmawati, L., and Tai, K. (2013). Classification-driven model selection approach of genetic programming in modelling of turning process. *International Journal of Advanced Manufacturing Technology*, 69(5-8), 1137-51.
- Garg, A., Tai, K., and Savalani, M. M. (2014). State-of-the-art in empirical modelling of rapid prototyping processes. *Rapid Prototyping Journal*, 20(2), 164-178.
- Garg, A., Vijayaraghavan, V., Mahapatra, S. S., Tai, K., and Wong, C. H. (2014a). Performance evaluation of microbial fuel cell by artificial intelligence methods. *Expert Systems with Applications*, 41(4), 1389-99.
- Garg, A., Tai, K., and Savalani, M. M. (2014). State-of-the-art in empirical modelling of rapid prototyping processes. *Rapid Prototyping Journal*, 20(2), 164-78.
- Garg, A., Tai, K., Lee, C. H., and Savalani, M. M. (2014b). A hybrid M5' -prime-genetic programming approach for ensuring greater trustworthiness of prediction ability in modelling of FDM process. *Journal of Intelligent Manufacturing*, 25(6), 1349-65.
- Garg, A., Vijayaraghavan, V., Mahapatra, S. S., Tai, K., and Wong, C. H. (2014). Performance evaluation of microbial fuel cell by artificial intelligence methods. *Expert systems with applications*, 41(4), 1389-99.
- Ghosh, A., and Mallik, A. K. (1986). *Manufacturing science*. Ellis Horwood, 1986.
- Giannatsis, J., and Dedoussis, V. (2009). Additive fabrication technologies applied to medicine and health care: a review. *The International Journal of Advanced Manufacturing Technology*, 40(1-2), 116-27.
- Gibson, I., Rosen, D., & Stucker, B. (2014). *Additive manufacturing technologies: 3D printing, rapid prototyping, and direct digital manufacturing*. Springer.
- Girod, S., Teschner, M., Schrell, U., Kevekordes, B., and Girod, B. (2001). Computer-aided 3-D simulation and prediction of craniofacial surgery: a new approach. *Journal of Cranio-Maxillofacial Surgery*, 29(3), 156-8.
- Gray IV, R. W., Baird, D. G., and Helge Bohn, J. (1998). Effects of processing conditions on short TLCP fiber reinforced FDM parts. *Rapid Prototyping Journal*, 4(1), 14-25.
- Greco, A., Licciulli, A., and Maffezzoli, A. (2001). Stereolithography of ceramic suspensions. *Journal of Materials Science*, 36(1), 99-105.
- Grida, I., and Evans, J. R. (2003). Extrusion free forming of ceramics through fine nozzles. *Journal of the European Ceramic Society*, 23(5), 629-35.
- Gungor, Z., and Arıkan, F. (2007). Using fuzzy decision making system to improve quality-based investment. *Journal of Intelligent Manufacturing*, 18(2), 197-207.

- Gurralla, P. K., and Regalla, S. P. (2014). Part strength evolution with bonding between filaments in fused deposition modelling: This paper studies how coalescence of filaments contributes to the strength of final FDM part. *Virtual and Physical Prototyping*, 9(3), 141-9.
- Hattiangadi, A., and Bandyopadhyay, A. (2000). Modeling of multiple pore ceramic materials fabricated via fused deposition process. *Scripta Materialia*, 42(6), 581-8.
- Heissler, E., Fischer, F. S., Boiouri, S., Lehrmann, T., Mathar, W., Gebhardt, A., and Bler, J. (1998). Custom-made cast titanium implants produced with CAD/CAM for the reconstruction of cranium defects. *International Journal of Oral and Maxillofacial Surgery*, 27(5), 334-8.
- Hinczewski, C., Corbel, S., and Chartier, T. (1998). Ceramic suspensions suitable for stereolithography. *Journal of the European Ceramic Society*, 18(6), 583-90.
- Hon, K. K. B. (2007, January). Digital Additive Manufacturing: From Rapid Prototyping to Rapid Manufacturing. In *Proceedings of the 35th International MATADOR Conference* (pp. 337-340). Springer London.
- Hon, K. K. B. (2007, January). Digital Additive Manufacturing: From Rapid Prototyping to Rapid Manufacturing. In *proceedings of the 35th international MATADOR conference*, Springer London, 337 – 40.
- Hopkinson, N., Hague, R., and Dickens, P. (Eds.). (2006). *Rapid manufacturing: an industrial revolution for the digital age*. John Wiley and Sons.
- Hsu, C. Y., Chen, D. Y., Lai, M. Y., and Tzou, G. J. (2008). EDM electrode manufacturing using RP combining electroless plating with electroforming. *The International Journal of Advanced Manufacturing Technology*, 38(9-10), 915-24.
- <http://www.plasticsintl.com/datasheets/ABS.pdf>.
- Im, Y. G., Cho, B. H., Seo, S. H., Son, J. H., Chung, S. I., and Jeong, H. D. (2007). Functional prototype development of multi-layer board (MLB) using rapid prototyping technology. *Journal of Materials Processing Technology*, 187, 619-622.
- Ippolito, R., Iuliano, L., and Gatto, A. (1995). Benchmarking of rapid prototyping techniques in terms of dimensional accuracy and surface finish. *CIRP Annals-Manufacturing Technology*, 44(1), 157-60.
- Jain, P. K., Pandey, P. M., and Rao, P. V. (2009). Effect of delay time on part strength in selective laser sintering. *The International Journal of Advanced Manufacturing Technology*, 43(1), 117-26.
- Kallrath, J., Altstädt, V., Schlöder, J. P., and Bock, H. G. (1999). Analysis of fatigue crack growth behaviour in polymers and their composites based on ordinary differential equations parameter estimation. *Polymer Testing*, 18(1), 11-35.
- Karapatis, N. P., Van Griethuysen, J. P. S., and Glardon, R. (1998). Direct rapid tooling: a review of current research. *Rapid Prototyping Journal*, 4(2), 77-89.

- Kengpol, A., and O'Brien, C. (2001). The development of a decision support tool for the selection of advanced technology to achieve rapid product development. *International Journal of Production Economics*, 69(2), 177-91.
- Koza, J. R. (1992). *Genetic programming: on the programming of computers by means of natural selection* (Vol. 1). MIT press.
- Krause, F. L., Ciesla, M., Stiel, C., and Ulbrich, A. (1997). Enhanced rapid prototyping for faster product development processes. *CIRP Annals-Manufacturing Technology*, 46(1), 93-6.
- Kruth, J. P., Leu, M. C., and Nakagawa, T. (1998). Progress in additive manufacturing and rapid prototyping. *CIRP Annals-Manufacturing Technology*, 47(2), 525-40.
- Kujawski, D., and Ellyin, F. (1995). A unified approach to mean stress effect on fatigue threshold conditions. *International Journal of Fatigue*, 17(2), 101-6.
- Kumar, S. (2009). Manufacturing of WC-Co moulds using SLS machine. *Journal of materials Processing Technology*, 209(8), 3840-48.
- Kumar, S., and Kruth, J. P. (2008). Wear performance of SLS/SLM materials. *Advanced Engineering Materials*, 10(8), 750-3.
- Kumar, S., and Kruth, J. P. (2010). Composites by rapid prototyping technology. *Materials and Design*, 31(2), 850-6.
- Lan, H. (2009). Web-based rapid prototyping and manufacturing system: a review. *Computer in Industry*, 60(9), 643-56
- Lan, H., Ding, Y., and Hong, J. (2005). Decision support system for rapid prototyping process selection through integration of fuzzy synthetic evaluation and an expert system. *International Journal of Production Research*, 43(1), 169-94.
- Lee, B. H., Abdullah, J., and Khan, Z. A. (2005). Optimization of rapid prototyping parameters for production of flexible ABS object. *Journal of Materials Processing Technology*, 169(1), 54-61.
- Lee, C. S., Kim, S. G., Kim, H. J., and Ahn, S. H. (2007). Measurement of anisotropic compressive strength of rapid prototyping parts. *Journal of Materials Processing Technology*, 187, 627-30.
- Lee, J., and Huang, A. (2013). Fatigue analysis of FDM materials. *Rapid Prototyping Journal*, 19(4), 291-9.
- Leuders, S., Thöne, M., Riemer, A., Niendorf, T., Tröster, T., Richard, H. A., and Maier, H. J. (2013). On the mechanical behaviour of titanium alloy TiAl6V4 manufactured by selective laser melting: Fatigue resistance and crack growth performance. *International Journal of Fatigue*, 48, 300-7.
- Levy, G. N., Schindel, R., and Kruth, J. P. (2003). Rapid manufacturing and rapid tooling with layer manufacturing (LM) technologies, state of the art and future perspectives. *CIRP Annals-Manufacturing Technology*, 52(2), 589-609.

- Lewis, G. K., and Schlienger, E. (2000). Practical considerations and capabilities for laser assisted direct metal deposition. *Materials and Design*, 21(4), 417-23.
- Li, C., Yi, J., and Zhao, D. (2009). Design of interval type-2 fuzzy logic system using sampled data and prior knowledge. *ICIC Express Letters*, 3(3).
- Liu, F. H., Shen, Y. K., and Liao, Y. S. (2011). Selective laser gelation of ceramic–matrix composites. *Composites Part B: Engineering*, 42(1), 57-61.
- Liu, Q., Leu, M. C., and Schmitt, S. M. (2006). Rapid prototyping in dentistry: technology and application. *The International Journal of Advanced Manufacturing Technology*, 29(3-4), 317-35.
- Lohfeld, S., McHugh, P., Serban, D., Boyle, D., O'Donnell, G., and Peckitt, N. (2007). Engineering Assisted Surgery™: A route for digital design and manufacturing of customised maxillofacial implants. *Journal of Materials Processing Technology*, 183(2), 333-8.
- Luo, R. C., Chang, C. L., Pan, Y. L., & Tzou, J. H. (2005, November). Rapid tooling using laser powered direct metallic manufacturing process. In *Industrial Electronics Society, 2005. IECON 2005. 31st Annual Conference of IEEE* (pp. 6-pp). IEEE.
- Ma, S., Gibson, I., Balaji, G., and Hu, Q. J. (2007). Development of epoxy matrix composites for rapid tooling applications. *Journal of Materials Processing Technology*, 192, 75-82.
- Mahapatra, S. S., and Sood, A. K. (2012). Bayesian regularization-based Levenberg–Marquardt neural model combined with BFOA for improving surface finish of FDM processed part. *The International Journal of Advanced Manufacturing Technology*, 60(9-12), 1223-35.
- Mahesh, M., Fuh, J. Y., Wong, Y. S., and Loh, H. T. (2005, August). Benchmarking for decision making in rapid prototyping systems. In *Automation Science and Engineering, 2005. IEEE International Conference on* (pp. 19-24). IEEE.
- Marissen, R., Schudy, D., Kemp, A. J., Coolen, S. M. H., Duijzings, W. G., Van Der Pol, A. and Van Gulick, A. J. (2001). The effect of material defects on the fatigue behaviour and the fracture strain of ABS. *Journal of Materials Science*, 36(17), 4167-80.
- Masood, S. H., and Al-Alawi, M. A. Z. E. N. (2002). The IRIS rapid prototyping system selector for educational and manufacturing users. *International Journal of Engineering Education*, 18(1), 66-77.
- Masood, S. H., and Song, W. Q. (2004). Development of new metal/polymer materials for rapid tooling using fused deposition modelling. *Materials and Design*, 25(7), 587-94.
- Masood, S. H., and Soo, A. (2002). A rule based expert system for rapid prototyping system selection. *Robotics and Computer-Integrated Manufacturing*, 18(3), 267-74.
- Minetola, P., and Iuliano, L. (2014). The reverse guillotine tribometer for evaluation of sliding wear of additive manufactured fixtures. *Rapid Prototyping Journal*, 20(2), 105-14.
- Montgomery DC (2003) *Design and Analysis of Experiments*. 5th ed. Singapore: John Wiley and Sons Inc.

- Monzon, M., Benítez, A. N., Marrero, M. D., Hernandez, N., Hernandez, P., and Aisa, J. (2008). Validation of electrical discharge machining electrodes made with rapid tooling technologies. *Journal of Materials processing technology*, 196(1), 109-14.
- Mostafa, N., Syed, H. M., Igor, S., and Andrew, G. (2009). A study of melt flow analysis of an ABS-Iron composite in fused deposition modelling process. *Tsinghua Science and Technology*, 14, 29-37.
- Mueller, B., and Kochan, D. (1999). Laminated object manufacturing for rapid tooling and patternmaking in foundry industry *Computers in Industry*, 39(1), 47-53.
- Nickel, A. H., Barnett, D. M., and Prinz, F. B. (2001). Thermal stresses and deposition patterns in layered manufacturing. *Materials Science and Engineering: A*, 317(1), 59-64.
- Noorani, R. (2006). *Rapid prototyping: principles and applications*. John Wiley and Sons Incorporated.
- Onuh, S. O., and Yusuf, Y. Y. (1999). Rapid prototyping technology: applications and benefits for rapid product development. *Journal of intelligent manufacturing*, 10(3-4), 301-11.
- Peng, A., Xiao, X., and Yue, R. (2014). Process parameter optimization for fused deposition modeling using response surface methodology combined with fuzzy inference system. *The International Journal of Advanced Manufacturing Technology*, 73(1-4), 87-100.
- Pham, D. T., and Gault, R. S. (1998). A comparison of rapid prototyping technologies. *International Journal of Machine Tools and Manufacture*, 38(10), 1257-87.
- Phatak, A. M., and Pande, S. S. (2012). Optimum part orientation in Rapid Prototyping using genetic algorithm. *Journal of Manufacturing Systems*, 31(4), 395-402.
- Rahmati, S., and Dickens, P. (2007). Rapid tooling analysis of Stereolithography injection mould tooling. *International Journal of Machine Tools and Manufacture*, 47(5), 740-7.
- Raja, V., Zhang, S., Garside, J., Ryall, C., and Wimpenny, D. (2006). Rapid and cost-effective manufacturing of high-integrity aerospace components. *The International Journal of Advanced Manufacturing Technology*, 27(7-8), 759-73.
- Ramesh, C. S., and Srinivas, C. K. (2009). Friction and wear behavior of laser-sintered iron–silicon carbide composites. *Journal of Materials Processing Technology*, 209(14), 5429-36.
- Rao, R. V., and Padmanabhan, K. K. (2007). Rapid prototyping process selection using graph theory and matrix approach. *Journal of Materials Processing Technology*, 194(1), 81-8.
- Rayegani, F., and Onwubolu, G. C. (2014). Fused deposition modelling (FDM) process parameter prediction and optimization using group method for data handling (GMDH) and differential evolution (DE). *The International Journal of Advanced Manufacturing Technology*, 73(1-4), 509-19.
- Rezaie, R., Badrossamay, M., Ghaie, A., and Moosavi, H. (2013). Topology optimization for fused deposition modeling process. *Procedia CIRP*, 6, 521-6.

- Riemer, A., Leuders, S., Thöne, M., Richard, H. A., Tröster, T. and Niendorf, T. (2014). On the fatigue crack growth behavior in 316L stainless steel manufactured by selective laser melting. *Engineering Fracture Mechanics*, 120, 15-25.
- Roylance, D. (2001). *Stress-strain curves*. Massachusetts Institute of Technology study, Cambridge.
- Sapkota, A., and Ohmi, K. (2009). Error detection and performance analysis scheme for particle tracking velocimetry results using fuzzy logic. *International Journal of Innovative Computing, Information and Control*, 5(12B), 4927-34.
- Searson, D. P. (2009). *GPTIPS: Genetic programming and symbolic regression for MATLAB. User Guide*, 2010.
- Sehrt, J. T., and Witt, G. (2010, January). Dynamic strength and fracture toughness analysis of beam melted parts. In *Proceedings of the 36th International MATADOR Conference* (pp. 385-388). Springer London.
- Shan, Z., Yan, Y., Zhang, R., Lu, Q., and Guan, L. (2003). Rapid manufacture of metal tooling by rapid prototyping. *The International Journal of Advanced Manufacturing Technology*, 21(7), 469-75.
- Shengxian, C., Yanhui, Z., Jing, Z., and Dayu, Y. (2012). Experimental Study on Dynamic Simulation for Biofouling Resistance Prediction by Least Squares Support Vector Machine. *Energy Procedia*, 17, 74-78.
- Singh, S., and Singh, R. (2015). Wear modelling of Al-Al₂O₃ functionally graded material prepared by FDM assisted investment castings using dimensionless analysis. *Journal of Manufacturing Processes*, 20(3), 507-14.
- Sood, A. K., Equbal, A., Toppo, V., Ohdar, R. K., and Mahapatra, S. S. (2012). An investigation on sliding wear of FDM built parts. *CIRP Journal of Manufacturing Science and Technology*, 5(1), 48-54.
- Sood, A. K., Ohdar, R. K., and Mahapatra, S. S. (2009). Improving dimensional accuracy of fused deposition modelling processed part using grey Taguchi method. *Materials and Design*, 30(10), 4243-52.
- Sood, A. K., Ohdar, R. K., and Mahapatra, S. S. (2010). Parametric appraisal of mechanical property of fused deposition modelling processed parts. *Materials and Design*, 31(1), 287-95.
- Sood, A. K. (2011). *Study on Parametric Optimization of Fused Deposition Modelling (FDM) Process* (Doctoral dissertation, NATIONAL INSTITUTE OF TECHNOLOGY ROURKELA).
- Spierings, A. B., Starr, T. L., and Wegener, K. (2013). Fatigue performance of additive manufactured metallic parts. *Rapid Prototyping Journal*, 19(2), 88-94.
- Subburaj, K., and Ravi, B. (2008). Computer aided rapid tooling process selection and manufacturability evaluation for injection mold development. *Computers in Industry*, 59(2), 262-76.

- Sun, Q., Rizvi, G. M., Bellehumeur, C. T., and Gu, P. (2008). Effect of processing conditions on the bonding quality of FDM polymer filaments. *Rapid Prototyping Journal*, 14(2), 72-80.
- Wohlers, T. (2012). *Wohlers report 2012*. Wohlers Associates, Inc.
- Tang, Y., Zhou, H., Hong, J., and Lu, B. (2002). RP-based abrading technique for graphite EDM electrode. *Journal of Material Science and Technology*, 18(6), 572-74.
- Tao, G., and Xia, Z. (2007a). An experimental study of uniaxial fatigue behavior of an epoxy resin by a new noncontact real-time strain measurement and control system. *Polymer Engineering and Science*, 47(6), 780-8.
- Tao, G., and Xia, Z. (2007b). Mean stress/strain effect on fatigue behavior of an epoxy resin. *International journal of fatigue*, 29(12), 2180-90.
- Todd Grimm, (2008) *Breakthroughs in Rapid Prototyping Materials*, Desktop Engineering (Magazine).
- Too, M. H., Leong, K. F., Chua, C. K., Du, Z. H., Yang, S. F., Cheah, C. M., and Ho, S. L. (2002). Investigation of 3D non-random porous structures by fused deposition modelling. *The International Journal of Advanced Manufacturing Technology*, 19(3), 217-23.
- Tromans, G. (2003). *Developments in rapid casting (Vol. 2)*. John Wiley and Sons.
- Upcraft, S., and Fletcher, R. (2003). The rapid prototyping technologies. *Assembly Automation*, 23(4), 318-30.
- Vaidya, O. S., and Kumar, S. (2006). Analytic hierarchy process: An overview of applications. *European Journal of operational research*, 169(1), 1-29.
- Vijayaraghavan, V., Garg, A., Lam, J. S. L., Panda, B., and Mahapatra, S. S. (2014). Process characterisation of 3D-printed FDM components using improved evolutionary computational approach. *The International Journal of Advanced Manufacturing Technology*, 78(5-8), 781-93.
- Villalpando, L., Eiliat, H., and Urbanic, R. J. (2014). An optimization approach for components built by fused deposition modeling with parametric internal structures. *Procedia CIRP*, 17, 800-5.
- Wang, T. M., Xi, J. T., and Jin, Y. (2007). A model research for prototype warp deformation in the FDM process. *The International Journal of Advanced Manufacturing Technology*, 33(11-12), 1087-96.
- Wang, T., Li, L., and Tong, S. (2010). Application of type-2 fuzzy logic system in indoor temperature control. *ICIC Express Letters*, 4(5B), 1919-24.
- Wang, W. L., Conley, J. G., Yan, Y. N., and Fuh, J. Y. (2000). Towards intelligent setting of process parameters for layered manufacturing. *Journal of Intelligent Manufacturing*, 11(1), 65-74.
- Wiedemann, B., and Jantzen, H. A. (1999). Strategies and applications for rapid product and process development in Daimler-Benz AG. *Computers in Industry*, 39(1), 11-25.

- Wohler, T., (2010) Additive Manufacturing State of the Industry Annual Worldwide Progress Report," Wohler associates, Colorado, USA.
- Wohlers, T. T. (1992). CAD meets rapid prototyping. *COMP. AIDED ENG.*, 11(4), 66-75.
- Wu, G., Langrana, N. A., Sadanji, R., and Danforth, S. (2002). Solid freeform fabrication of metal components using fused deposition of metals. *Materials and design*, 23(1), 97-105.
- Yan, Y., Li, S., Zhang, R., Lin, F., Wu, R., Lu, Q., and Wang, X. (2009). Rapid prototyping and manufacturing technology: principle, representative technics, applications, and development trends. *Tsinghua Science and Technology*, 14, 1-12.
- Yang, X. S. (2010). *Engineering optimization: an introduction with metaheuristic applications*. John Wiley and Sons.
- Yen, H. C., Chiu, M. L., and Tang, H. H. (2009). Laser scanning parameters on fabrication of ceramic parts by liquid phase sintering. *Journal of the European Ceramic Society*, 29(8), 1331-6.
- Zhang, W., Srivastava, I., Zhu, Y. F., Picu, C. R., and Koratkar, N. A. (2009). Heterogeneity in epoxy nanocomposites initiates crazing: significant improvements in fatigue resistance and toughening. *Small*, 5(12), 1403-7.
- Zhang, Y. M., Li, P., Chen, Y., and Male, A. T. (2002). Automated system for welding-based rapid prototyping. *Mechatronics*, 12(1), 37-53.
- Zhang, Y., and Chou, K. (2008). A parametric study of part distortions in fused deposition modelling using three-dimensional finite element analysis. *Proceedings of the Institution of Mechanical Engineers, Part B: Journal of Engineering Manufacture*, 222(8), 959-68.
- Zhang, Y., and Liu, H. (2009). Application of rapid prototyping technology in die making of diesel engine. *Tsinghua Science and Technology*, 14, 127-31.
- Zhang, Y., Chen, Y., Li, P., and Male, A. T. (2003). Weld deposition-based rapid prototyping: a preliminary study. *Journal of Materials Processing Technology*, 135(2), 347-57.
- Zhang, Y., He, X., Du, S., and Zhang, J. (2001). Al₂O₃ ceramics preparation by LOM (laminated object manufacturing). *The International Journal of Advanced Manufacturing Technology*, 17(7), 531-534.
- Zhong, W., Li, F., Zhang, Z., Song, L., and Li, Z. (2001). Short fiber reinforced composites for fused deposition modeling. *Materials Science and Engineering: A*, 301(2), 125-30.
- Ziemian, S., Okwara, M., and Ziemian, C. W. (2015). Tensile and fatigue behavior of layered acrylonitrile butadiene styrene. *Rapid Prototyping Journal*, 21(3), 270-8.

Dissemination

PATENTS

1. Design registration for Portable Water Bottle (265832) patented on 18.09.2014, (**Swayam Bikash Mishra**, Siba Sankar Mahapatra, Sandip Mondal and Raj Kishore Patel).
2. Patent applied for Gravity Flow Portable Water Bottle with Filtration System (961/KOL/2014) on 22.09.2014. (**Swayam Bikash Mishra**, Siba Sankar Mahapatra, Sandip Mondal and Raj Kishore Patel). (Examination Awaited).

JOURNAL ARTICLES

1. **Mishra, S. B.** and Mahapatra, S. S. Improvement in Tensile Strength of FDM Built Parts by Parametric Control. Applied Mechanics and Materials. 2014; 592:1075-9.
2. **Mishra, S. B.**, Malik, R. and Mahapatra, S. S. Enhancement of Flexural Strength of FDM Build Parts using a Metaheuristic Approach. Additive manufacturing (under review).
3. **Mishra, S. B.** and Mahapatra, S. S. Strain controlled fatigue behaviour of FDM build parts. Engineering failure analysis (under review).
4. **Mishra, S. B.** and Mahapatra, S. S. Effect of raster fill pattern and contour number on mechanical property in fused deposition modelling parts. Robotics and computer integrated manufacturing (under review).
5. **Mishra, S. B.** and Mahapatra, S. S. Parametric analysis of wear behaviour on fused deposition modelling parts. International journal of productivity and quality management (under review).

CONFERENCE PRESENTATIONS

1. **Mishra, S. B.** and Mahapatra, S. S. (2014), "Improvement in tensile strength of FDM build parts using a parametric approach" International Mechanical Engineering Congress 2014, NIT Tiruchirappalli, June 13-15.
2. **Mishra, S. B.**, Malik, R. and Mahapatra, S. S. (2015), "An experimental investigation on Flexural strength of FDM process parts" Advances in Materials, Manufacturing and Applications 2015, NIT Tiruchirappalli, April 09-11
3. **Mishra, S. B.** and Mahapatra, S. S. (2015), " Parametric assessments of FDM build part", National Seminar on Recent Advancements in Mechanical and Production Engineering 2015, Nalanda institute of technology Bhubaneswar, October 10-11.

Vitae

Swayam Bikash Mishra

Ph.D. Research Scholar,
National Institute of Technology Rourkela
Sundargarh, Odisha 769008
Tel: +91-9937175116; 06721-270289;
Email: swayambikash86@gmail.com
DOB: 27th May 1987, Male, Indian

EDUCATION / ACADEMIC BACKGROUND

2015	Ph.D. (Production Engineering, NIT Rourkela, India) (Continuing)
2012	M.Tech (Heat and Power, SOA University, Odisha, India)
2009	B.Tech (Mechanical Engineering, BPUT, Odisha, India)

WORK EXPERIENCE

Designation: Ph.D. Scholar

Duration: July 2012-till date

Organisation: National Institute of Technology, Rourkela

Job Profile: Research and Development in the area of Rapid Prototyping with special importance on Fused Deposition Modelling and its applications. Designed a water bottle by R.P technique which can purify water itself without the help of any external machine.

Designation: Assistant Professor

Duration: Jan 2011-July 2012

Organisation: Aryan Institute of Engineering and Technology, Bhubaneswar

Job Profile: Responsible for assisting in the educational and social development of B.Tech final and pre-final students. Conducted classes and labs in the area of thermal and automobile engineering.

Duties:

1. Planning & delivering well-structured lessons which engage & motivate students.
2. Planning and organising visits, field studies and special activities connected with the teaching of the subject.
3. Organising and supporting a range of extra-curricular activities.
4. Achieving and maintain high standards of care and education.
5. Planning, preparing and reviewing the school curriculum with other staff.

Designation: Graduate Engineer Trainee

Duration: Nov 2009-Dec 2010

Organisation: Central Tool Room and Training Centre, Bhubaneswar

Job Profile: Responsible for conducting classes of CATIA, SOLID WORKS and other such mechanical systems softwares.

Teaching Attributes:

1. Able to create a vibrant and effective learning environment.
2. Familiar with a variety of approaches to teaching pupils.
3. Having the ability to motivate and earn the respect of students.

SKILLS

Hands on Experience in:

1. CATIA
2. Pro-E
3. SOLID WORKS
4. Auto CAD
5. Uni-Graphics
6. ANSYS
7. MINITAB
8. MATLAB
9. Design of Experiments

Proficiency in:

MS Office

MEMBERSHIP

1. Regular Student Membership "American Society of Mechanical Engineers (ASME)", USA.
2. Associate Membership "The Institute of Engineers (IE)" India.
3. Life Membership "Additive Manufacturing Society of India (AMSI)", India.

RESEARCH EXPERIENCE

Doctoral Research

- Parametric assessments of Fused Deposition Modelling (FDM) build parts on Mechanical strength viz. Tensile, Compressive, Impact and Flexural strength.
- Experimental investigation of the Effect of build Parameters on the Fatigue life of FDM Build Parts and the best parameter setting improving the fatigue life has been suggested.
- Wear behaviour of the FDM build parts have been studied considering six important controllable process parameters.
- The effect of process parameters on the circularity and the surface roughness of build part are studied.
- Split Mould and Pattern Manufactured using FDM machine within minimum time and less material waste.
- The FDM build parts are made conductive for manufacturing of internal circuit board design.
- FDM build parts are made as replica using electrolysis and electro-less processes for the preservation of the antique artefacts.

Master's Research

- Study of internal flow characteristics of an internal pinned fin tube at variable Reynolds number and variable finned number.
- Applying the optimisation technique for best parameter setting is suggested to maximize the heat transfer rate through the internal pinned fin tube.

PUBLICATIONS

Patents

- Design registration for Portable Water Bottle (265832) patented on 18.09.2014, (Swayam Bikash Mishra, Siba Sankar Mahapatra, Sandip Mondal and Raj Kishore Patel).
- Patent applied for Gravity Flow Portable Water Bottle with Filtration System (961/KOL/2014) on 22.09.2014. (Swayam Bikash Mishra, Siba Sankar Mahapatra, Sandip Mondal and Raj Kishore Patel). (Examination Awaited).

Referred journals

1. *Mishra, S. B.* and Mahapatra, S. S. Improvement in Tensile Strength of FDM Built Parts by Parametric Control. *Applied Mechanics and Materials*. 2014; 592:1075-9.
2. *Mishra, S. B.*, Malik, R. and Mahapatra, S. S. Enhancement of Flexural Strength of FDM Build Parts using a Metaheuristic Approach. *Additive manufacturing* (under review).
3. *Mishra, S. B.* and Mahapatra, S. S. Strain controlled fatigue behaviour of FDM build parts. *Engineering failure analysis* (under review).
4. *Mishra, S. B.* and Mahapatra, S. S. Effect of raster fill pattern and contour number on mechanical property in fused deposition modelling parts. *Robotics and computer integrated manufacturing* (under review).
5. *Mishra, S. B.* and Mahapatra, S. S. Parametric analysis of wear behaviour on fused deposition modeling parts. *International journal of productivity and quality management* (under review).
6. *Mishra, S. B.* and Mahapatra, S. S. Parametric appraisal of compressive strength on the FDM build parts. Under process
7. *Mishra, S. B.* and Mahapatra, S. S. An experimental investigation on circularity and surface roughness of the FDM build parts. Under process

Conference publications

8. **Mishra, S. S.** (2012), "Characteristics of heat flow through internal finned tube under mixed condition", National seminar on Advancement in production technology and engineering materials 2012, Aryan institute of technology Bhubaneswar, February 11-12.

9. **Mishra, S. B.** and Mahapatra, S. S. (2013), "Optimisation of performance and analysis of internal finned tube heat exchanger under mixed flow condition", AEOTIT 2013, SVNIT Surat, July 01-03.
10. **Mishra, S. B.** and Mahapatra, S. S. (2014), "Improvement in tensile strength of FDM build parts using a parametric approach" IMEC 2014, NIT Tiruchirappalli, June 13-15.
11. **Mishra, S. B.**, Malik, R. and Mahapatra, S. S. (2015), "An experimental investigation on Flexural strength of FDM process parts" AMMA 2015, NIT Tiruchirappalli, April 09-11
12. **Mishra, S. B.** and Mahapatra, S. S. (2015), " Parametric assessments of FDM build part", NSRAMPE 2015, Nalanda institute of technology Bhubaneswar, October 10-11

PROJECTS HANDLED

1. "Design and development of moulds by RP route" for IFGL Refractories Limited Kalunga Odisha for Rs. 34,996/- on 13.06.2014.
2. "End use part design for Gupchup machine" project undertaken by Prof. S. S. Mahapatra and Dr. S. Panda, Mechanical Engineering department, NIT Rourkela. 14.06.2014
3. "Design and development of moulds by RP route" for IFGL Refractories Limited Kalunga Odisha for Rs. 49,900/- on 08.08.2014.
4. "Design and manufacturing of portable water filter" project under taken by Prof. S. S. Mahapatra, Mechanical Engineering Department, NIT Rourkela. 12.08.2014.
5. "Design and fabrication of casting core by RP route" for IFGL Refractories Limited Kalunga Odisha for Rs. 30,000/- on 20.10.2014.
6. "Pattern manufacturing using FDM technique" For Eastern alloy Pvt. Ltd Kalunga Odisha for Rs. 54,000/- on 19.02.2015.
7. "Design and manufacturing of end use parts for portable washing machine" For Estinno Pvt. Ltd, Rourkela Odisha for Rs. 40,609/- on 10.07.2015.
8. "External fin design and manufacturing for under water robot" DRDO project undertaken by Prof. B. Subudhi, Electrical Engineering Department, NIT Rourkela.

ORGANISING COMMITTEE MEMBER FOR STTP

1. A three day short term course on Design of Experiments: An Optimisation Tool (DOEOT-2013) during 27th Dec. – 29th Dec. 2013 at Mechanical Engineering Department of NIT Rourkela (a self-sponsored course for faculty, research scholars and industry professionals (No. of participants 75)
2. A three day short term course on Multi-Objective Optimisation Methods and Applications in Manufacturing (MOOMAM-14) during 6th June 8th June 2014 at Mechanical Engineering Department of NIT Rourkela (a self-sponsored course for faculty, research scholars and industry professionals (No. of participants 36).
3. A four day short term course on Design of Experiments: An Optimisation Tool (DOEOT-2014) during 22nd Dec. – 25th Dec. 2014 at Mechanical Engineering Department of NIT Rourkela (a self-sponsored course for faculty, research scholars and industry professionals (No. of participants 68).
4. A four day short term course on Design of Experiments: An Optimisation Tool (DOEOT-2015) during 21nd Dec. – 24th Dec. 2015 at Mechanical Engineering Department of NIT Rourkela (a self-sponsored course for faculty, research scholars and industry professionals (Expected participation 60).

REFEREES

Dr. Siba Sankar Mahapatra

Professor, NIT Rourkela, Odisha, India. Email: ssm@nitrkl.ac.in

Dr. Saurav Datta

Asst. Professor, NIT Rourkela, Odisha, India. Email: sdatta@nitrkl.ac.in

Dr. Manasa Behera

Asst. Professor, IIT Bombay, Maharashtra, India. Email: manasa.rb@iitb.ac.in

Date: January 22, 2016

Swayam Bikash Mishra
Ph.D. Research Scholar, NIT Rourkela